AD-A277 178

RESEARCH TRIANGLE INSTITUTE

RTI/5294/94-Quarterly

DTIC
S ELECTE
MAR 1 7 1994
F D

February 1994

HETEROEPITAXIAL DIAMOND GROWTH

Final Report
1 January 1993 - 31 December 1993

94-08660

R. J. Markunas
R. A. Rudder
R. E. Thomas
J. B. Posthill

94 3 16 186

BALLISTIC MISSILE DEFENSE ORGANIZATION
Innovative Science and Technology Office

POST OFFICE BOX 12194 RESEARCH TRIANGLE PARK, NORTH CAROLINA 27709-2194

REPORT DOCUMENT PAGE

Public reporting burden for this collection of information is estimated to average 1 hour per response, including the time for reviewing instructions, searching existing data sources, gathering and maintaining the data needed, and completing and reviewing the collection of information. Send comments regarding this burden estimate or any other aspect of this collection of information, including suggestions for reducing this burden to Washington Headquarters Services, Directorate for Information Operations and Reports, 1215 Jefferson Davis Highway, Suite 1204 Arlington, VA 22202-4302, and to the Office of Management and Budget Paperwork Reduction Project (0704-088), Washington, DC 20503

1. AGENCY USE ONLY *(Leave blank)*	2. REPORT DATE February 1994	3. REPORT TYPE AND DATES COVERED Final Report January 1, 1993 -- December 31, 1993

4. TITLE AND SUBTITLE

Heteroepitaxial Diamond Growth

5. FUNDING NUMBERS

N00014-92-C-0081

6. AUTHOR(S)

R. J. Markunas, R. A. Rudder, J. B. Posthill, R. E. Thomas, G. Hudson

7. PERFORMING ORGANIZATION NAME(S) AND ADDRESS(ES)

Research Triangle Institute
P. O. Box 12194
Research Triangle Park, NC 27709

8. PERFORMING ORGANIZATION REPORT NUMBER

83U-5294

9. SPONSORING/MONITORING AGENCY NAME(S) AND ADDRESSES(ES)

Office of Naval Research
800 N. Quincy Street
Arlington, VA 22217-5000

10. SPONSORING/MONITORING AGENCY REPORT NUMBER

11. SUPPLEMENTARY NOTES

12a. DISTRIBUTION/AVAILABILITY STATEMENT

Approved for public release; unlimited distribution

12b. DISTRIBUTION CODE

13. ABSTRACT

Technical highlights from 1993 include the following:

Growth Chemistries. A clear correlation was observed between ionization potential of feedstock gasses and critical power necessary for inductive coupling of the plasma and consequent diamond growth.

Substrate preparation and epitaxial film quality. Ion-implantation of C and O has been coupled with either electrochemical etching or acid cleaning for surface preparation prior to homoepitaxial growth.

Reactor modifications. Key improvements were made to the rf reactor to allow for long growths to consolidate substrates. Liquid mass flow controllers were added to precisely meter both the water and selected alcohol.

Ion-Implantation and lift off. Lift off of diamond platelets has been achieved with two processes. Ion-implantation of either C or O followed by annealing and implantation of either C or O followed by water based electrolysis.

Diamond characterization. Development of novel defect characterization techniques. 1.) Etch delineation of defects by exposure to propane torch flame. 2.) Hydrogen plasma exposure to enhance secondary electron emission and provide non-topographical defect contrast.

Acetylene will react at room temperature with sites created by partial desorption of oxygen from the (100) diamond surface.

Thermal desorption measurements give an apparent activation energy for CO desorption from diamond (100) of 45 kcal/mol.

Quantum chemical calculations indicate an activation energy of 38 kcal/mol for CO desorption. (Collaboration, M. Frenklach Penn. St. U).

Ab initio calculations on (100) surfaces indicates that oxygen adsorbed at one dimer site has an effect on the dimerization of an adjacent site. (Collaboration, J. Whitten NCSU).

14. SUBJECT TERMS

15. NUMBER OF PAGES

16. PRICE CODE

17. SECURITY CLASSIFICATION OF REPORT UNCLASSIFIED	18. SECURITY CLASSIFICATION OF THIS PAGE UNCLASSIFIED	19. SECURITY CLASSIFICATION OF ABSTRACT UNCLASSIFIED	20. LIMITATION OF ABSTRACT

TABLE OF CONTENTS

1.0 INTRODUCTION AND TECHNICAL HIGHLIGHTS

This is the final report on the Heteroepitaxial Diamond Growth Program Contact No. N-00014-92-C-0081 at Research Triangle Institute.

Two approaches have been taken in the development of diamond substrates for electronic applications. In the first we are attempting to consolidate natural diamond substrates into a large area template from which thin sections can be cleaved to act as single crystal seeds for subsequent substrate production. Thus a single reusable template could provide an arbitrary number of "seeds" for growth of large area substrates. In the second approach we are developing substrate preparation techniques for direct heteroepitaxial growth of diamond substrates on non-diamond substrates.

The final report is organized as follows. The introduction provides a brief background for the project and program highlights for 1993. Additional information on progress in both large area substrate development and heteroepitaxial growth is provided in the two subsequent sections that provide summaries of individual papers presented and published in 1993. Detailed descriptions of the experimental methods, results and analyses are provided in copies of the journal articles reproduced in the appendix.

Substantial progress was made in both program areas and the following section provides technical highlights from 1993 program activities.

1.1 Large Area Substrate Development Via Tiling.

Production of large area substrates by a tiling process requires the integration of several key steps: consolidation of natural substrates via homoepitaxial growth, ion-implantation and lift-off of diamond sheets, and subsequent homoepitaxial growth on the cleaved "seed".

Growth Studies:

- Growth Chemistries. A clear correlation was observed between ionization potential of feedstock gasses and critical power necessary for inductive coupling of the plasma and consequent diamond growth. The water based growth chemistries also allow growth at substantially lower substrate temperatures.

1

- Substrate preparation and epitaxial film quality. Ion-implantation of C and O has been coupled with either electrochemical etching or acid cleaning for surface preparation prior to homoepitaxial growth.

- Reactor modifications. Key improvements were made to the rf reactor to allow for long growths to consolidate substrates. Liquid mass flow controllers were added to precisely meter both the water and selected alcohol. This allows long growths without changes in concentration seen in premixed solutions. An optical feedback loop was added to control the tuning of the reactor and maintain the high-power inductively coupled mode.

Ion-Implantation and lift off:

- Lift off of diamond platelets has been achieved with two processes. 1) Ion-implantation of either C or O followed by annealing. 2) Implantation of either C or O followed by water based electrolysis. Maximum lift off size to date is 2 mm x 2 mm.

Diamond characterization:
- Development of novel defect characterization techniques.

    1.) Etch delineation of defects by exposure to propane torch flame.
    2.) Hydrogen plasma exposure to enhance secondary electron emission and provide non-topographical defect contrast.

- Detailed correlations between defects in natural and PECVD-grown diamond have been made using plan-view TEM, scanning cathodoluminescence, SEM, electron beam induced current and etch delineation by oxidizing flames.

1.2 Heteronucleation Development

- A variety of carbon sources local to the silicon surface are found to enhance nucleation of diamond growth.

- Thermal desorption studies of oxygenated diamond (100) surfaces reveals that some CO desorbs from the surface a relatively low temperatures, < 300°C, which results in open sites for carbon addition.

- Acetylene will react at room temperature with sites created by partial desorption of oxygen on the (100) diamond surface.

2

- Thermal desorption measurements give an apparent activation energy for CO desorption from diamond (100) of 45 kcal/mol

- Quantum chemical calculations indicate an activation energy of 38 kcal/mol. (Collaboration, M. Frenklach Penn. St. U).

- Ab initio calculations on (100) surfaces indicates that oxygen adsorbed at one dimer site has an effect on the dimerization of an adjacent site. (Collaboration, J. Whitten NCSU).

4

2.0 LARGE AREA SUBSTRATE DEVELOPMENT.

Substantial progress was made in 1993 on development of key areas for large area diamond substrate production via a tiled array of natural diamonds. This section incorporates a more detailed review of published results and a review of recent unpublished work. Following the format of the introduction, three areas of concentration are described: growth studies, ion-implantation for lift off, and characterization of natural diamond and CVD diamond.

2.1 Growth Studies.

Growth experiments during this phase of the project have concentrated on developing reactor conditions, substrate surface preparation techniques and reactor improvements to allow long duration, high quality, homoepitaxial diamond growth. Particularly troublesome has been morphology variations in homoepitaxial films grown on natural diamond substrates which have received only basic cleaning procedures. A variety of acid cleans including chromic/sulfuric, sulfuric/hydrogen peroxide, "RCA" cleans, and aqua regia have been tried to remove residual contaminants and damage from the mechanical polishing process. No clear correlation has been observed between a given cleaning process and the resulting film morphology. To overcome this difficulty and recover a "true" diamond surface, ion-implantation to generate a subsurface or surface graphite layer has been coupled with either an electrochemical etch or one of the above acid etches. Natural diamond crystals subjected to this treatment have shown improved surface morphologies following homoepitaxial growth. This cleaning process also allows recovery of the diar. ⊃nd surface following ion-implantation for lift off. A key component of the tiling process.

Reactor modifications were also implemented during this phase to allow for stable reactor operation during long duration growths. Delivery of the water/alcohol feedstocks was upgraded from a premixed tank fed through a leak valve to separate water and alcohol sources metered through liquid mass flow controllers. The premixed tanks suffered from variations in water/alcohol ratio due to differences in the vapor pressures of the constituents. This was not a problem for short trial growths but is a concern for long duration growths, >10 hours. Process parameters can also be more reproducibly set with the mass flow controllers than with a leak valve. Stability of the discharge was addressed with addition of an optical monitoring and feedback system to maintain the plasma in the inductively coupled mode.

Water alcohol was chosen as the growth chemistry to concentrate development efforts on for several reasons [1,2,3]. The water alcohol process is able to grow diamond at lower

temperatures than traditional hydrogen/methane chemistries. Lower growth temperatures puts fewer demands on the bonding system used to hold the tiled array during consolidation. In addition work has shown that lowering the ionization potential of the feedstock gasses allows one to achieve inductive coupling at lower applied power levels. A clear trend towards lower power and lower temperature growth is observed as one goes from hydrogen to water to acetic acid as the primary hydrogen source.

2.2   Ion-Implantation for Lift Off.

Two lift off processes have been developed involving ion-implantation. A buried damage layer is first created using either C or O implants. Release of the diamond platelet thus created is achieved by either through furnace annealing to graphitize the damage layer [4] or through water based electrolysis. Lift off of 2 mm x 2 mm platelets from type IIa substrates was achieved following both C and O implants. As noted above, process steps have been developed to recover the diamond surface for subsequent homoepitaxial growth. Water based electrolysis was found to have a substantial advantage over furnace annealing to achieve lift off. Much lower doses, 8E15 O^{++}/cm^2 versus 3E17 O^{++}/cm^2 could be used for electrolytic lift off as compared with annealing for lift off. The advantage of such a low dose is that virtually all the near-surface damage can annealed out as revealed by RBS/channeling spectra of annealed and virgin diamonds. We have not yet attempted to lift off platelets from a consolidated array of natural diamonds. This is expected to occur at the beginning of the next phase of the project.

2.3   Characterization of Polycrystalline and Homoepitaxial CVD Diamond.

Semiconductor material destined for electronic applications requires the lowest possible defect and impurity concentrations. A major thrust in the last phase of the program was to develop the tools needed to rapidly assess the quality of the CVD diamond prepared by various growth chemistries. The most detailed microstructural information is provided by transmission electron microscopy. However sample preparation on natural substrates is an arduous task. Ion milling requires on the order of 100 hours of mill time to prepare a sample. Work was done to both improve sample preparation times and to develop new techniques to rapidly assess diamond quality.

In collaboration with JPL a rapid method for thinning single crystal diamonds for transmission electron microscopy was developed [5]. Below band-gap laser ablation was used to thin natural diamond substrates. Thinning was performed in air, using an excimer laser operated at 248 nm (KrF) at a pulse rate of 5 Hz., and with an output energy of 600mJ, at normal and

6

glancing angle (22°) incidence. Glancing incidence provided excellent thin areas for electron microscopy with no post-milling processing necessary. Dramatic reductions in the time necessary to produce a sample were realized, going from approximately 100 hours for argon ion-milling to less than 1 hour with excimer laser milling.

In related work a number of new techniques were developed in this phase to allow assessment of diamond quality. These techniques are rapidly and easily performed, allowing us to determine which samples are worth detailed analysis by transmission electron microscopy. In the first technique the diamond sample is exposed to an oxidizing flame, in this case a propane torch for several seconds [6]. Defects intersecting the surface are selectively etched allowing relatively simple analysis in a scanning electron microscope with no further sample preparation. The second technique exposes natural substrates to a hydrogen plasma for approximately 1 minute [7]. The surface is saturated with hydrogen as a result of the plasma exposure and SEM analysis shows a dramatically enhanced secondary electron yield. The enhanced yield in turns gives rise to non-topographic contrast mechanisms at the surface. The nature and density of the dark areas seen at high magnifications corresponds quite closely with defects observed by the oxidizing flame and by direct observation in transmission electron microscopy [8, 16]. The contrasting areas are therefor thought to arise from defects intersecting the free surface. Both techniques offer the potential for rapid and easy assessment of diamond quality. With these techniques the growth conditions and growth chemistries can be fine tuned to provide high quality diamond homoepitaxial films.

3.0 HETEROEPITAXIAL SUBSTRATE DEVELOPMENT

Work on heteroepitaxial diamond growth progressed in parallel with the tiling development. Studies of heteroepitaxial growth were roughly divided into three areas, substrate engineering via surface modifications of heterosubstrates, detailed experimental studies of surface processes and detailed theoretical studies of surface processes.

3.1 Substrate Modifications for Heteroepitaxy

Growth studies on silicon substrates have shown that a variety of carbon sources when in close proximity to the surface, can considerably enhance nucleation of diamond [11]. Surface pre-treatments of photoresist, sucrose, Teflon, and graphite were tested. A tendency was shown for longer carbon chain species to promote greater nucleation. Of the substances tested, graphite showed the densest nucleation. Graphite has the additional advantage that it can be applied without damage to the surface. The enhanced activity of graphite can be attributed to the slower dissolution rate of graphite in the plasma, as compared to long chain hydrocarbons, carbohydrates, and fluorocarbons.

Based on theoretical studies by J. Whitten of NCSU, nickel samples were implanted with Na. Dr. Whitten's calculations indicate that methyl radicals attached to the nickel surface have a greater barrier to planarization if electropositive species such as Na are located in sites just below the surface. Early results were promising in that dense nucleation was observed in one area of a nickel sample. There were questions however concerning the purity of the nickel surface following the implant process. We have prepared a new set of nickel samples by directly reacting metallic Na with single crystal nickel. This avoids the contamination associated with the implant process and provides a far higher concentration of Na near the surface than can be achieved through ion-implantation. We are currently optimizing a reactor for standard hydrogen/methane growths and we expect nucleation experiments will continue in the early part of the next phase.

3.2 In-situ Surface Studies.

Surface studies in this phase have concentrated on understanding interactions of oxygen with the diamond surface and the role oxygen plays in the growth process. Detailed studies using thermal desorption from oxygenated diamond surfaces have shown that both fully and partially covered surfaces will lose oxygen via CO desorption at temperatures less than 300°C [12]. Analysis of the thermal desorption data indicates an effective activation energy of 45

kcal/mol for CO desorption from the (100) surface. This has been corroborated by MNDO calculations described below which provide a low energy pathway for CO desorption from the surface. Desorption of CO from the (100) surface leaves behind two dangling bonds to carbon atoms. These dangling bonds appear able to react with acetylene at room temperature. This provides a simple mechanism for diamond growth from water alcohol mixtures at relatively low temperatures. EELS studies of both hydrogen and oxygen terminated surfaces have shown that as the surfaces lose the respective adsorbates a new loss feature appears at approximately 5eV from the elastic peak [13]. This peak appears distinct from the 6eV pi-plasmon observed on graphite and rather seems to be related to dangling bonds on the surface.

Ultraviolet photoemission analysis of a hydrogen plasma-treated C(100)-(100) surface has shown the presence of an intense low-energy emission peak which can be extinguished upon exposure to a 20% oxygen/argon plasma or upon high-temperature annealing. The intense low-energy emission feature has been attributed to photo excitation of inelastically scattered electrons into unoccupied H-induced states near the conduction band edge which can escape into the vacuum.

3.3   Modeling of Surface Processes.

Collaborations continued with Prof. J. Whitten (NCSU) and Prof. M. Frenklach (PSU). Both groups have applied analytic techniques to model surface processes on diamond. The collaborations have resulted in stimulation of new avenues of research in both the experimental work and the theoretical work.

Calculations by Prof. Whitten's group of oxygen on the diamond (100) surface have shown that oxygen adsorbed at one dimer site can have an influence on adjacent dimer sites[14]. The influence however is not sufficient to prevent dimerization of the adjacent pair of carbon atoms. Additional oxygen to the surface will result in conversion of the 2 x 1 surface to the 1x1 configuration, but adsorption at adjacent sites is not sufficient to open dimer bonds for carbon addition.

As mentioned above, mechanisms have been modeled for CO desorption from the diamond surface. Calculations by Prof. Frenklach's group indicate a possible desorption pathway for CO from the diamond surface with a value of 38 kcal/mol as the largest barrier in the sequence of steps [15]. This is in quite good agreement with the measured value of 45 kcal/mol described above.

APPENDIX (Referenced Papers)

1. R.A. Rudder, R.E. Thomas, G.C. Hudson, J.B. Posthill, D.P. Malta, R.J. Markunas, *Low Temperature Diamond Growth: Development of Water-Based Techniques for Diamond CVD*, Third Int. Symp. on Diamond Materials (ECS), Hawaii, 1993, p. 372.

2. R.A. Rudder, R.J. Markunas, R.E. Thomas, J.B. Posthill, G.C. Hudson, D.P. Malta, R.C. Hendry, T.P. Humphreys, R.J. Nemanich, *Growth of Diamond Films from Water-Based Chemical Vapor Deposition Systems*, Presentation at the Applied Diamond Conference, Tokyo, August. 1993, p. 139.

3. J.B. Posthill, D.P. Malta, R.A. Rudder, G.C. Hudson, R.E. Thomas, R.J. Markunas, *Homoepitaxial Diamond Layers Grown with Different Gas Mixtures in a rf Plasma Reactor*, to be presented at the Third International Symposium on Diamond Materials (as part of the 183rd Meeting of The Electrochemical Society), Honolulu, Hawaii, May 16-21, 1993, p. 303.

4. N.R. Parikh, J.D. Hunn, E. McGucken, M.L. Swanson, C.W. White, R.A. Rudder, D.P. Malta, J.B. Posthill, and R.J. Markunas, *Single-Crystal Diamond Plate Liftoff Achieved by Ion Implantation and Subsequent Annealing*. Appl. Phys Lett 61, 1992, 3124.

5. T. George, M.C. Foote, R.P. Vasquez, E.P. Fortier, J.B. Posthill, *Below Band-Gap Laser Ablation of Diamond for Transmission Electron Microscopy*, published May 31, 1993, Applied Physics Letter, 62 (22), pages 2880-2882.

6. D.P. Malta, J.B. Posthill, R.A. Rudder, G.C. Hudson, and R.J. Markunas, *Etch-delineation of defects in diamond by exposure to an oxidizing flame*, Published in J. Mater. Res., Vol. 8, No. 6, June, 1993, p. 1217-1219, 1993 Materials Research Society.

7. D.P. Malta, J.B. Posthill, R.E. Thomas, G.G. Fountain, R.A. Rudder, G.C. Hudson, M.J. Mantini, and R.J. Markunas, T.P. Humphreys, NC State University, *Secondary Electron Emission Enhancement and Defect Contrast from Diamond by Exposure to Atomic Hydrogen*, submitted to Applied Physics Letters, Nov. 11, 1993.

8. D.P. Malta, J.B. Posthill, E.A. Fitzgerald, R.A. Rudder, G.C. Hudson, R.J. Markunas, *A Correlative Investigation of Defects in Natural and PECVD-Grown Diamond*, Third Int. Symp. on Diamond Materials (ECS), Hawaii, 1993, p. 647.

11

9. D.P. Malta, E.A. Fitzgerald, J.B. Posthill, R.A. Rudder, G.C. Hudson, R.J. Markunas, *Characterization of Epitaxial Diamond on Natural Diamond Substrates by Cathodoluminescence*, Published by San Francisco Press, Proc. 51st Annual Meeting of the Microscopy Society of America, p. 614-615.

10. T.P. Humphreys, P.K. Baumann, K.F. Turner, R.J. Nemanich, K. Das, R.G. Alley, D.P. Malta, J.B. Posthill, *Growth and Characterization of SiGe Contacts on Semiconducting Diamond Substrates*, published Third Intl. Symp. on Diamond Materials (ECS), Hawaii, 1993, p. 580.

11. R.A. Rudder, G.C. Hudson, J.B. Posthill, R.J. Markunas, *The Effect of Local Carbon Sources on Diamond Nucleation*, abstract submitted to Int. Conf. on Metallurgical Coatings and Thin Films, April 19-23, 1993, San Diego, CA.

12. R.E. Thomas, R.A. Rudder, R.J. Markunas, *Diamond Surface Studies of Growth Mechanisms from Water-Alcohol Deposition Chemistries*, Third Int. Symp. on Diamond Materials (ECS), Hawaii, 1993, p. 71.

13. R.E. Thomas, R.A. Rudder, and R.J. Markunas, *Surface Processes Associated with Diamond Growth from Water Alcohol Deposition Chemistries*. Submitted to Proceedings of IUMRS-ICAM-93, Tokyo, Japan, 1993.

14. J.L. Whitten and Pietro Cremaschi, and R.E. Thomas, R.A. Rudder and R.J. Markunas, *Effects of Oxygen on Surface Reconstruction of Carbon*, published Appl. Surf. Sci. 75, 1993, 45.

15. M. Frenklech and D. Huang, R.E. Thomas, R.A. Rudder and R.J. Markunas, *Activation Energy and Mechanism of CO Desorption from (100) Diamond Surface*, published Applied Physics Letters, 63, 1993, 3090..

16. J.B. Posthill, T. George, D.P. Malta, T.P. Humphreys, R.A. Rudder, G.C. Hudson, R.E. Thomas, and R.J. Markunas, *Electron Microscopy of Natural and Epitaxial Diamond*, published by San Francisco Press Proc. 51st Annual Meeting of the Microscopy Society of America, p. 1196-1197, 1993.

LOW TEMPERATURE DIAMOND GROWTH: DEVELOPMENT OF WATER-BASED TECHNIQUES FOR DIAMOND CVD

R.A. Rudder, R.E. Thomas, G.C. Hudson, J. B. Posthill, D. P. Malta, and R.J. Markunas
Research Triangle Institute, Research Triangle Park, NC 27709

Low temperature diamond deposition techniques have been developed using low-pressure rf-induction plasmas coupled with water-based chemical vapor deposition. Both the low-pressure rf-induction plasma and the water chemistry are critical to the production of diamond films at low temperature (less than 500°C). This work elaborates on the interdependencies between plasma-chemistry and induction coupling at 13.56 MHz. A critical power must be applied to the rf coil to achieve induction coupling. Empirically, we have determined that the power threshold for induction coupling is a strong function of the gas-pressure and the ionization potentials of the source gasses. Low-pressure plasmas containing water-vapor facilitate induction coupling at modest power levels (300 - 500 W). At these levels, induction heating of the sample stage is restricted to low temperatures (less than 500°C), and diamond growth at low temperature can be evaluated.

INTRODUCTION

Recently we have demonstrated, and others have reproduced, chemical vapor diamond deposition from water solutions containing alcohols and organic acids. These techniques have been quite successful in depositing diamond at temperatures well below 500°C. These demonstrations have taken place in low pressure rf induction plasma systems and in low pressure microwave ECR systems.(1-4) Diamond deposition at temperatures below 600°C allows for the application of diamond thin films on materials which can not survive high temperature growth. Our work has concentrated on diamond growth from low pressure rf induction plasmas. These plasmas have shown a great propensity for diamond deposition. Diamond growth from low pressure rf induction plasmas occurs when sufficient power is applied to the rf coils to inductively couple to the plasma gas. Diamond growth below this critical power level proceeds very slowly, if at all. This can be understood by considering the plasma density differences between capacitive coupling and induction coupling. Inductively-coupled discharges have a two-order of magnitude higher plasma density than do capacitively-coupled discharges. Along with inducing currents in the plasma gas, the radiation field from the rf coil also produces eddy currents in the sample and the sample stage. For low temperature diamond deposition, the applied power needs to be reduced in order to avoid substantial substrate heating. We have found that diamond growth can be obtained at lower applied powers 1) if the molecular hydrogen is replaced by alternative sources of atomic hydrogen which have lower ionization potentials and 2) if the operating pressure is reduced.

EXPERIMENTAL APPROACH

These experiments have been conducted in a standard plasma system consisting of a water-cooled 50 mm diam quartz tube surrounded by a 2-turn helical coil. This system has been described in more detail elsewhere. A schematic of the system showing the simple water vapor delivery system is shown in Figure 1. To date, solutions containing water, alcohol, and organic-acids have been connected to the low-pressure rf-plasma system by a leak valve which permits

the composite vapor pressure of the constituents in the solution to be pumped into the plasma system. The proportion of water to alcohol to organic-acid is controlled by the molar concentration in the solution. For extended growths, depletion of the higher vapor pressure component is a concern. But for the work presented here, depletion is not great. The samples are located on a graphite susceptor positioned a few mm removed from the rf coil. The graphite susceptor is not necessary for diamond growth from the water-based solutions. However, its presence actively contributes carbon to the vapor phase by gasification. The graphite susceptor also serves as a sample heater. Circulating currents in the rf will produce eddy currents in the graphite susceptor which resistively heat the susceptor. Consequently, lower applied powers result in lower growth temperatures.

Diamond growth proceeds by admitting gasses into the reactor vessel (maintained at a constant pressure) and by applying sufficient power to the rf coil to inductively couple. Induction-coupling is distinguished by a sudden change in plasma intensity as the applied power is increased. The abrupt change in luminosity is a manifestation of the two-order magnitude increase in the plasma density. This dramatic increase in plasma density results in plasma densities at 13.56 MHz that is comparable to plasma densities in microwave systems ($\sim 10^{12}/cm^3$.)

Induction-coupling via high frequency discharges has been long-studied.(5) At low power, a discharge is initiated inside the rf coil by the electric field which exists due to the potential drop across the length of the coil. Once the plasma initiates, the interior of the plasma is screened from the applied electric field. Thus, electrons in this region do not have sufficient energy to create ionization and sustain the plasma. However, the magnetic field permeates this low density plasma. At 13.56 MHz, the rapidly changing magnetic field produces an induced electric field or electromotive force. Free electrons in the plasma are accelerated by this force. Provided the field strength is high enough or the mean free path to collision is long enough, these electrons can gain sufficient energy to produce impact ionization with neutral molecules or atoms in the gas. Once this occurs, a rapid increase in plasma density follows as free electrons in the plasma (previously not contributing to plasma-ionization) promote electron-impact ionization. Thus, induction coupling proceeds when the product of induced electric field strength and the mean free path for electron-neutral collision is greater than the ionization potential of the gas.

EXPERIMENTAL RESULTS

Empirically, we have found that the critical power level necessary to inductively couple and, in turn, the critical power necessary for diamond growth, falls as one introduces gasses with lower ionization potentials. Furthermore, we have observed that the critical power level is a strong function of the growth pressure. Figure 2 shows the critical power that is necessary to inductively couple as a function of pressure for pure water discharges and for pure hydrogen discharges. At low pressure, there is not a pronounced difference. However, at more typical growth pressures (above 1 Torr), the water discharges require considerably lower power input than does the molecular H_2.

While water/alcohol discharges require considerably less power than the molecular hydrogen discharges to achieve induction coupling, addition of acetic acid to the water solution allows diamond growth at even lower input power. As a consequence, the addition of acetic acid allows diamond growth to proceed at very low temperatures, perhaps as low as 250° C. Figure 3 shows SEM micrographs from a sample deposited using vapors from an acetic-acid:methanol:water solution. The input power to the rf coil was ~ 500 W. For the limited deposition time, a continuous film was not obtained. Discrete diamond particles were produced. The diamond particles grew in a very anisotropic fashion. Micro-Raman from these crystals

shows (Figure 3) these crystals to have a very narrow FWHM of 2.9 cm^{-1} with negligible amorphous carbon or graphitic component.

Recently, acetic-acid solutions have produced at low temperature ($\_$ 500°C) a continuous film which also displays highly anisotropic grain growth. It also had a fairly narrow Raman FWHM of 5.0 cm^{-1}, but exhibited a broad band around 1500 cm^{-1}, perhaps originating from material in the grains.

DISCUSSION

In considering the low-temperature growth of diamond, the propensity for diamond deposition at low temperatures from the water-based solutions is consistent with the work of others who using H_2-based microwave plasmas have been able to reduce substrate temperatures required for diamond growth through O_2 or H_2O addition.(6-8) The role of oxygen on the diamond growth surface must be critical to low temperature growth. Surface chemistry studies by Thomas et. al. have provided considerable insight.(9-10) Oxygen on the diamond surface behaves quite different from hydrogen on the diamond surface. On diamond (100), oxygen eliminates surface dimerization; it desorbs as CO at temperatures far lower than hydrogen which desorbs as H_2; and it serves to stabilize the (1 × 1) bulk surface termination. Of particular importance to this work is the extremely low-temperature desorption (onset at 200 - 300°C, peak at 550°C) and the desorption product CO. It is speculated that, in diamond growth using the water chemistry, water contributes O to the diamond surface. As a consequence sites become available on the growth surface at low temperature through CO desorption. These open sites are sites for radical addition and hence growth propagates. If this mechanism accounts for the low temperature growth phenomena with oxygen present than at least C_2 species must be contributing to the growth. CO desorption removing one carbon atom must be followed by insertion of at least a C_2 species in order for the diamond crystal to grow.

It is certainly encouraging that high quality material can be produced at relatively low temperatures. Preliminary experiments have been undertaken to determine a low temperature limit to the process by actively cooling the sample stage. These experiments indicate that the low temperature limit to the acetic-acid water-based diamond deposition process appears to be between 200°C and 250°C. The quality of the diamond, once again, does not appear to degrade as the temperatures is reduced below 300°C. However, at 200°C, no carbon deposition occurred. It is yet to be determined if this result is a consequence of a nucleation problem or a deposition problem.

SUMMARY

Low temperature diamond growth has been facilitated using low-pressure rf-induction plasmas and water-based chemistries. In order to study low-temperature growth in the rf-induction plasma system, the critical power necessary to achieve induction coupling had to be reduced. Low pressure operation as well as the inclusion of low ionization potential gasses (H_2O, CH_3COOH) enabled these experiments. Our results indicate that high quality diamond particles and continuous films can be produced at low temperatures (250 - 450° C). At the present time, diamond deposition appears restricted to temperatures above 200°C. The low temperature limit is consistent with oxygen desorption data showing the onset of CO desorption around 250°C.

ACKNOWLEDGEMENTS

REFERENCES

1) R. A. Rudder, G. C. Hudson, J. B. Posthill, R. E. Thomas, R. C. Hendry, D. P. Malta, R. J. Markunas, T. P. Humphreys, and R. J. Nemanich, Appl. Phys. Lett., 60, 329 (1992).

2) R. A. Rudder, J. B. Posthill, G. C. Hudson, D. P. Malta, R. E. Thomas, R. J. Markunas, T. P. Humphreys, and R. J. Nemanich, Mater. Res. Soc. Symp. Proc., 242, 23 (1992).

3) R. K. Singh, D. Gilbert, R. Tellshow, R. Koba, R. Ochoa, J. H. Simmons, P. H. Holloway, J. Rodgers, and K. Buckle, Mater. Res. Soc. Symp. Proc., 31 (1992).

4) Shu Jin and T. D. Moustakas, Diamond 1992 Abstract ff 8.69. August 31 - September 4, 1992, Heidelberg, Germany.

5) K. Z. Mackinnon, Philus. Mag. 8, 605 (1929).

6) Y. Liou, A. Inspektor, R. Weimer, D. Knight, and R. Messier, J. Mat. Res. 5, 2305 (1990)

7) Y. Saito, K. Sato, K. Gomi and H. Miyaderu, J. Mat. Sci. 25, 1246 (1990)

8) Y. Saito, K. Sato, H. Tanaka, K. Fujita, and S. Matuda, J. Mat. Sci. 23, 842 (1988).

9) R. E. Thomas, R. A. Rudder, R. J. Markunas, J. Vac. Sci. Tech., A 10(4), Jul/Aug 1992, 2451 - 2457.

10) R. E. Thomas, R. A. Rudder, R. J. Markunas, Diamon Surface Studies of Growth Mechanisms from Water-Alcohol Deposition Chemistries, submitted to Third Int. Symp. on Diamond Materials (ECS), Hawaii, 1993.
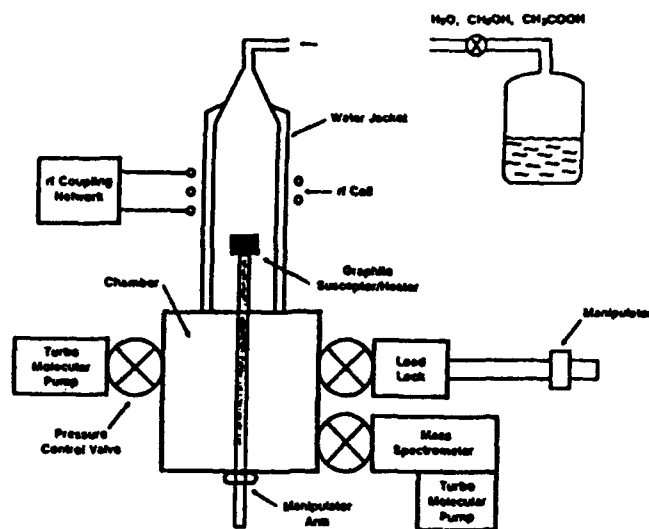
Figure 1.   Schematic of low-pressure rf-plasma assisted chemical vapor deposition system
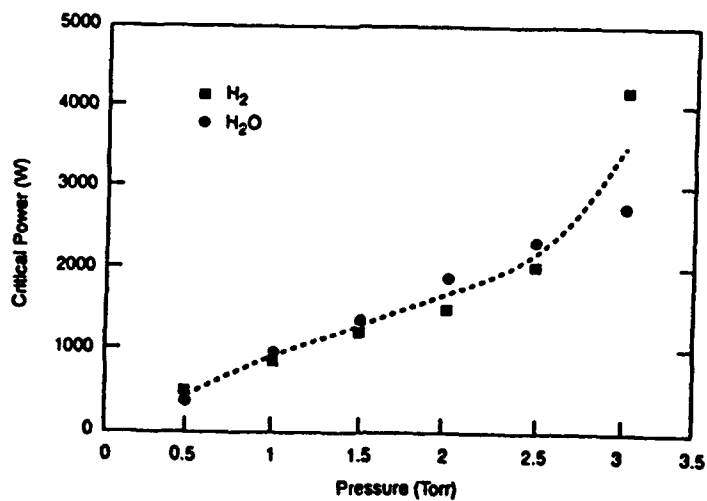

Figure 2.   Dependence of critical power necessary to inductively-couple as a function of reactant choice (H_2O or H_2) and as a function of pressure.
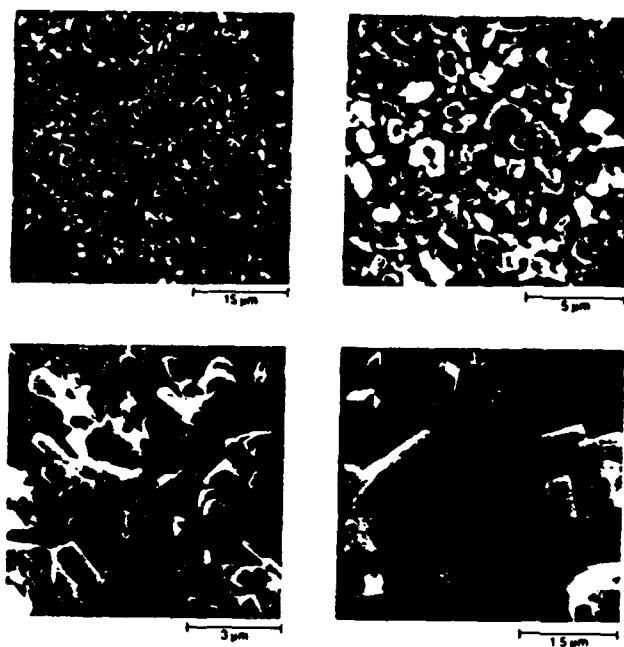
Figure 3. SEM micrographs of diamonds deposited at 250°C.

GROWTH OF DIA`.!OND FILMS FROM WATER-BASED CHEMICAL VAPOR DEPOSITION SYSTEMS

R.A. Rudder[1], R.J. Markunas[1], R.E. Thomas[1], J.B. Posthill[1], G.C. Hudson[1], D.P. Malta[1]
R.C. Hendry[1,] T.P. Humphreys[2], and R.J. Nemanich[2]

[1]Research Triangle Institute, Research Triangle Park, NC 27709 U.S.A.

[2]Department of Physics, North Carolina State University, Raleigh, NC 27695 U.S.A.

Abstract

Diamond research has clearly demonstrated that high quality diamond films can be produced from a variety of chemical vapor deposition systems using a wide variety of source gasses. Unfortunately, the high costs involved in the production (capital, labor, gas, electricity, etc.) have precluded widespread commercialization of diamond products. Research must target development of chemical and physical systems wherein diamond can be produced at reduced cost. This paper reports on the chemical vapor deposition of diamond films using vapors from water-based solutions. Application of water-based solutions for the growth of diamond will dramatically reduce the process gas cost. In addition, growth rates obtained in low pressure rf- induction plasmas using water-based feedstocks are comparable to those obtained using hydrogen-methane feedstocks. It is thus anticipated that the water-based solutions will incur no higher energy costs than the traditional hydrogen-based methods.

1.0 INTRODUCTION

Chemical vapor deposition has been widely used for the production of diamond films.[1 - 10] The majority of diamond film production has occurred from gasses residing in the C-H-O system. P. K. Bachmann has derived an empirical diagram to predict the relative atomic fraction of C,H, and O required for diamond growth.[8] This diagram permits one to rapidly converge on parameters suitable for diamond growth. Workers interested in cost reduction are then free to investigate a great variety of feedstocks provided that the relative mixture of feedstock gasses can be adjusted to produce diamond growth. In comparison to the traditional hydrogen-based processing, workers can now choose gasses which are relatively inexpensive in comparison to hydrogen-methane, which impose fewer fire and explosion hazards, and which are readily ionizable thereby facilitating easy power coupling from the electromagnetic applicator to the plasma gas. In short, one has tremendous flexibility in the selection of starting materials.

This paper compares the growth of diamond from water-based feedstocks to the growth of diamond from hydrogen-based feedstocks. Vapors from water-based solutions

have a number of distinct advantages which should simplify the manufacturing tool. Vapors from water-based solutions 1) have lower ionization potentials than hydrogen-methane, 2) have bond strengths comparable to hydrogen-methane, 3) evaporate from subatmospheric liquid sources, and 4) are quite inexpensive compared to hydrogen-methane.

We have compared the growth of diamond from both chemical systems in a low-pressure rf induction plasma deposition system that is quite proficient in diamond growth. We have found no technical reason to preclude the water-based solutions as a diamond manufacturing technology. Indeed, our results indicate that water-based feedstocks would be comparable to traditional hydrogen-based feedstocks and not impose the hazards and safety controls demanded for the storage and handling of copious amounts of hydrogen.

2.0 EXPERIMENTAL METHOD

The low pressure rf-induction plasma system used in this work consists of a 2 1/2 turn copper coil surrounding a 50 mm diameter quartz tube. [11-16] The sample rests in the CVD chamber on a graphite susceptor isolated from ground underneath the rf coil. All samples were abraded with 1 μm diamond paste prior to introduction into the reactor. H_2-CH_4 gasses are metered into the system through mass flow controllers connected to high-pressure cylinders. Water:alcohol vapors are metered in the system through a leak valve connected to a room-tempature liquid reservoir. In this work, the liquids are held in a common reservoir, and the proportion of water to alcohol is dictated by the molar concentration in the liquid. The process pressure is controlled by an automatic butterfly valve. Sufficient power is applied to the coil to insure induction coupling (i.e. currents in the rf coil induce currents in the plasma gas). The onset of induction coupling is manifest through an abrupt intensity change in the plasma luminosity.[17]

With H_2-CH_4, the abrupt intensity change is also accompanied by a distinct change in the visible color of the plasma. Prior to achieving induction coupling, emissions through the H_2-CH_4 plasma have a characteristic blue color originating from an anti-bonding molecular hydrogen continuum. Upon achieving induction coupling, the emission has a characteristic red color dominated by atomic H emission at 656 nm. For diamond growth in this system, it is critical that induction coupling be achieved. For water-based solutions, the abrupt intensity change concomitant with achieving induction coupling does not produce a distinct change in the visible color of the plasma. However, spectral analysis of the emission from the water-based solutions does show intense atomic H emission once inductive coupling has been realized. Prior to inductive coupling, OH emissions dominate the spectrum.

The propensity for this system to produce diamond from both H_2-based and water-based systems permits one to use this system to compare and contrast processing conditions necessary for diamond growth. It is speculated that differences discovered between hydrogen-based and water-based feedstocks in the low pressure rf induction

plasma system will be similar to differences that might be experienced in other plasma systems producing diamond.

3.0 EXPERIMENTAL RESULTS

The great variety of hydrocarbons that can be mixed with either the hydrogen-based or water-based feedstocks permits enormous lattitude in the choice of hydrocarbon. For the purposes of comparing a hydrogen-base process to a water-base process, we chose a H_2-CH_4-H_2O mixture which used a small amount of water (3%). Water addition improves the crystalline quality of crystals deposited from H_2-CH_4 system. From the water-based feedstocks, we chose the H_2O-CH_4O family. Water and methanol are miscible and thus can be stored in solution with vapors above the liquid serving as the gas feedstock to the CVD system. H_2O-CH_4O represents the simplest of the water-alcohol systems. Correspondingly, H_2-CH_4 represents the simplest of the hydrogen-hydrocarbon system.

3.1 H_2-CH_4 (H_2O-minor) Growth

Shown below in Table I are growth conditions typical for diamond deposition from both hydrogen and water-based chemistries. As previously noted, the hydrogen-based results depicted here use H_2-CH_4 along with a small amount of water. Growth at higher pressures from this mixture is certainly possible but requires even higher input rf power to achieve induction coupling. Growth at lower pressures is possible, but the nucleation density and quality suffer. Figure 1 shows SEM micrographs from the H_2-CH_4 growth depicted in Table 1. One can see that the diamonds are well-faceted and reminiscent of polycrystalline diamond deposited by other techniques. A cleaved cross-sectioned view such as the one that is shown in Figure 1c shows the deposition rate under these conditions to be 0.4 μm/hr.

Table I
A comparison of hydrogen and water chemistries.

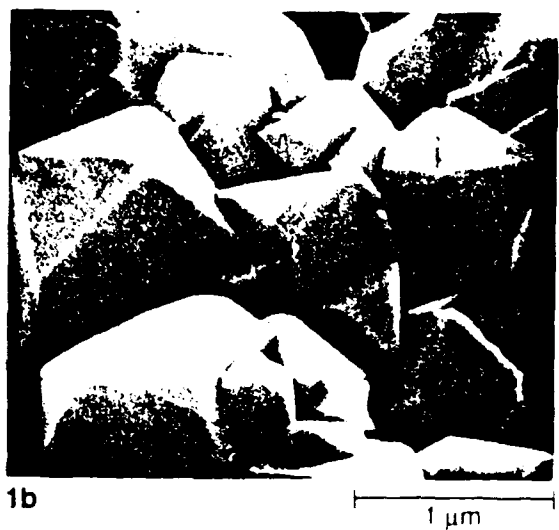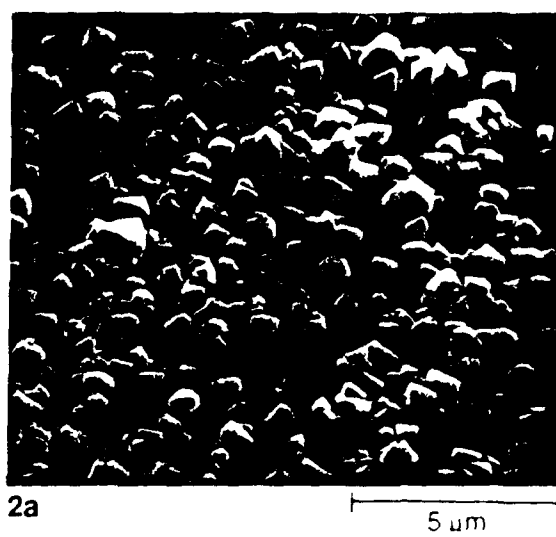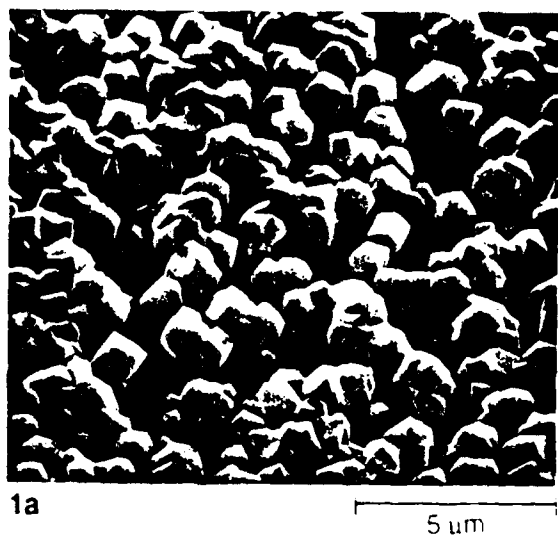|	H_2-CH_4-H_2O	H_2O-CH_4O
Gas Phase Concentrations (%)	95:02:03	27:73
Pressure (Torr)	5.0	1.0
rf Power (W)	2100	1300
Temperature (°C)	850	600
Deposition rate (μm/hr)	0.40	0.25
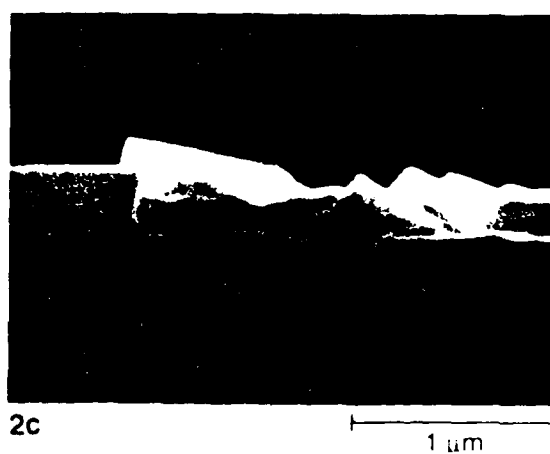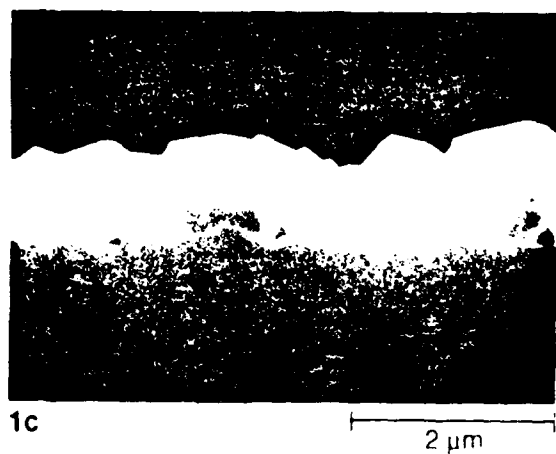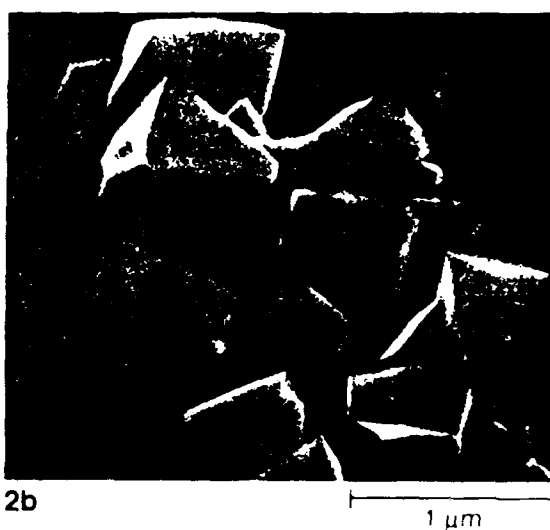
Figure 1. SEM micrographs of diamond
grown from H_2-CH_4-H_2O

Figure 2. SEM micrographs of diamond
grown from H_2O - CH_4O

3.2 H_2O-CH_4O Growth

Also shown in Table I are growth conditions that we have employed for diamond deposition from the water-based chemistry. The water-based processes routinely operates at pressures lower than the 5 Torr used for the H_2-CH_4 chemistry. Figure 2 shows SEM micrographs from H_2O-CH_4O growth at 1.0 Torr. At lower pressures, the input power required to achieve induction-coupling is less. Consequently, the graphite susceptor containing the substrate is maintained at a lower temperature. The micrographs show well-faceted diamond growth. The high concentration of water in the reactor promotes aggressive etching of the crystallites. Like the H_2-CH_4 growth, the crystallite faces show little if any secondary nucleation and growth. A cleaved cross-sectional view such as the one that is shown in Figure 2c shows the deposition rate for the water-based conditions depicted in Table I to be 0.25 μm/hr.

4.0 CONCLUSIONS

Diamond has been produced using the water-based process at comparable growth rates and quality to the traditional H_2 - CH_4 process. The water-based process shows nearly comparable diamond growth at lower pressures (implying a higher carbon yield), at low input power (implying reduced power costs) and at lower temperatures (permitting the application of diamond to more materials). Our work to date has not shown any significant disadvantage to the water-based process. While this paper does not show the results, the water-based process has also been successfully used for homoepitaxial growth on natural stones.[10] Future work will concentrate on process control and refinement to enable high quality thick film diamond production.

ACKNOWLEDGMENTS

REFFRENCES

1. B. Derjaguin and V. Fedoseev, Rus. Chem. Rev., **39** (1970) 783.
2. B. V. Spitsyn, L. L. Bouilov and B. V. Derjaguin, J. Cryst. Growth, **52** (1981) 219.
3. S. Matsumoto, Y. Sato, M. Kamo and N. Setaka, Jpn. J. Appl. Phys., **21** (1982) 183.
4. Y. Hirose and Y. Teresawa, Jpn. J. Appl. Phys., **25** (1986) L51.
5. M. Kamo, Y. Sato, S. Matsumoto and N. Setaka, J. Cryst. Growth, **62** (1983) 642.
6. L. M. Hanssen, W. A. Carrington, J. E. Butler and K. A. Snail, Mater. Lett., **7** (1988) 289.
7. G. Janssen, W. J. P. Van Enckevort, J. J. D. Schaminee, W. Vollenberg, L. J. Giling and M. Seal, J. Cryst. Growth, **104** (1990) 752.
8. Peter K. Bachmann, Dieter Leers and Hans Lydtin, Diamond Relat. Mater., **1** (1991) 1.

9.   M. Buck, T. J. Chuang, J. H. Kaufman and H. Seki, Mater. Res. Soc. Symp. Proc., **162** (1990) 97.

10.   R. Beckmann, W. Kulisch, H. J. Frenck and R. Kassing, Applications of Diamond Films and Related Materials, Mater. Sci. Monograph, **73** (1991) 543.

11.   R. A. Rudder, G. C. Hudson, Y. M. LeGrice, M. J. Mantini, J. B. Posthill, R. J. Nemanich and R. J. Markunas, MRS Extended Abstracts **EA19**, (1989) 89.

12.   R. A. Rudder, G. C. Hudson, R. C. Hendry, R. E. Thomas, J. B. Posthill and R. J. Markunas, Applications of Diamond Films and Related Materials, Mater. Sci. Monograph, **73** (1991) 583.

13.   R. A. Rudder, G. C. Hudson, J. B. Posthill, R. E. Thomas, R. J. Markunas, R. J. Nemanich, Y. M. LeGrice and T. P. Humphreys. Electrochem. Soc. Proc. **Vol. 91-8**, (1991), 209 - 216.

14.   R. A. Rudder, G. C. Hudson, J. B. Posthill, R. E. Thomas and R. J. Markunas, Appl. Phys. Lett., **59** (1991) 791.

15.   R. A. Rudder, G. C. Hudson, R. C. Hendry, R. E. Thomas, J. B. Posthill and R. J. Markunas, Applications of Diamond Films and Related Materials, Mater. Sci. Monograph, **73** (1991) 395.

16.   R. A. Rudder, G. C. Hudson, J. B. Posthill, R. E. Thomas, R. C. Hendry, D. P. Malta, R. J. Markunas, T. P. Humphreys and R. J. Nemanich,. Appl. Phys. Lett., **60** (1992) 329.

17.   J. Amorim, H. S. Maciel and J. P. Sudano, J. Vac. Sci. Technol. **B, 9** (1991) 362.

18.   J. B. Posthill, T. George, D.P. Miller, T.P. Humphreys, R.A. Rudder, G.G. Hudson, R. E. Thomas, and R. J. Markunes, ""Electron, Microscopy of Natural and Epitaxial Diamond", Proc. of the Microscopy Soc. of America, 1993, in press.

HOMOEPITAXIAL DIAMOND LAYERS GROWN WITH DIFFERENT GAS MIXTURES IN AN RF PLASMA REACTOR

J.B. Posthill, D.P. Malta, R.A. Rudder, G.C. Hudson, R.E. Thomas, and R.J. Markunas
Research Triangle Institute, Research Triangle Park, North Carolina 27709-2194

T.P. Humphreys and R.J. Nemanich
Department of Physics, North Carolina State University
Raleigh, North Carolina 27695-8202

Homoepitaxial diamond films have been grown using rf-driven plasma-enhanced chemical vapor deposition. Certain CH_4/H_2 chemistries are shown to be inadequate for extended deposition times; the addition of an oxygen-containing species being required to maintain smooth topography. CO and H_2O additions were found to be beneficial for CH_4/H_2-based gas mixtures. Elimination of the methane completely and using water/alcohol mixtures exclusively was found to yield excellent results with respect to surface topography, minimal impurity introduction and defect density.

INTRODUCTION

The thermal and electrical properties of diamond make it an excellent candidate for electronic applications in extreme environments, but significant device development in this materials system cannot take place unless larger area single crystals are available. While significant progress has been made towards increasing the areal size of diamond crystals by different means [e.g. 1,2], it is also recognized that a reliable and inexpensive method of growing high-quality epitaxial diamond will be necessary to grow device structures and to increase the thickness of diamond crystals and films. To this end, we have examined the effect of gas phase chemistry on the homoepitaxial growth of diamond on natural diamond single crystals. This paper outlines some of these results obtained in an rf-driven plasma-enhanced chemical vapor deposition (PECVD) reactor.

EXPERIMENTAL PROCEDURES

The substrates used in this study were nominally (100) oriented [± 3°] natural type Ia diamonds. It has been established previously by both X-ray topography and ion channeling studies that type Ia substrates are crystallographically superior [3], and it is believed that this would result in improved diamond homoepitaxial films. Transmission electron microscopy (TEM) of a type Ia diamond showed the expected presence of nitrogen-containing platelets lying on {100}-type planes (Fig. 1). However, no dislocations could be seen in the field of view, hence the dislocation density is $< 10^5$ cm^{-2}. This contrasts with substantially larger dislocation densities observed in type IIb substrates [4]. Prior to loading into the reactor, the standard substrate preparation

involved swabbing in deionized water and blow drying with clean nitrogen. Swabbing has been shown to remove particles from the diamond surface, thereby minimizing the sporadic regions of polycrystallinity that are thought to be caused by this contamination [3]. One other diamond substrate preparation method is also described herein and compared with our standard preparation.

The system used for the growth of homoepitaxial diamond consists of a 13.56 MHz inductively-coupled plasma-enhanced chemical vapor deposition (PECVD) system. The sample is positioned near the rf coil on a graphite susceptor, and the growth temperature was achieved by a combination of rf inductive coupling to the susceptor and additional heating from an independently driven radiative source beneath the susceptor. A variety of different gas mixtures have been used for diamond growth. In addition to conventional CH_4/H_2 mixtures, we have also explored oxygen-containing mixtures which utilized combinations of CO, CH_4, and H_2. Recently, polycrystalline diamond has been grown using water/alcohol and water/alcohol/organic acid mixtures [5,6]. This new method of CVD diamond growth using inexpensive liquids has been extended to homoepitaxial diamond growth in this study.

RESULTS

CH_4/H_2 and $CH_4/CO/H_2$ Chemistries

Fig. 2 shows an SEM micrograph taken from an epitaxial film grown on a (100) substrate with a 0.33%CH_4/99.67%H_2 mixture at a pressure of 5 Torr and temperature of ~ 900°C for 6 hours. An extensively "shingled" morphology is evident. The surface topography has been roughened, not planarized, by this process. These results were unexpected. Micro-Raman spectroscopy taken from the near-surface region of this sample was not found to be severely degraded; the full-width at half-maximum (FWHM) of the diamond LO phonon line at 1332 cm^{-1} was measured to be 2.8 cm^{-1}. To observe the transition from the polished as-received surfaces to this rough "shingled" morphology, an epitaxial growth was performed for a slightly longer duration, but by interrupting the deposition at 1 hour, 3 hours, and 6.5 hours. Figures 3a, 3b, and 3c show SEM micrographs from these epitaxial layers. The topography after the 6.5 hour interrupted growth was distinctly smoother than the "shingled" topography observed previously for the uninterrupted 6 hour growth using CH_4/H_2 chemistry.

The interruption and exposure to room ambient proved beneficial. We suspected that the graphite susceptor above transfer into the room ambient absorbed considerable water vapor. Upon reintroduction into the vacuum environment of the deposition system and upon heating, the susceptor would desorb the water into the system. Water vapor released from the heated susceptor would be adsorbed onto the nearby water-cooled quartz walls. Water vapor would be slowly released from the quartz walls resulting in the system having a prolonged memory for water and thereby a significant oxygen source at the beginning of each run; lasting for some amount of time before depleting.

To begin to address this hypothesis, feedstock gases containing oxygen were deliberately introduced for extended homoepitaxial growths. Figure 4 shows a SEM micrograph from a diamond deposition using 1.14%CO/0.43%CH$_4$/98.43%H$_2$, uninterrupted for 6.5 hours. The surface topography appears nearly identical to the SEM micrograph from the 6.5 hour interrupted growth using 0.33% CH$_4$ in H$_2$. Oxygen addition in the form of CO or H$_2$O (see below) is beneficial to the growth of smooth (100) homoepitaxy.

CH$_3$OH/H$_2$O Chemistries

Fig. 5 shows the surface of a (100) homoepitaxial film grown by introducing the vapor pressure of a 30%CH$_3$OH/70%H$_2$O liquid mixture at P = 1 Torr and T ≅ 500°C for 50 minutes. The diamond epilayer shows no roughness. It was then ion milled from the back-side for plan-view TEM examination. Fig. 6 shows the dislocations observed by TEM in the film. The average dislocation density was found to be ~ 5 × 10^6 cm^{-2}, and no other types of defects were observed. This dislocation density would be considered high by single crystal Si standards, but it does represent the current benchmark for diamond epitaxy. We are certain we are observing the epilayer because of the absence of nitrogen-containing platelets. Micro-Raman spectroscopy results were obtained from this back-thinned TEM sample. Spectra acquired from the region near the center, where the epitaxial film is expected to dominate the signal, yielded a FWHM of 2.7 cm^{-1} for the 1332 cm^{-1} LO phonon mode. This contrasts with the slightly improved FWHM of 2.5 cm^{-1} observed from the edge of the sample, which would be dominated by the bulk type Ia natural single crystal substrate. These results show that growth of homoepitaxial diamond can be achieved on natural type Ia diamond to a reasonable standard. In other words, the presence of the nitrogen-containing platelets in the substrate does not result in catastrophic dislocation densities in the diamond epilayer, nor in a severely broadened Raman diamond line width.

Perhaps the most remarkable aspect of the water/methanol-grown diamond films is the measured concentrations for some of the common (and potentially detrimental) elemental impurities. Secondary ion mass spectrometry (SIMS) depth profiling on another homoepitaxial film grown in a similar manner (33.3%CH$_3$OH/66.7%H$_2$O, 1 Torr, T ≅ 500°C) showed that Si, B, and N were at measured instrumental background, while H and O were measured to be 2 × 10^{18} cm^{-3} and 2 × 10^{18} cm^{-3}, respectively. All these values are lower than we have observed in any of our high-temperature-grown homoepitaxial diamond films to date. No special distillation/purification was performed to the liquid reagents to achieve this result. It appears that water/alcohol mixtures can be used where a low temperature diamond epitaxial process is desired or required.

Substrate Preparation

Although discussed briefly earlier [3], the issue of properly preparing a diamond single crystal substrate for CVD growth is still important. This was illustrated by

growing an epitaxial film on two diamond (100) substrates, which were prepared differently, in the same run. One substrate was only given an ethanol/water swab and blown dry, whereas the other substrate was additionally subjected to an ethanol/water pressurized jet before being blown dry. SEM after cleaning looked very similar and featureless, and few particulates were observed on either sample (Fig. 7). A subsequent 2-hour epitaxial growth on both using a 1.5%CH_4/98.5%H_2 mixture with H_2O added continuously to the process showed a considerable difference in the resulting morphology (Fig. 8). While the standard preparation yielded a relatively smooth topography, the ethanol/water-jet-prepared sample showed large (~10 μm) pyramidal hillocks and smaller nodules of apparent polycrystallinity. These features have been observed by other researchers that have grown homoepitaxial diamond on (100) single crystals [7,8]. The precise origin of the detrimental features seen in this study is currently unknown, but appears to result from contamination introduced by applying the ethanol/water jet.

DISCUSSION AND SUMMARY

The epitaxy of diamond can be severely effected by the gas chemistries, other reactor variables, and the nature of the substrate surface upon which homoepitaxial diamond nucleation is to occur. In particular, we have found that the introduction of oxygen via CO or H_2O into a CH_4/H_2-based chemistry is highly desirable to maintain a topographically smooth epitaxial film. It should be mentioned that earlier results with CO/H_2 plasmas showed extensive incorporation of Si into polycrystalline diamond films [8], thereby raising suspicion with regards to CO introduction. Although we do not have sufficient data to currently recommend H_2O introduction into a CH_4/H_2-based diamond growth chemistry as a solution to the Si incorporation problem, we find the SIMS results from the CH_3OH/H_2O diamond growth encouraging. One epitaxial film grown with this chemistry also showed the lowest dislocation density reported to date for a diamond epitaxial film. Future work in this area will focus on diamond substrate preparation.

ACKNOWLEDGMENT

REFERENCES

1.   M.W. Geis, H.I. Smith, A. Argoita, J. Angus, G.-H.M. Ma, J.T. Glass, J. Butler, C.J. Robinson, and R. Pryor, *Appl. Phys. Lett.*, **58**, 2485 (1991).

2.   B.P. Siener and J.T. Glass, *Appl. Phys. Lett.*, **60**, 698 (1992).

3.   J.B. Posthill, R.A. Rudder, G.C. Hudson, D.P. Malta, G.G. Fountain, R.E. Thomas, R.J. Markunas, T.P. Humphreys, R.J. Nemanich, and D.R. Black, *Proc. of the 2nd Intl. Symp. on Diamond Materials*, 91-8, [The Electrochemical Society], 274 (1991).

4.   D.P. Malta, J.B. Posthill, E.A. Fitzgerald, R.A. Rudder, G.C. Hudson, and R.J. Markunas, [this proceedings].

5.   R.A. Rudder, G.C. Hudson, J.B. Posthill, R.E. Thomas, R.C. Hendry, D.P. Malta, R.J. Markunas, T.P. Humphreys and R.J. Nemanich, *Appl. Phys. Lett.*, **60**, 329 (1992).

6.   R.A. Rudder, J.B. Posthill, G.C. Hudson, D.P. Malta, R.E. Thomas, R.J. Markunas, T.P. Humphreys and R.J. Nemanich, *Mater. Res. Soc. Symp. Proc.*, **242**, 23 (1992).

7.   W.J.P. van Enckevort, G. Janssen, W. Vollenberg, M. Chermin, L.J. Giling, and M. Seal, *Surf. and Coating Tech.*, **47**, 39 (1991).

8.   M. Kamo, H. Yurimoto and Y. Sato, *Appl. Surf. Sci.*, **33 - 34**, 553 (1988).

9.   R.J. Graham, J.B. Posthill, R.A. Rudder, and R.J. Markunas, *Appl. Phys. Lett.*, **59**, 2463 (1991).
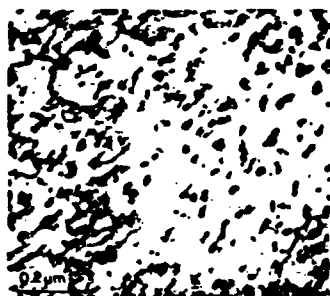
Fig. 1. TEM of natural type Ia diamond substrate showing ~50 nm diameter nitrogen platelets on {100}-type planes. No dislocations were observed.
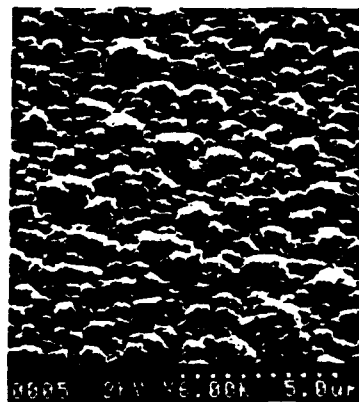

Fig. 2. SEM of 0.33%CH$_4$/99.67%H$_2$ homoepitaxial (100) diamond after 6 hours.
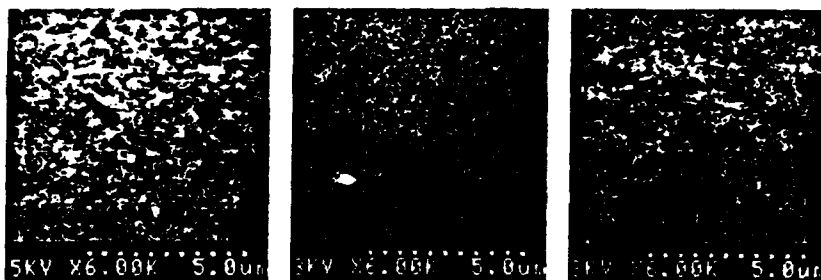
Fig. 3 SEM of 0.33%CH₄/99.67%H₂ "interrupted" homoepitaxial (100) diamond.
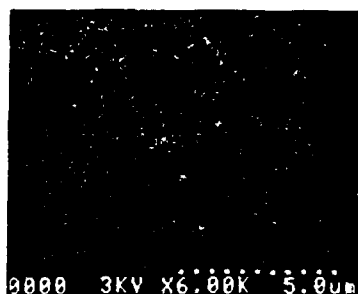After: (a) 1 hour, (b) 3 hours, and (c) 6.5 hours.

Fig. 4 SEM of 1.14%CO/0.43%CH₄/
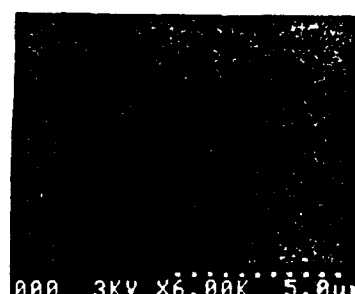98.43%H₂ homoepitaxial (100)
diamond after 6.5 hours.

Fig. 5. SEM of 30%CH₃OH/70%H₂O
(100) homoepitaxial diamond
after 50 minutes.

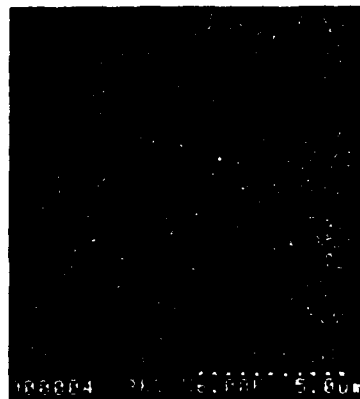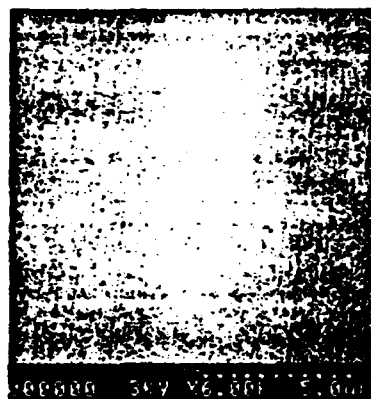Fig. 6. Plan-view TEM of 30%CH₃OH/70%H₂O homoepitaxial (100) diamond.

Fig. 7. SEM of diamond (100) substrates after: (a) ethanol/water swab and blow dry and (b) ethanol/water swab, ethanol/water jet, and blow dry.
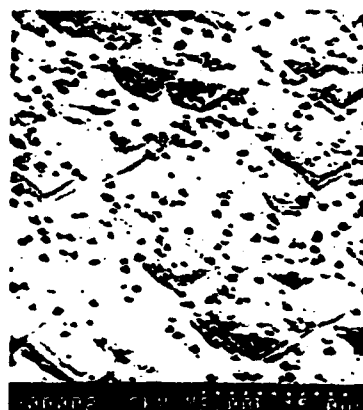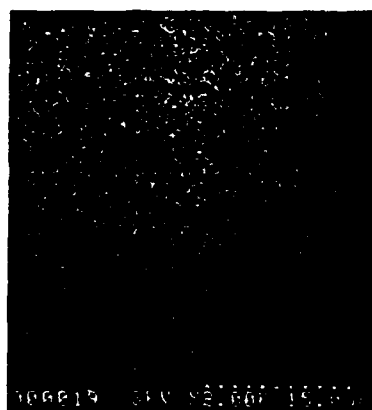

Fig. 8. SEM from same substrates after diamond homoepitaxy using 1.5%CH$_4$/98.5%H$_2$ with H$_2$O addition for 2 hours; (a) ethanol/water swab and blow dry and (b) ethanol/water swab, ethanol/water jet, and blow dry.

Single-crystal diamond plate liftoff achieved by ion implantation and subsequent annealing

N. R. Parikh, J. D. Hunn, E. McGucken, and M. L. Swanson
University of North Carolina, Chapel Hill, North Carolina 27599-3255

C. W. White
Oak Ridge National Laboratory, Oak Ridge, Tennessee 37831-6048

R. A. Rudder, D. P. Malta, J. B. Posthill, and R. J. Markunas
Research Triangle Institute, Research Triangle Park, North Carolina 27709-2194

We describe a new method for removing thin, large area sheets of diamond from bulk or homoepitaxial diamond crystals. This method consists of an ion implantation step, followed by a selective etching procedure. High energy (4–5 MeV) implantation of carbon or oxygen ions creates a well-defined layer of damaged diamond that is buried at a controlled depth below the surface. For C implantations, this layer is graphitized by annealing in vacuum, and then etched in either an acid solution, or by heating at 550–600 °C in oxygen. This process successfully lifts off the diamond plate above the graphite layer. For O implantations of a suitable dose (3×10^{17} cm^{-2} or greater), the liftoff is achieved by annealing in vacuum or flowing oxygen. In this case, the O required for etching of the graphitic layer is also supplied internally by the implantation. This liftoff method, combined with well-established homoepitaxial growth processes, has considerable potential for the fabrication of large area single crystalline diamond sheets.

An essential hurdle yet to be cleared, before one can fabricate diamond electronic devices, is the creation of large area, flat, single crystalline diamond layers. A very promising beginning has been made by Pryor et al.,[1] who have shown that homoepitaxial diamond layers can be grown by chemical vapor deposition onto a matrix of oriented diamond microcrystallites, which are imbedded in an array of etch pits on a Si substrate. However, this method is both costly and time-consuming, and the crystallites are only poorly oriented, thus causing low angle grain boundaries. We propose to combine homoepitaxial growth with liftoff technology to permit large area diamond sheets to be economically fabricated from a master template. For example, such diamond films could be fabricated by tiling together several small diamond crystals on which one then deposits a single crystalline layer; and then removing thin sheets of single crystalline diamond from the surface using a liftoff process. In this way, a large diamond template could be fabricated, from which large diamond sheets could be removed ad infinitum. In this letter, we shall describe the use of ion implantation to lift thin sheets of diamond from a single-crystal substrate.

In our liftoff method, we have used ion implantation to create a buried damaged layer in a polished bulk diamond crystal, and then removed that damaged layer by selective etching, thus lifting a thin sheet of diamond from the surface. The fundamental concepts of the method are the following. (a) Most of the damage caused by ion implantation occurs at the end of the ion range, and thus is confined to a buried layer of material at a controllable depth. (b) The damaged layer can be graphitized by annealing, and the graphitized layer has sharp boundaries because of the well-defined critical damage density necessary for conversion of diamond to graphite.[2,3] (c) The graphitic layer can

be preferentially etched at a much more rapid rate than that of the adjacent diamond.

It is known[2,3] that ion beam damage caused by carbon implantation at low temperatures in diamond can be divided into four general regimes.

(i) At low doses ($< 1.5 \times 10^{15}$ C^+ ions/cm^2 at 100 keV, corresponding to a Frenkel defect concentration of ~7%), the damage is almost completely recoverable by thermal annealing at about 900 °C in vacuum.

(ii) At doses between 1.5×10^{15} and 1×10^{16} C^+ ions/cm^2 at 100 keV, a stable damaged diamond structure (green diamond[3]) may be formed by annealing at 950 °C.

(iii) At doses greater than about 10^{16} C^+ ions/cm^2 at 100 keV, the damaged diamond is graphitized by thermal annealing at moderate temperatures (about 600 °C).

(iv) At very high doses, diamond is spontaneously graphitized. It should be noted, however, that diamond is much more resistant to such graphitization when the damaged layer is buried, perhaps because of the constraint on expansion due to the relatively undamaged overlying diamond.[4]

The depth profile of ion beam damage can be calculated using Monte Carlo computer programs, such as TRIM.[5] Because high energy ions lose most of their energy via electronic collisions, there is relatively little damage near the surface of an ion-implanted sample. The damage is confined to a relatively narrow buried region near the end of the ion range, where the ions lose most of their energy via nuclear collisions. Thus, by varying the initial ion energy, the depth of the buried damaged layer can be controlled. The thickness of the buried damaged layer is almost independent of the ion energy. Consequently, a buried thin layer of graphite can be created in diamond by ion implantation followed by low-temperature annealing.

Selective etching of the graphitic layer can be achieved by several methods.

(1) Since a hot chromic-sulfuric acid solution etches graphite much more rapidly than diamond, it is apparent that liftoff could be achieved by the graphitizing of a buried layer followed by an acid etch. However, the penetration of the acid into the narrow graphitic layer may be slow.

(2) The graphitic layer can be etched by annealing in an oxygen atmosphere,[6] i.e., burning the graphite to form CO or CO_2.

(3) In method (2), the oxygen must be supplied via diffusion from the edge of the sample. However, if the implanted species is oxygen, the implantation serves the dual role of creating the damaged layer and providing the required oxygen for etching.

Natural diamond types Ia and IIa crystals, in the form of polished thin plates 2×2 or 3×3 or 4×4 mm areal dimensions and 0.25 mm thick (from Dubbeldee Harris Diamond Corp.), were implanted with C^+ or O^+ ions to doses of 6×10^{16} cm^{-2}–10^{18} cm^{-2} at energies of 4–5 MeV. The ranges for 4 MeV C^+ and 5 MeV O^+ are 1.95 and 1.86 μm, and the straggling 0.07 and 0.05 μm, respectively. The C implanted samples were annealed in vacuum to graphitize the damaged layers, and then annealed in air or flowing oxygen. Some samples were etched in a chromic-sulphuric acid solution. The O implanted samples were annealed in vacuum at 500–900 °C to form CO_x in the damaged layer, and in some cases a further anneal in O_2 was used to complete the liftoff process. The samples were examined by both optical and scanning electron microscopy to monitor the etching.

One set of samples was implanted with 4 MeV C^+ ions to a fluence of 6×10^{16} cm^{-2}, with the substrate at a temperature of approximately 80 K. These samples were annealed in a vacuum of approximately 10^{-6} Torr for 30 min at 950 °C to graphitize the buried damaged layers, and then annealed at successively higher temperatures in air to selectively etch the graphitized layers. A sample that was annealed for 2 h in air at 550 °C showed undercutting of the diamond surface layer by about 9–13 μm from the edges, as demonstrated by interference fringes caused by an air gap between the partially undercut surface layer and the substrate. The etching rate at 550 °C was ~5–10 μm/h for the first 4 h. After ~20 μm had been undercut, the rate decreased markedly with time. Presumably the etch rate was limited by the penetration of the O in from the edge, and/or by removal of the reaction products CO_x out of the constricted layer. The etching rate at 600 °C was higher than at 550 °C but the diamond overlayer was also slowly etched at that temperature.

After the 950 °C vacuum anneal, one of these samples was etched in hot chromic-sulphuric acid, which also caused undercutting by removal of the graphitic layer. A 5 min etch gave an undercut depth of 0.35 μm, and the overlying natural diamond layer was 2 μm thick.

A second set of samples was implanted with 4 MeV C^+ ions to a fluence of 1×10^{18} cm^{-2}, also with the substrate at 80 K. These samples were annealed in flowing oxygen at 550 °C for 1 h. This annealing produced a partially under-

0.5 mm

FIG. 1. Optical micrograph of lifted-off diamond layer (on the right) beside the original diamond crystal template (on the left). This liftoff was achieved by an implantation of 4 MeV C ions to a fluence of 1×10^{18} cm^{-2}, followed by an anneal at 550 °C for 5 h in flowing oxygen.

cut surface layer, again shown by interference fringes. This sample was then annealed at 550 °C for 4 more hours in flowing oxygen. The diamond overlayer had separated when the sample was removed from the furnace, demonstrating that complete liftoff required less than 5 h at 550 °C in flowing oxygen. Both the lifted-off plate and the diamond substrate are shown in Fig. 1. The lifted plate (on the right) is darker than the diamond substrate (on the left). Since darker coloring indicates more irradiation defects, this effect demonstrates that the maximum depth of ion implantation has a sharp cutoff; hence the diamond crystal template has less damage. The line near the edge of both the lifted-off layer and the substrate corresponds to the etching depth after the first hour (about 120 μm). The black areas on both the lifted plate and the substrate are unetched graphite. The etching rate at 550 °C was determined to be between 120 and 140 μm/h, which is much greater than that for the lower dose C implanted sample described previously.

Several samples were implanted at ~80 K with 5 MeV ^{16}O ions to fluences of 10^{17}–10^{18} cm^{-2}. The highest dose was chosen to give a peak oxygen concentration equal to the concentration of host C atoms in the graphitic layer. One of the 10^{18} cm^{-2} samples was annealed at 950 °C for 1 h in vacuum. Most of the diamond overlayer flaked off the surface (Fig. 2), presumably because of the high pressure from the reaction products CO and CO_2 at high temperature. A unique mesa structure resulted, as shown in Fig. 2(a), where a well-defined cleavage plane traces are visible.
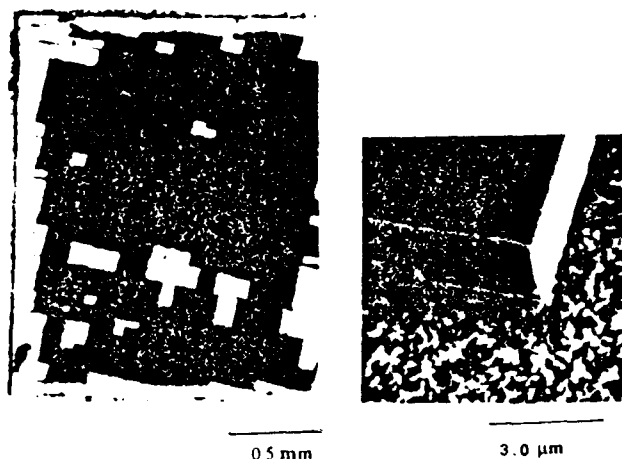
0 5 mm   3.0 µm

FIG. 2. (a) Optical micrograph of a diamond crystal after implantation with 5 MeV O ions to a fluence of 10^{18} cm^{-2}, followed by annealing at 950 °C for 1 h in vacuum. Most of the overlayer was lost, but a few rectangular-shaped pieces of the overlayer remained, and are seen as bright areas in the photograph. (b) Scanning electron micrograph of one edge of a piece of diamond overlayer from the sample of Fig. 3(a). The thickness of the layer was 2 µm.

A scanning electron micrograph of one of the remaining pieces on the surface is shown in Fig. 2(b). Here residual graphitic layers are visible both on the sample surface and on the underside of the undercut diamond layer. One method by which this unwanted graphite can be removed is by annealing in flowing oxygen.

A second 4×4 mm diamond sample that had been implanted to 10^{18} O ions/cm^2 was etched in flowing oxygen at 550 °C for 1 h. Most of the 4×4 mm layer of diamond was removed in one piece, but it broke into 3 pieces while being handled. One of the pieces (4×1.5 mm) was then annealed in vacuum (10^{-5} Torr) at 950 °C for 1 h to remove the residual damage. This annealing increased the transparency of the lifted diamond, leaving it curled with a translucent brownish hue, as shown in the SEM micrograph (Fig. 3).

To determine the minimum dose of oxygen needed to lift off a diamond layer, single crystals were implanted with 5 MeV ^{16}O$^+$ to fluences of 1×10^{17}, 3×10^{17}, and 7×10^{17} cm^{-2} at 80 K. A dose of 1×10^{17} cm^{-2} was not sufficient to amorphize the diamond or to cause liftoff. However, successful liftoff was achieved for a dose of 3×10^{17} cm^{-2}. The sample was annealed in flowing oxygen for 4 h at 550 °C. The top layer, which lifted off in one piece, was darker than the diamond substrate, as in Fig. 1. The 3×10^{17} cm^{-2} fluence should produce a Frenkel defect concentration of ~10% in the near-surface layer,[5] which is close to the damage concentration that is completely recoverable, according to our earlier annealing results.[3] To avoid the curling of the lifted diamond layer, it would be necessary to deposit a thick (~10 µm) homoepitaxial layer before the
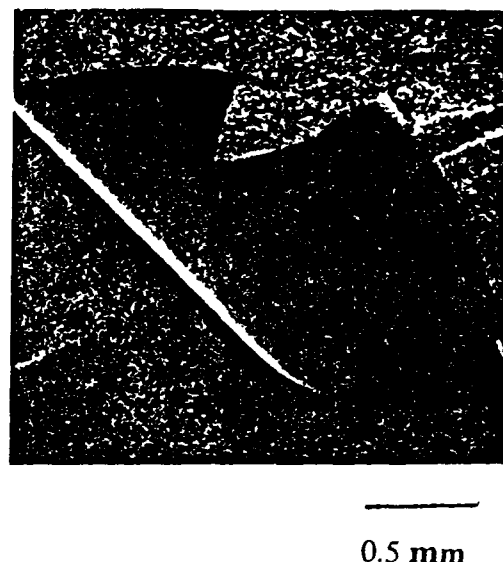

0.5 mm

FIG. 3 Scanning electron micrograph of a lifted-off diamond layer. The liftoff was achieved by implantation with 5 MeV O ions to a fluence of 10^{18} cm^{-2}, followed by annealing in flowing oxygen at 550 °C for 1 h. The sample was then vacuum annealed at 950 °C for 1 h to remove radiation damage.

liftoff in order to endow the top layer with greater mechanical strength.

We have demonstrated that square millimeter-sized areas of diamond can be lifted off intact from natural diamond crystals through a technique combining implantation and selective etching. Both 4 MeV C implantation, followed by selective etching in oxygen or in chromic acid, and 5 MeV O implantation, followed by vacuum annealing and/or annealing in O_2, were used. Sheets up to 4×4 mm in size were lifted off by the O implantation method.

[1] R. W. Pryor, M. W. Geis, and H. R. Clark, Mater. Res. Soc. Symp. Proc. 242 (1992).
[2] G. Braunstein, A. Talmi, R. Kalish, T. Bernstein, and R. Beserman, Radiat. Eff. 48, 138 (1980).
[3] J. D. Hunn, M. L. Swanson, E. A. Hill, N. R. Parikh, and G. Hudson, in New Diamond Science and Technology, edited by R. Messier (MRS, Pittsburgh, 1991), p. 929.
[4] G. S. Sandhu, B. Liu, N. R. Parikh, J. D. Hunn, M. L. Swanson, Th. Wichert, M. Deicher, H. Skudlik, W. N. Lennard, and I. V. Mitchell, Mater. Res. Soc. Symp. Proc. 162, 189 (1990).
[5] J. F. Ziegler, Transport of Ions in Matter (TRIM), IBM Corp software (1991).

Below band-gap laser ablation of diamond for transmission electron microscopy

T. George, M. C. Foote, R. P. Vasquez, and E. P. Fortier
*Center for Space Microelectronics Technology. Jet Propulsion Laboratory.
California Institute of Technology. Pasadena. California 91109*

J. B. Posthill
Research Triangle Institute. Research Triangle Park. North Carolina 27709-2194

A 248 nm excimer laser was used to thin naturally occurring type Ia diamond substrates at normal and glancing (22°) incidence. Perforation of a 250-μm-thick substrate was achieved in about 15 min at normal incidence. While the substrate thinned at glancing incidence was found to have large electron-transparent areas, that thinned at normal incidence required additional argon-ion milling to achieve electron transparency. X-ray photoelectron spectroscopy of the back surface of the diamond failed to detect any graphite or glassy carbon, confirming that damage due to laser ablation occurs only at the incident surface. Samples prepared using this technique imaged in the transmission electron microscope were observed to have retained the nitrogen platelets characteristic of such type Ia diamonds.

Recently, interest in diamond as a bulk substrate and as a coating material has grown for a variety of applications.[1] Transmission electron microscopy (TEM), both in the conventional and analytical modes, will continue to be an important technique for the characterization of diamond based materials. However, the main barrier to the widespread use of TEM as a characterization tool is the lack of a suitable technique to produce electron transparent thin foils in a controlled and timely manner. Natural diamond is the hardest substance known and, consequently, the thinning of diamond has been a centuries-old problem, particularly among manufacturers of diamond jewelry. Traditionally the grinding and polishing of diamond is achieved with diamond-based abrasives and is a time consuming process. Alternatively, argon-ion milling[2] oxidation[3] in a furnace, and laser ablation[4] have been used as means of obtaining electron-transparent specimens. The furnace oxidation approach suffers from a lack of controllability in the desired area for TEM examination and possible surface structural modification, making the technique unsuitable for producing TEM specimens from homoepitaxial samples. Argon-ion milling is a time-consuming process with a very low sputter rate of approximately 1 μm/h.[3] Laser ablation has been attempted previously although only using radiation above the band gap (193 nm).[4] This letter describes the results of an in-depth study of the laser ablation approach using below band-gap laser radiation with a view towards its applicability in producing TEM specimens from homoepitaxial samples without significantly damaging the epitaxial layers. The use of below band-gap laser radiation confines most of the energy of the laser pulse in the surface carbon layer formed during ablation and minimizes the absorption and consequent structural damage in the bulk of the diamond.

In this work, 2 mm $\times$ 2 mm $\times$ 0.25 mm, (100) oriented, type Ia diamond substrates were used. The substrates were mounted in a copper holder in the as-received condition without the use of optically absorbent coatings.

Thinning was performed in air, using an excimer laser (Questek 2960) operated at 248 nm (KrF), at a pulse rate of 5 Hz, and with an output energy of 600 mJ, at normal and glancing (22°) incidence. Although the band gap of natural diamond is around 5.48 eV (226 nm), a high concentration of nitrogen impurities in type Ia diamond lowers the UV absorption edge to 340 nm.[5] The laser output was first reduced in size by passing the beam through a 3-mm-diam aperture; the remaining 15 mJ was focused onto the diamond substrate using a 30 cm focal-length fused-quartz lens. The substrate was placed near the focal point of the lens to produce a laser spot of approximately 300 $\times$ 500 μm at normal incidence. The fluence at the center of this spot is estimated to be 20 J/cm^2.

Following laser thinning the resultant surface morphology was studied using scanning electron microscopy (SEM). TEM observations were conducted at 200 kV. The diamond substrate thinned at glancing incidence could be imaged directly. However, the substrate thinned at normal incidence required the removal of the layer formed on the ablated surface of graphitic and amorphous carbon by argon-ion milling at 5 kV and 0.5 mA for electron transparency. X-ray photoelectron spectroscopy (XPS) data were taken with a Surface Science Instruments SSX100-501 spectrometer using monochromatic Al $K\alpha$ x rays (1486.6 eV) with a beam of diameter 150 or 300 μm. Prior to XPS measurements, the diamond samples were degreased in hot trichloroethylene, acetone, and methanol to minimize surface organic contaminants. The effects of sample charging XPS data accumulation were minimized with the use of a low-electron flood gun.

Low-magnification SEM micrographs of the laser-thinned diamond substrates are shown in Fig. 1. The laser-exposed surfaces on both substrates are rough whereas the unexposed back surfaces retain their original surface polish. It was found that an absorbent coating was not necessary to initiate the laser-thinning process. A black surface layer, presumably a mixture of graphitic and amorphous
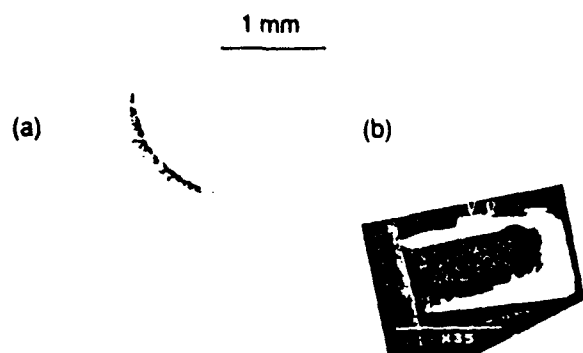
1 mm

(a)   (b)

FIG. 1. Low-magnification scanning electron micrographs of diamond substrates thinned at (a) normal incidence and (b) glancing incidence (the sample has cleaved in half, arrows point to the groove ablated by the laser).

50nm

FIG. 2. Transmission electron micrograph of a diamond substrate laser thinned at glancing incidence showing electron-transparent areas exhibiting thickness fringes.

carbon, forms very soon in the ablation process. This layer is consistent with the results from earlier furnace-oxidation studies of diamond which have shown the formation of a surface carbon (nondiamond) layer.[3] These studies determined that above 850 °C a carbon (nondiamond) layer appeared on the (100) surface of the diamond. The formation of a surface carbon layer would reduce the absorption depth of the laser radiation significantly and also have a lower thermal diffusivity than the underlying diamond, leading the localization of the laser pulse energy within the surface layer.[4,6] Rothschild, Armone, and Ehrlich have proposed that thinning in such circumstances involves a sustained process of conversion of diamond to a graphite/amorphous carbon layer followed by evaporation or reaction of this layer with the ambient. However, unlike their etching method which used above band-gap 193 nm laser radiation, this work uses a laser energy below the band gap of the diamond, with the bulk of the pulse energy being absorbed in the surface carbon layer thus minimizing absorption in the interior of the diamond. Although an optically absorbent coating was not used in the present study to initiate the thinning, such a coating could potentially be used with lasers having wavelengths in the optical transmission regime for diamond but within the absorption range for graphite or glassy carbon. The only requirement would be that the lasers have sufficiently high-energy densities for substaining the ablation process.

For the laser-thinning technique to be utilized in future TEM studies of homoepitaxial diamond layers, it is necessary to demonstrate that there is negligible damage in the form of graphitization to the back surface of the substrate. The presence of a surface graphite/amorphous carbon layer can be detected using XPS. Although both diamond and graphite contain only carbon and have C 1s core level XPS peaks at the same binding energy of 284.3 eV, the C 1s signals for these materials are distinguishable by their line shapes and characteristic energy losses. Diamond is an insulator with a C 1s signal which is symmetric, while graphite is a semimetal whose C 1s signal exhibits a pronounced asymmetry on the high binding energy side and a characteristic energy-loss peak at 291 eV which is absent in the signal from diamond.[7,8] Glassy carbon also exhibits

spectral characteristics similar to those of graphite.[7] The diamond substrate laser thinned at a glancing angle was selected for the XPS study. The C 1s signals from the samples measured in this work, including a virgin diamond crystal, consist of a single main peak with shoulders at both low and high binding energy. The only significant contaminant is O, which is present at a level of ~0.5-1 monolayer assuming surface localization. Surface C—O or C—OH bonding may account for the high binding energy shoulder on the main C 1s peak. Alternatively, the C 1s line shape may indicate some differential charging of the sample surface. However, the 291 eV energy-loss peak characteristic of graphite or glassy carbon was not observed, even near the spot where the laser has ablated completely through the sample. This result demonstrates that laser-induced heating does not damage the back surface of the diamond substrate in these experiments.

Figure 2 shows a TEM micrograph of a diamond substrate thinned at glancing incidence. This specimen contains electron-transparent regions which exhibit thickness fringes. The substrate thinned at normal incidence, however, required argon-ion milling at 12° for an hour following laser ablation to achieve electron transparency. Also, very small areas were available for observation as compared to the sample thinned at glancing angle, due to presence of steep sidewalls surrounding the perforated region. The presence of graphitic and amorphous carbon as initially proposed by Rothschild, Armone, and Ehrlich[6] on the ablated surface of the diamond thinned at normal incidence was confirmed via electron diffraction. Figure 3 contains a diffraction pattern obtained from a $\langle \bar{1}2\bar{1}1 \rangle$ ori-

(a)   (b)

$\bullet$ $\bullet$
$\bar{1}\bar{1}03$ $0\bar{1}13$

$\bullet$ $\bullet$ $\bullet$
$10\bar{1}0$ 0000 $\bar{1}010$
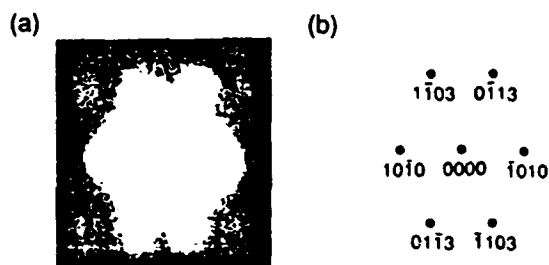
$\bullet$ $\bullet$
$01\bar{1}3$ $\bar{1}103$

FIG. 3. $\langle \bar{1}2\bar{1}1 \rangle$ diffraction pattern obtained from a graphite particle present on a diamond substrate laser thinned at normal incidence.

5nm

FIG. 4. {100} oriented nitrogen platelets characteristic of type Ia diamond found in the substrate laser thinned at normal incidence.

In summary, a novel technique for the rapid thinning of diamond using below band-gap laser radiation is described. An optically absorbent surface carbon layer is formed during irradiation which then sustains the ablation process. XPS measurements were not able to detect the damage in the form of graphitic/amorphous carbon formation on the unexposed side of the diamond substrate.

ented graphite particle found on the diamond substrate laser thinned at normal incidence. It was found that the graphitic and amorphous carbon layer could be removed by extended ion milling. Figure 4 contains a high magnification electron microscope showing the presence of nitrogen platelets lying on {100} planes in the diamond thinned at normal incidence, which is characteristic of type Ia natural diamond. These results provide ample evidence for the viability of laser ablation as a TEM specimen preparation process.

[1] For a recent review in this field see, "Status and applications of diamond and diamond-like materials: An emerging technology" Report of the committee on superhand materials, National Materials Advisory Board, NMAB-445, National Academy Press, Washington, DC, 1990.

[2] T. Myers and J. B. Posthill (unpublished).

[3] T. Evans, in *Physical Properties of Diamond*, edited by R. Berman (1965), pp. 122-124.

[4] M. W. Geis, M. Rothschild, R. R. Kunz, R. L. Aggarwal, K. F. Wall, C. D. Parker, K. A. McIntosh, N. N. Efremow, J. J. Zayhowski, D. J. Ehrlich, and J. E. Butler, Appl. Phys. Lett. 55, 2295 (1989).

[5] O. Madelung, Ed., *Physics of Group IV Elements and III-V Compounds*, Vol. 17a of Landolt-Börnstein, New series (Springer, 1982), p. 36.

[6] M. Rothschild, C. Armone, and D. J. Ehrlich, J. Vac. Sci. Technol. B 4, 310 (1986).

[7] F. R. McFeely, S. P. Kowalczyk, L. Ley, R. G. Cavell, R. A. Pollak, and D. A. Shirley, Phys. Rev. B 9, 5268 (1974).

[8] R. P. Vasquez, Surf. Sci. Spectra 1, 188 (1992); 1, 238 (1992).

Etch-delineation of defects in diamond by exposure to an oxidizing flame

D. P. Malta, J. B. Posthill, R. A. Rudder, G. C. Hudson, and R. J. Markunas
Research Triangle Institute, Research Triangle Park, North Carolina 27709-2194

An experimental study of the etching properties of defects in diamond using propane flame exposure in air is presented. Both natural diamond crystals and polycrystalline diamond films were exposed to a flame for an optimum time of 3–4 s. This process topographically delineates defects in diamond via an accelerated etch rate at defect sites. Using transmission electron microscopy (TEM) to determine the exact nature and density of defects present in the diamond, we have found a direct correlation between topographical delineation observed by scanning electron microscopy (SEM) and the defect structure observed by TEM.

Diamond has several properties that make it desirable for electronic applications.[1] Foremost are diamond's high thermal conductivity (~ 2000 W m^{-1} K^{-1}) and wide band gap (5.48 eV). However, before the impressive attributes of diamond can be fully exploited for electronic device purposes, several manufacturing technologies must be developed. First among these is the growth of electronic-quality diamond thin films of high microstructural perfection. Considerable worldwide effort has gone into developing chemical vapor deposition (CVD) techniques for growing high-quality diamond,[2,3] and considerable progress has been made. And, by analogy with the historical development of other semiconductor materials, techniques are evolving to determine accurately the crystalline quality of grown diamond. For example, Raman spectroscopy has been used extensively to ascertain the presence of unwanted sp^2 bonding in diamond films.[4] In other semiconductor material technologies, wet chemical etch delineation is used to ascertain defects at the per cm^2 level. But this technique is lacking in diamond technology, as diamond is virtually impervious to standard wet chemical etchants. This communication describes a defect delineation method for diamond, which involves anisotropic defect etching using a propane torch.

Previous etching studies on diamond have been undertaken to investigate feasibility of patterning,[5] to determine etch removal rates,[6–11] to identify the role of non-diamond phase removal during the growth process,[5] and to assess crystalline quality through preferential etching of defects,[8,12] to name a few. Several methods that have proven successful in etching both diamond and non-diamond phases have employed both (a) an oxygen-containing gas and (b) an activation mechanism. Etching under these conditions is generally believed to occur via the oxidation and volatilization of the carbon

phase(s). It has been suggested that etching of diamond proceeds through graphitization followed by oxidation of the graphitic phase.[8] Several observations regarding etch rates have been made: (1) non-diamond phases etch faster than diamond,[5,7,9,11] (2) natural diamond etches faster than plasma-enhanced chemical vapor deposition (PECVD)-grown diamond,[6,9,11] and (3) diamond etches faster at grain boundaries and other defects than non-defective regions.[8,9,11,12] Oxidation/etching experiments recently reported have employed either a temperature-activated[6,8–11] or plasma-activated[5,7,12] process using air or oxygen-containing gas mixtures. We have achieved temperature-activated etching of diamond using only a short exposure to an oxidizing flame. Our results indicate that accurate, reproducible etch-delineation of defects is possible with minimal investment. These results have been correlated with TEM analysis.

A continuous polycrystalline film was grown at 450 °C by low pressure rf-induction PECVD on Si(100) using an acetic acid/water/methanol mixture at 1 Torr, similar to results described elsewhere.[3] For comparison, a natural type IIb semiconducting diamond stone sectioned into thin (100 μm) wafers with (100) orientation was obtained from a commercial vendor. Both sample types were examined by TEM in order to assess crystalline quality. TEM samples were prepared by ion milling. Each sample type was immersed in a propane flame for various lengths of time and then topographically examined by field-emission scanning electron microscopy (FESEM).

Plan-view TEM of the polycrystalline diamond film revealed a high degree of microtwinning within the grains [Fig. 1(a)]. After immersion of the sample in the flame for an optimum time of 3–4 s [Fig. 1(b)], the microtwin boundaries were clearly delineated as were grain boundaries which were attacked more vigorously (arrow).
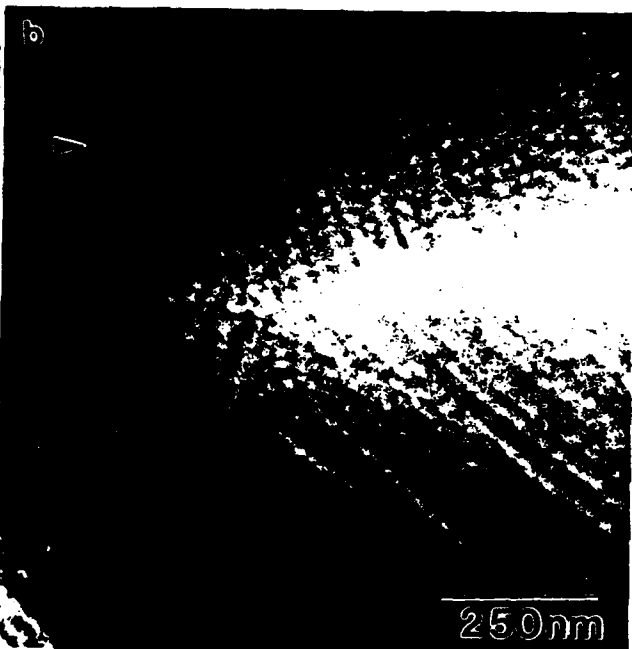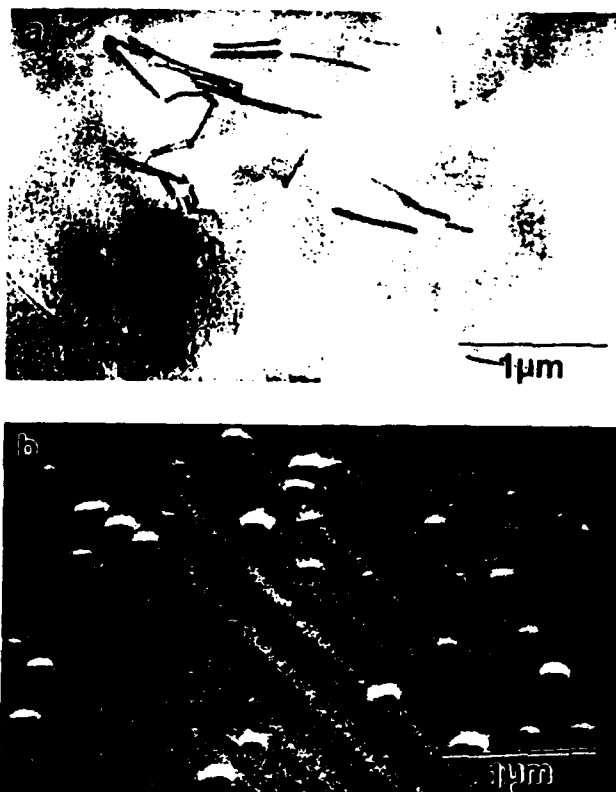
FIG. 2. (a) Plan-view TEM of natural type IIb diamond shows dislocations. Examination of large areas found that dislocations tended to cluster and the overall density was $\sim 10^8$ cm^{-2}. (b) Etch pits in natural type IIb diamond formed at dislocation sites upon exposure to an oxidizing flame. Density measured over large areas was averaged to be $\sim 10^8$ cm^{-2}. Both results were obtained from the exact same crystal; the etching work was followed by ion milling the 100 μm thick wafer from both sides to electron transparency.

FIG. 1. Microscopic images of PECVD-grown polycrystalline diamond; (a) plan-view TEM shows a very high density of microtwins, and (b) FESEM image of sample after exposure to an oxidizing flame which shows delineated microtwin boundaries (parallel grooves) and a grain boundary (arrow).

TEM analysis of the type IIb natural diamond over relatively large areas found only line defects with an area density of $\sim 10^8$ cm^{-2} [Fig. 2(a)]. Immersion of the diamond in the flame for an optimum time of 3–4 s produced roughly square etch pits with an equivalent area density of $\sim 10^8$ cm^{-2} [Fig. 2(b)]. Note that after this exposure the remnants of the unidirectional scratches left over from the commercial polishing process are still evident. Shorter exposure times resulted in fewer, smaller pits; longer exposure resulted in larger (but few additional) pits and a roughened surface no longer showing scratches.

The results are consistent with those obtained by furnace annealing in an oxygen atmosphere at 700 °C–800 °C for several hours[8] and by air microwave plasma etching for 15–30 min.[12] In this work, the accelerated etch rate obtained through flame exposure produced verified topographical defect delineation requiring only several seconds at negligible cost. The value of this method for routine and rapid evaluation of diamond is considerable. Future research will extend this technique to homoepitaxial diamond films grown by PECVD.

ACKNOWLEDGMENTS

REFERENCES

1. *The Properties of Diamond*, edited by J. E. Field (Academic Press, London, 1979).

2. R. A. Rudder, G. C. Hudson, J. B. Posthill, R. E. Thomas, R. C. Hendry, D. P. Malta, R. J. Markunas, T. P. Humphreys, and R. J. Nemanich, Appl. Phys. Lett. **60**, 329 (1992).

3. R. A. Rudder, J. B. Posthill, G. C. Hudson, D. P. Malta, R. E. Thomas, R. J. Markunas, T. P. Humphreys, and R. J. Nemanich, in *Wide Band-Gap Semiconductors* edited by T. D. Moustakas, J. I. Pankove, and Y. Hamakawa (Mater. Res. Soc. Symp. Proc. **242**, Pittsburgh, PA, 1992), p. 23.

4. R. J. Nemanich, J. T. Glass, G. Lucovsky, and R. E. Shroder, J. Vac. Sci. Technol. A **6**, 1783 (1988).

5. R. Ramesham and B. H. Loo, J. Electrochem. Soc. **139** (7), 1988 (1992).

6. Q. Sun and M. Alam, Proc. 2nd Int. Symp. on Diamond Materials, Washington, DC, The Electrochemical Society Proceedings, Vol. 91-8, 463 (1991).

7. G. S. Sandhu and W. K. Chu, Appl. Phys. Lett. **55** (5), 437 (1989).

8. W. Zhu, X. Hong Wang, A. Badzian, and R. Messier, in *New Diamond Science and Technology*, edited by R. Messier, J. T. Glass, J. E. Butler, and R. Roy (Mater. Res. Soc. Symp. Int. Proc. NDST-2, Pittsburgh, PA, 1990), p. 812.

9. A. Joshi, R. Nimmagadda, and J. Herrington, J. Vac. Sci. Technol. A **8** (3), 2137 (1990).

10. K. Tankala and T. DebRoy, in *New Diamond Science and Technology*, edited by R. Messier, J. T. Glass, J. E. Butler, and R. Roy (Mater. Res. Soc. Symp. Int. Proc. NDST-2, Pittsburgh, PA, 1990), p. 827.

11. L. S. Plano, S. Yokota, and K. V. Ravi, Proc. 1st Int. Symp. on Diamond Materials, Los Angeles, CA, The Electrochemical Society Proceedings, Vol. 89-12, 380 (1989).

12. Y. Sato, C. Hata, T. Ando, and M. Kamo, in *New Diamond Science and Technology*, edited by R. Messier, J. T. Glass, J. E. Butler, and R. Roy (Mater. Res. Soc. Symp. Int. Proc. NDST-2, Pittsburgh, PA, 1990), p. 537.

Secondary Electron Emission Enhancement and Defect Contrast From Diamond by Exposure to Atomic Hydrogen

D.P. Malta, J.B. Posthill, R.E. Thomas, G.G. Fountain, R.A. Rudder, G.C. Hudson, M.J. Mantini, and R.J. Markunas
Research Triangle Institute, Research Triangle Park, North Carolina 27709-2194

T.P. Humphreys
Department of Physics, North Carolina State University, Raleigh, North Carolina 27695-8202

Abstract

Polished nominal (100) surfaces of four types of diamonds were exposed to atomic hydrogen by hot filament cracking of H_2 gas or by immersion in a H_2 plasma discharge. Both type IIa and IIb (100) diamond surfaces exhibited the following characteristic changes: (a) secondary electron (SE) yield increased by a factor of ~30 as measured in a scanning electron microscope (SEM), (b) near-surface, non-topographical defects were observable directly using the conventional SE mode of the SEM, (c) surface conductance increased by up to 10 orders of magnitude. These changes were observed only weakly in nitrogen-containing type Ia and Ib diamonds

Diamond has several properties such as high thermal conductivity (~2000 W m^{-1}K^{-1})and wide bandgap (5.48eV) that make it a desirable candidate material for electronic device applications. Considerable research world-wide has been undertaken to optimize diamond growth processes and significant work has focused on the interaction of the diamond surface with reactive gas species in an effort to better understand the process of growth from the gas phase. Hydrogen, because of its critical role in most diamond growth processes, has received the most attention. Surface studies on (100) natural diamond[1] have shown that the clean surface becomes H-terminated upon exposure to atomic H and that H can be desorbed from the surface upon annealing above ~950°C or alternatively displaced by oxygen in an atomic O environment. Hydrogen-treated diamond surfaces have been known to demonstrate negative electron affinity (NEA). For example, photoemission studies by van der Weide et al.[2] on (111) diamond indicate that the H-terminated diamond surface exhibits NEA such that the energy position of the vacuum level lies below the conduction band minimum. Higher electrical conductivities have also been associated with H-treated diamond surfaces[3,4].

In this letter, we report on the enhancement and control of the secondary electron yield and surface conductance on diamond through exposure to atomic H, atomic O and high temperature annealing processes. We present, for the first time, near-surface, non-topographical defect images from H-treated natural single crystal diamond surfaces using conventional secondary electron contrast in the SEM.

Four types of diamond crystals commercially cut and polished to nominally (100) orientation (types Ia, Ib, IIa, and IIb), were exposed to atomic hydrogen. Each sample was exposed by immersion in a hydrogen rf-plasma at 50W with a sample temperature of 380°C and hydrogen partial pressure of 7×10^{-3} Torr or alternatively by immersion in a H/H_2 gas flow over a hot tungsten filament with a hydrogen partial pressure of 2×10^{-6} Torr and the sample at room temperature. Both systems are ultra-high vacuum (UHV) with base pressures $<5 \times 10^{-10}$ Torr. Time of exposure was varied from 1sec to several hours. Samples were then removed and characterized by SEM and by two-point probe, current-voltage surface conductance measurements. One of the following steps was then used to remove H from the diamond: (a) annealing in UHV at ~1000°C for 15 minutes, (b) exposure to a 20%oxygen/argon plasma for 1min, (c) immersion in an O/O_2 gas flow over a hot iridium filament for 1 min with an oxygen partial pressure of 2×10^{-6} Torr and the sample at room temperature or (d) immersion in boiling CrO_3/H_2SO_4 for 15 mins followed by boiling aqua-regia for 15 mins. SEM and conductance measurements were then repeated.

Natural type IIa (highly insulating) and IIb (semiconducting, p-type) diamond (100) surfaces exposed to the H_2 plasma for 1min showed a large increase in electron emission as observed by SEM using a conventional Everhart-Thornley SE detector (see Fig. 1). In the example shown in Fig. 1, Ni dots that were evaporated on the diamond through a shadow mask illustrate the relative electron yields. In all cases, Pt wires were used to suture the diamonds to a graphite puck. Areas of the diamond shadowed from the plasma by the wires showed much lower electron emission in the SE mode; however, no

contrast was observed using a solid-state Si backscattered electron (BSE) detector indicating that yield enhancement was of the much lower energy (0-50eV) SE's. This shadowing effect indicates that the emission enhancement is intensified in areas that received directional dosing from ion bombardment in the plasma. Exposure to an O_2/Ar plasma for 1min resulted in a decrease of SE yield from the diamond surface to below that of the Ni dots and Pt wires, (Fig. 1b). Highly insulating type Ia (containing nitrogen platelets) and Ib (containing nitrogen in solution) (100) diamond surfaces showed only weak enhancement of SE yield when treated with a H_2 plasma under the same conditions for up to 100 mins.

The total electron yield, σ, can be deduced fairly readily by measuring the beam current I_b with a Faraday cup and the specimen current I_s with an electrometer and using the current balance relation

$$I_b = \sigma I_b + I_s \qquad (1)$$

where

$$\sigma = \delta + \eta \qquad (2)$$

δ is the SE yield and η is the BSE yield[5]. Values of σ measured from the natural type IIb (100) diamond in the SEM using a 3keV/70pA beam were $\sigma = 1.3$ following an anneal at 1000°C for 15min and $\sigma = 37.7$ following a H_2 plasma exposure for 1min. η is small for

low atomic number elements and on the order of 0.09 for carbon at 3keV[6]. Assuming this value for η and that it did not change upon atomic H exposure, which is supported by BSE images,

$$\delta = (\sigma - \eta) \sim \sigma \quad \text{since} \quad \eta \ll \sigma \qquad (3)$$

and therefore $\delta \sim 37.7$. To the best of our knowledge, this value of δ is the highest SE yield measured to date for any material[7].

Enhancement of SE yield was not as pronounced in samples dosed with atomic hydrogen produced by a hot filament but showed increases with longer exposures over several hours. These long exposures were more than adequate to leave the diamond surface H-terminated[1], however, the hot filament method of dosing does not involve ion bombardment, an apparent contributing factor to SE yield enhancement, as does the plasma method. SE enhancement was, however, achieved fully by a 1sec exposure to a H_2 plasma when preceded by an anneal at 1000°C in UHV for 15mins. It is interesting to note that the enhancement effect degraded very little upon storage of a H-exposed diamond in air for several weeks.

Specific processing steps were found to reduce the SE emission and surface conductance to more typical levels. Annealing, O_2/Ar plasma exposure or treatment in an oxidizing acid bath appeared to be equally effective. Surface conductance on the type IIa

(100) diamond following the high temperature anneal was extremely low (<1fA at 100V); and increased more than 10 orders of magnitude following the 1 min H_2 plasma exposure (10μA at 100V); it was subsequently decreased again upon O_2/Ar plasma exposure (<1fA at 100V). The increased surface conductance upon hydrogen exposure is consistent with results by Landstrass et al.[3] and Nakahata et al.[4] on polycrystalline and homoepitaxial diamond, respectively.

SE images from H-exposed type IIa and IIb single crystal diamond surfaces that showed SE emission enhancement also showed non-topographical, near-surface defect contrast. A similar observation was first reported by Harker, et al.[8] following high temperature iron metal polishing of polycrystalline diamond in a hydrogen atmosphere. Fig. 2a is a low magnification SE micrograph taken from a *natural type IIa (100) diamond surface following H_2 plasma* exposure clearly delineating an orthogonal array of defects showing directional preference. Plan-view transmission electron microscopy (TEM) examination of another natural type IIa (100) diamond confirmed the presence of an orthogonal dislocation substructure with preference to lie in <011> directions (Fig. 2b). Isolated dislocations were also observed. Higher magnification SEM images on the type IIb diamond surface after H_2 plasma exposure show a portion of the characteristic cell structure of dislocations as previously observed by TEM, cathodoluminescence and electron beam-induced current[9] (Fig. 3a) and resolution of *individual defects (Fig. 3b)* with directional preference. Reversal of the SE defect contrast effect by O_2/Ar plasma exposure yields the more typical topographical image showing polishing scratches (Fig.

3c). The defect contrast was observed at all beam energies (0.5 - 25keV) and sample tilt (0° - 80°) and was not observed using a BSE detector.

These new observations have considerable apparent utility and points can be made about the increased SE emission and the accompanying defect contrast. To permit the detection of secondary electrons created within the solid, the secondary electrons must be able to: (1) migrate to the surface without being trapped and (2) overcome any surface potential energy barrier between the solid surface and the vacuum. We present the hypotheses of two possible mechanisms to account for the observed increase in secondary electron yield with H plasma exposure: (1) H exposure has created a surface potential which establishes an attractive electric field that effectively increases the maximum escape depth for secondary electrons, and (2) the H-exposed C(100) surface is exhibiting negative electron affinity[2], meaning that any mobile electron at the surface of the diamond can "drop" into the vacuum level as opposed to having to overcome an energy barrier. Both possibilities can explain the increased secondary electron yield, δ, and it is interesting to note that they are not necessarily mutually exclusive. It could then be reasoned that mobile secondary electrons migrating in the near-surface region could be trapped by a dislocation or by a deep-level-creating impurity such as nitrogen. This would appear to explain the defect contrast in type IIa and IIb diamond and the lower degree of secondary electron emission enhancement from nitrogen-containing type Ia and Ib diamonds and is consistent with observations by Hoffman, et al.[10] indicating that the SE yield is sensitive to near-surface damage in diamond. If we are correct in our interpretation of our results, then this technique has potential utility beyond dislocation observation and

characterization. In principle, a simple measurement of secondary electron yield from a H-exposed diamond surface can be employed as a useful measure of electrical quality, in a manner that would be analogous to minority-carrier diffusion length measurements derived from the electron-beam-induced current (EBIC) technique.

In summary, we have demonstrated a factor of ~30 increase in SE yield to $\delta = 37.7$ from a type IIb diamond crystal. Yield enhancement observed on both type IIa and IIb diamonds was eliminated upon removal of hydrogen by exposure to an oxygen plasma, high temperature annealing, or by treatment with an oxidizing acid solution. H-exposed type IIa and IIb surfaces also exhibited considerable surface conductance and showed defect contrast in the SE mode of the SEM. The authors gratefully acknowledge the support of this work by the BMDO/IST through ONR (Contract No. N00014-92-C-0081) and we thank Dr. David C. Joy and Mr. Max N. Yoder for insightful discussions.

References

[1]R.E. Thomas, R.A. Rudder, and R.J. Markunas, J. Vac. Sci. Technol. A, **10**, 2451 (1992)

[2]J. van der Weide and R.J. Nemanich, Appl. Phys. Lett.**62** 1878 (1993)

[3]M.I. Landstrass and K.V. Ravi, Appl. Phys. Lett. **55** 975 (1989)

[4]H. Nakahata, T. Imai, and N. Fujimori, Proc. of the 2nd Intl. Symp. on Diam. Mat., ECS, Vol. 91-8, p. 487

[5]For a complete review, see H. Seiler, J. Appl. Phys. **54** R1 (1983)

[6]P. Palluel, Compt. Rendu, **224**, 1492 (1947)

[7]D.C. Joy, "A Data Base on Electron-Solid Interactions", non published document.

[8]A.B. Harker, J.F. DeNatale, and J.F. Flintoff, Appl. Phys. Lett. **62** 3105 (1993)

[9]D.P. Malta, J.B. Posthill, E.A. Fitzgerald, R.A. Rudder, G.C. Hudson, and R.J Markunas, Proc. of the 3rd Intl. Symp. on Diam. Mat., ECS, Vol. 93-17, p. 647

[10]Alon Hoffman and Steven Prawer, Appl. Phys. Lett. **58** 361 (1991)

<u>Figure Captions</u>

Figure 1 - Secondary electron-mode images of a (100) natural type IIb diamond wafer with epitaxial Ni dots (a) after exposure to a H_2 plasma for 1min (notice the diagonal shadow lines where the wire sutures were) and (b) after exposure to an O-plasma for 1min. The SE yield (δ) from the H-treated diamond surface was ~30 times greater than that from the O-treated surface.

Figure 2 - (a) Low magnification secondary electron map of near-surface non-topographical defects lying in <011> directions in highly-insulating natural type IIa (100) diamond after exposure to a H_2 plasma for 1min. (E_b=25keV; surface conductance is high; no charging observed) (b) Plan-view TEM image of natural type IIa (100) diamond showing dislocations in cell walls with <011> directional preference and individual dislocations within cells.

Figure 3 - Secondary electron images of the surface of natural type IIb (100) diamond after 1 min exposure to a H_2 plasma [(a) and (b)] and after a desorb step in UHV at 1000° C for 15mins (c). (a) Shows a portion of the characteristic cellular wall structure of dislocations and <011> preference. (b) shows individual near-surface dislocations. The more typical surface topographical image of polishing scratches is observed (c) after H desorption by high temperature annealing.
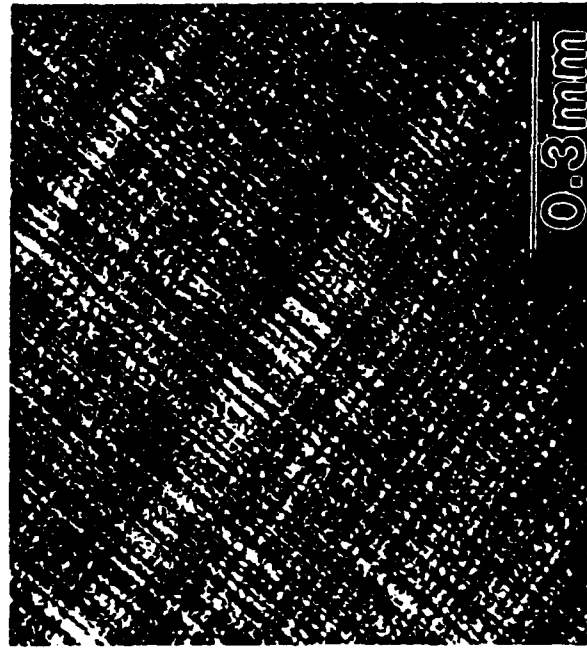
(a)   (b)

Figure 1

(b)

011
01̄1

(a)
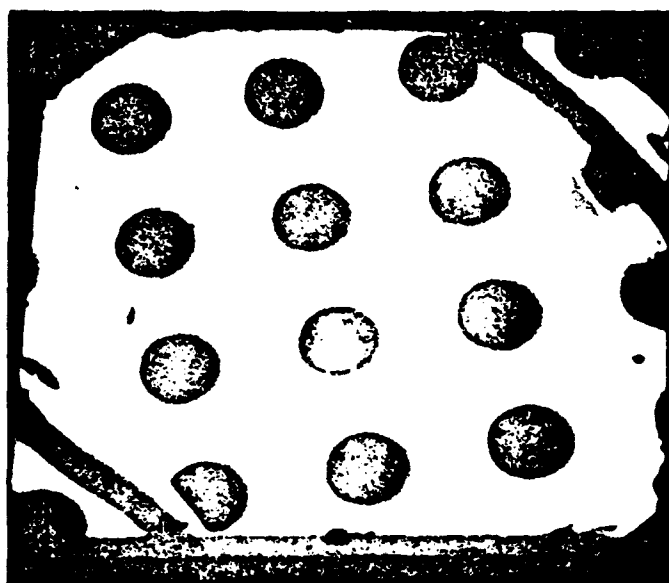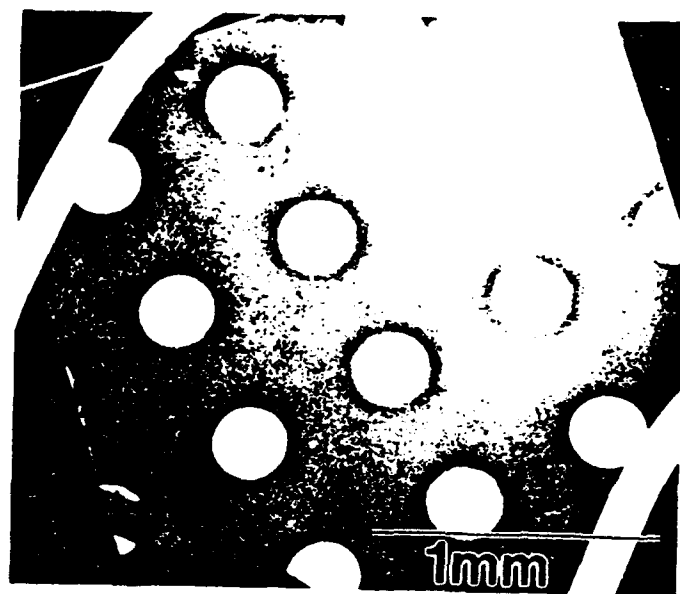
Figure 2

(a)   (b)   (c)

Figure 3

A CORRELATIVE INVESTIGATION OF DEFECTS
IN NATURAL AND PECVD-GROWN DIAMOND

D.P. Malta, J.B. Posthill, E.A. Fitzgerald[*], R.A. Rudder,
G.C. Hudson and R.J. Markunas

Research Triangle Institute
Research Triangle Park, North Carolina 27709-2194
[*]AT&T Bell Laboratories, Murray Hill, New Jersey 07974

Defects contained in natural type IIb single crystal diamonds and
polycrystalline diamond films grown by plasma-enhanced chemical
vapor deposition (PECVD) were characterized using several dif-
ferent techniques. Dislocations in a cellular-like network in
natural IIb diamond were electrically active and luminescent
predominantly at 430nm. A high density of microtwins was
present in the PECVD polycrystalline diamond. All defect types
etched faster than surrounding diamond when exposed to an oxi-
dizing flame creating readily observable topographical delineation.

The potential for utilizing the many superior qualities of diamond in
electronics applications has driven a large effort toward the advancement of
diamond materials technologies. Diamond film growth technologies have
recently been developed that are safe and relatively inexpensive and therefore
promising for large-scale applications (1).

Active electronic device applications require a smooth diamond surface
and a low defect density. As diamond growth technologies progress toward
this goal, focus will shift from the achievement of epitaxial registration to
defect reduction in the epitaxial growth. In order to attain defect control,
methods of routine and accurate assessment are necessary for an understand-
ing of the nature, origin and propagation of defects in diamond (2). Unlike
other semiconductors, diamond is inert to wet chemical attack thus preclud-
ing the use of common wet chemical etch techniques for defect delineation.
Also highly electrically insulating in some forms, the use of electron-beam-
based techniques can be difficult.

We have conducted a correlative investigation of structural, electrical,
optical, and oxidation properties of defects in natural and PECVD-grown dia-
mond and present a new technique for the routine, accurate assessment of
the crystalline quality of diamond.

EXPERIMENTAL

A natural type IIb semiconducting diamond stone sectioned into three 2.0x2.0x0.10mm wafers with (100) face orientations was obtained from a commercial vendor. Type IIb diamonds have relatively low electrical resistivity (10^5-10^7 ohm-cm) and are p-type with boron as the predominant impurity (3). The small thickness (0.10mm) was specified to minimize ion milling time during transmission electron microscopy (TEM) sample preparation. The sections were analyzed as follows: (a) Wafer No.1 was subject to a defect etch delineation technique (described in detail elsewhere (4)) by immersion in a propane flame for 3 sec followed by scanning electron microscopical (SEM) observation. This wafer was then ion-thinned from both sides to electron transparency and observed in plan-view by TEM (b) Wafer No.2 was analyzed using wavelength-resolved cathodoluminescence (CL) spectroscopy in an SEM at a sample temperature of $6°K$. (c) Wafer No.3 was imaged using a scanning panchromatic CL signal collected by an annular solid state Si detector. Thin (10nm) Au Schottky diodes were then fabricated to facilitate plan-view imaging by electron beam-induced current (EBIC) which followed.

The polycrystalline diamond film was grown on Si(100) by low pressure rf-induction plasma-enhanced chemical vapor deposition (PECVD) using an acetic acid/water/methanol mixture in the ratio 2:2:1 at 1 Torr and a substrate temperature of 450 C (1). Part of the sample was observed in plan-view by TEM and part was etched via flame exposure for 3 sec followed by SEM observation.

RESULTS

Natural Type IIb Diamond

Oxidation/etching of wafer No.1 of the type IIb natural diamond crystal via flame exposure created roughly square etch pits on the surface as observed by SEM (Fig. 1a). The density of pits counted over large areas was $\sim 10^8$cm^{-2}. Plan-view TEM also on wafer No.1 following ion-thinning from both sides revealed a relatively high density of dislocations (Fig. 1b). Examination of large areas indicated a density of $\sim 10^8$cm^{-2} dislocations. The dislocations were arranged in clusters. No other type of defect was observed.

A CL spectrum collected from wafer No.2 of the natural diamond crystal (Fig. 2) gave strong emission at 430nm, which has been termed "band A" emission and has been associated with donor-acceptor recombination due to

nitrogen and boron impurities (5), respectively. Minor CL peaks were observed at 589nm and 618nm. Emission at 589nm is near the emission generally associated with a nitrogen-vacancy complex at 575nm (6). The origin of the emission at 618nm is unknown.

Panchromatic CL and EBIC images collected from wafer No.3 of the natural diamond crystal (Figs. 3a and 3b, respectively) indicated that active sites were arranged in a cellular-like network. Bright regions in Fig. 3a correspond to luminescent sites in the diamond within ~3-4μm from the surface. As indicated by the CL spectra, most of the luminescence that composes this image is of a wavelength of 430nm (2.88eV) which is within the sensitivity range of the Si solid state detector. The dark regions in the EBIC image of Fig. 3b are sites where carrier recombination takes place. Individual sites were not resolved in either imaging mode likely due to small spacing between active sites and the relatively large electron beam interaction volume diameter (~4μm at 25KeV).

Polycrystalline Diamond

Oxidation/etching via flame exposure of the polycrystalline diamond film on Si(100) followed by SEM examination (Fig. 4a) revealed delineated grain boundaries (arrow) and closely spaced parallel grooves within the grains. Plan-view TEM of the same polycrystalline film (Fig. 4b) showed a high density of microtwins within the crystals with spacing and geometry very similar to the topographical grooves shown in Fig. 4a.

Attempts at imaging using the SEM-based EBIC and CL techniques were unsuccessful, probably due to the small defect spacing relative to the electron beam interaction volume diameter and/or a high density of nonluminescent sites.

DISCUSSION AND CONCLUSIONS

It is likely that dislocations in the natural diamond crystal observed by TEM were etched preferentially during the flame exposure process since etch pits in a similar arrangement and density were observed by SEM. This observation indicates that surface-terminated dislocations in natural semiconducting diamond, when exposed to an oxidizing environment, behave similarly to dislocations in other semiconductors when exposed to wet chemical etchants (eg. 7). Since diamond is virtually inert to wet chemical etchants, this result is significant. EBIC analysis showed a network of (electrically active) carrier recombination sites similar in structure and density to the dislocation

network observed by TEM. Due to the limited resolution of the EBIC technique, only clusters of sites were resolved. Nevertheless, this observation suggests that the dislocations *are* the electrically active sites. It does not confirm, however, that *all* dislocations are electrically active. Comparison of EBIC images and panchromatic CL images shows much similarity in the arrangement of active sites. This further indicates that indeed some or all electrically active sites (dislocations) are *also* luminescent. Others have concluded in a CL/TEM study of natural type IIb diamond that all CL in the range of ~500nm-700nm originated from dislocations but not all dislocations were luminescent in that range (8).

The high density of microtwins observed by TEM in the polycrystalline diamond film grown on Si(100) likely prevented resolved panchromatic CL images. Likewise, resolved EBIC images have not been possible previously on polycrystalline diamond films. Band A CL emission has been observed in PECVD polycrystalline diamond films (9). however, it is not known if this emission is associated with microtwins as it has been with dislocations. Our studies have shown that microtwin and grain boundaries in PECVD diamond etch in an oxidizing environment faster than surrounding diamond material. As in the case of natural diamond, the potential usefulness of this quick and simple method for defect delineation is significant.

In summary, we have studied and compared the microstructure and properties of defects in natural and PECVD-grown diamond. This study has identified a dense ($\sim 10^8 \text{cm}^{-2}$) cellular-like dislocation structure in natural type IIb diamond with the following properties: (a) some or all are electrically active, (b) some or all of those electrically active are luminescent, (c) the predominant emission of those that luminesce is at 430nm, (d) the surface-terminated dislocation sites etch faster than the surrounding diamond when exposed to a flame creating readily observable pits, (e) no other defect types were observed. The PECVD-grown polycrystalline diamond film contained a high density of microtwins. The CL emission and induced current signal were insufficiently low for imaging. Both grain and twin boundaries etched faster than the surrounding diamond when exposed to a flame creating readily observable topographical delineation.

ACKNOWLEDGEMENT

REFERENCES

1. R.A. Rudder, J.B. Posthill. G.C. Hudson. D.P. Malta, R.E. Thomas, R.J. Markunas, T.P. Humphreys and R.J. Nemanich, Mat. Res. Soc. Symp. Proc., 23 (1992).

2. D.P. Malta, S.A. Willard, R.A. Rudder, G.C. Hudson, J.B. Posthill, R.E. Thomas and R.J. Markunas. Proceedings of the 49th Annual Meeting of the Electron Microscopy Society of America (Ed. G.W. Bailey, San Francisco Press, 1991)p. 880.

3. From "Properties of Diamond", distributed by DeBeers Diamond Research Laboratory. Johannesburg 2000, South Africa

4. D.P. Malta, J.B. Posthill, R.A. Rudder, G.C. Hudson and R.J. Markunas, J. Mater. Res., 8, 1217 (1993), in press.

5. R.J. Graham, T.D. Moustakas, M.M. Disko, J. Appl. Phys., 5, 3212 (1991)

6. L.H. Robins, L.P. Cook, E.N. Farabaugh and A. Feldman, Phys. Rev. B, 39, 13367 (1989)

7. D.J. Stirland, B.W. Straughan, Thin Solid Films, 31, 139 (1976)

8. N. Yamamoto, J.C.H. Spence and D. Fathy, Phil. Mag. B, 6, 609 (1984)

9. R.J. Graham, J.B. Posthill, R.A. Rudder and R.J. Markunas, Appl. Phys. Lett., 59, 2463 (1991)
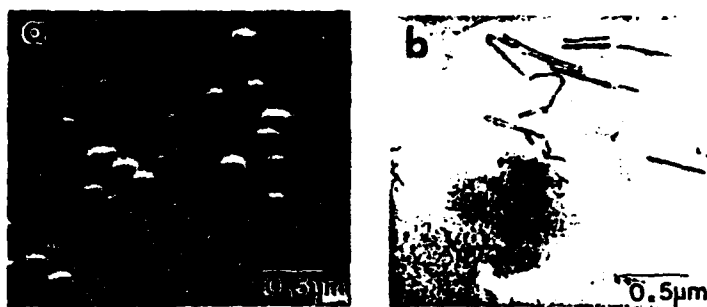
FIGURE 1: (a)SEM of the natural type IIb diamond surface following exposure to an oxidizing flame showing etch pits at dislocation sites. Etch pit density is $\sim10^8 cm^{-2}$. Notice that the polishing scratches are still visible. (b)Plan-view TEM of the same wafer shows dislocations. Examination of large areas found that dislocations tended to cluster and overall density was $\sim10^8 cm^{-2}$.
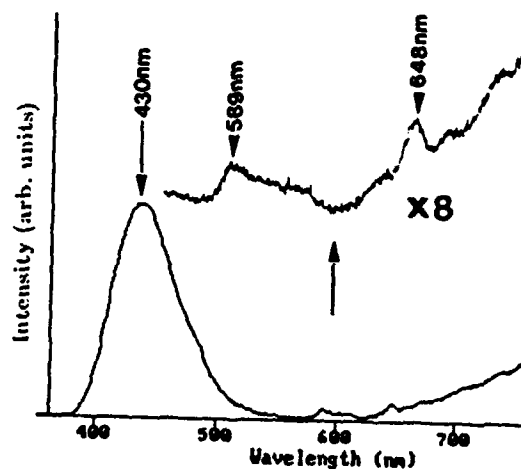

FIGURE 2: CL spectrum acquired from the same natural type IIb diamond examined in Fig. 1 showing the characteristic band A emission at 430nm and smaller peaks at 589nm and 648nm.
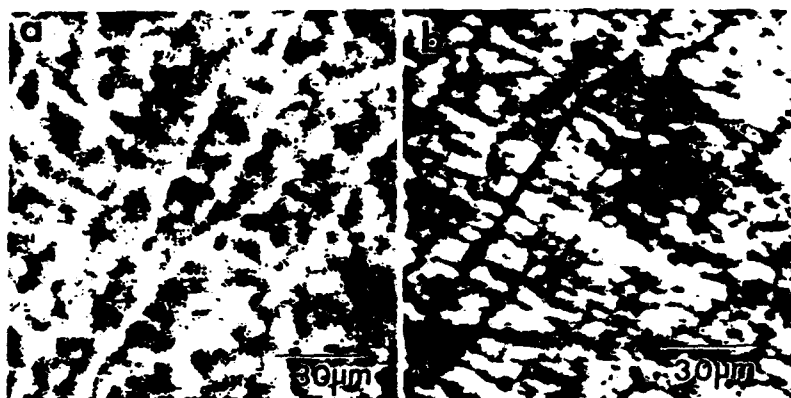
FIGURE 3: Large area maps of defect distributions in the same natural Type IIb diamond: (a) panchromatic CL image: bright regions represent *luminescent* electron-hole recombination sites. (b) EBIC image: dark regions represent *all* electron-hole recombination sites.
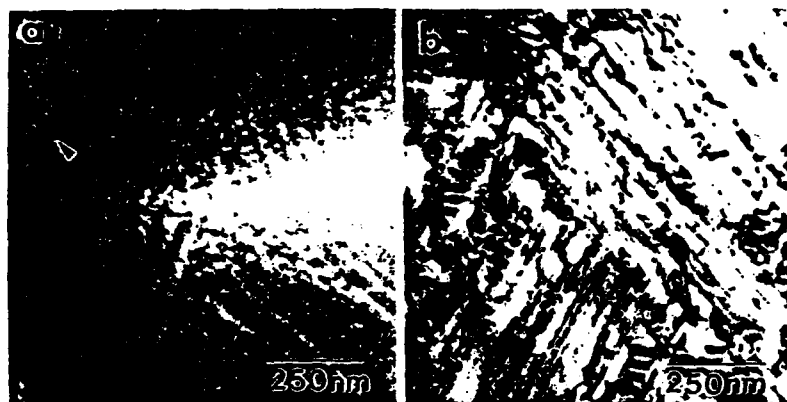

FIGURE 4: Images of PECVD-grown polycrystalline diamond: (a) SEM after exposure to an oxidizing flame delineates microtwin boundaries (grooves) and a grain boundary (arrow). (b) bright field TEM image confirms the high density of microtwins.

CHARACTERIZATION OF EPITAXIAL DIAMOND ON NATURAL DIAMOND SUBSTRATES BY CATHODOLUMINESCENCE

D.P. Malta, E.A. Fitzgerald[*], J.B. Posthill, R.A. Rudder, G.C. Hudson, R.J. Markunas

Research Triangle Institute. Research Triangle Park, NC 27709-2194

[*]AT&T Bell Laboratories, Murray Hill, NJ 07974

A large effort continues in the development of diamond growth technologies for the production of electronic-grade diamond epitaxy[e,8,1]. Diamond has several properties such as a wide band gap (5.48 eV) and high thermal conductivity (2000 W $m^{-1}K^{-1}$) that make it desirable for electronic applications. Characterization of diamond with cathodoluminescence (CL) spectroscopy yields information on impurity and defect distributions with both spatial and energy resolution, providing insight into the growth process.

Diamond films were grown by plasma-enhanced chemical vapor deposition (PECVD) on natural type Ia 1mm × 1mm × 0.25mm diamond substrates. The results of microstructural studies on this type substrate are discussed elsewhere in these proceedings[2]. Two films were selected for CL analysis based on their strikingly different surface morphologies but similar growth conditions. Both were grown for 6 hours at a substrate temperature of ~750°C and a pressure of 5 Torr. The gas mixtures were varied: $CO/CH_4/H_2$ was used in one case and CH_4/H_2 in the other. Growth rates for both processes were estimated at 0.5μm/hr thus giving film thicknesses of ~3μm. Films were examined topographically by field emission scanning electron microscopy (FESEM). Wavelength-resolved CL spectroscopy was performed in another SEM using a 15keV electron beam and a sample temperature of 6°K.

The CL spectrum from the film grown with the CO-containing gas mixture (Fig. 1a) showed a major peak at 432nm with a shoulder at 472nm and minor peaks at 575nm and 602nm. The film grown with CH_4/H_2 (Fig. 1b) showed major peaks at 444nm and 478nm with a shoulder at 384nm. In both spectra, appearance of the large peaks in the 800-900nm range was attributed to second harmonics due to the unavailability of appropriate filters; their large size is due to the increased sensitivity of the detector in that range. Corresponding surface morphologies are presented in Figs. 1c and 1d. The $CO/CH_4/H_2$-grown film appeared very smooth with a speckled contrast. The CH_4/H_2-grown film contained pyramid-like protrusions and scattered crystalline diamond particles.

Emissions at 384nm and 575nm have been attributed to N-vacancy complexes[3]. Emissions at 472nm and 478nm are unknown, however, they have been observed in polycrystalline diamond[4]. An emission at 737nm attributed[5] to di-Si interstitials and possibly N was not observed in either case but could have been obscured by the second harmonic peaks. Emissions at 432nm and 444nm are termed "band A" emissions and have been associated with closely spaced donor-acceptor (D-A) pairs likely due to nitrogen and boron impurities segregated at defects[6]. Emission at 602nm has also been observed previously[4] in CVD diamond and is thought to be due to band A emission from more widely spaced D-A pairs. Monochromatic CL images (not shown) from the $CO/CH_4/H_2$-grown film using the 432nm peak revealed a cellular structure similar to that observed in natural diamonds[7]. TEM on those natural diamonds indicated the cellular structure was composed of dislocations. Images from the CH_4/H_2-grown film using the 444nm and 478nm peaks independently indicated non-radiative sites corresponding with the pyramid-like features shown in Fig. 1d on a uniform background. In studying individual diamond grains using CL in the TEM, Graham[6] has determined that grains containing moderate densities of defects emit band A CL strongly and those with very high or low defect densities emit very weakly. By analogy, our observations appear to indicate that the pyramid-like features on the CH_4/H_2-grown film have a different defect density than the surrounding epitaxial film. Independent of whether the defect density in the hillock regions is higher or lower, these features are undesirable,

614

The fact that pyramid-like defects are not observed in the $CO/CH_4/H_2$-grown film and spatial uniformity is observed with respect to band A luminescence, suggests the potential superiority of CO-containing growth chemistries over the more widely used CH_4, H_2 mixtures for homoepitaxial diamond growth[8].

References

1. R.A. Rudder et al., Appl. Phys. Lett. **60**, 329, (1992)

2. J.B. Posthill et al., This proceedings

3. L.H. Robins et al. Phys. Rev. B **39**, 13367 (1989)

4. R.J. Graham et al., Appl. Phys. Lett. **59**, 2463 (1991)

5. A.T. Collins et al., J. Mat. Res. 5 2507 (1990)

6. R.J. Graham et al., J. Appl. Phys. **69**, 3212 (1991)

7. Unpublished results obtained in our laboratory

8. The authors gratefully acknowledge the support of this work by the SDIO/IST through ONR (Contract No. N00014-92-C-0081)
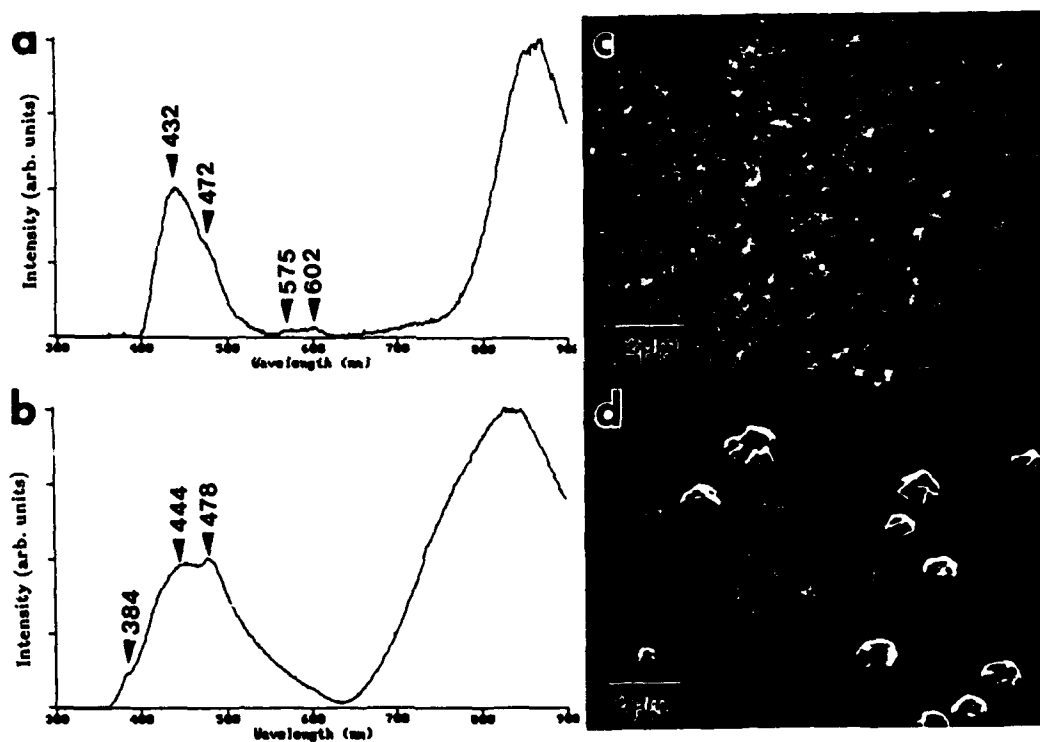
FIGURE 1: CL spectra and SEM topographical images of epitaxial diamond films grown by PECVD using gas mixtures of $CO/CH_4/H_2$ (a and c) and CH_4/H_2 (b and d)

615

GROWTH AND CHARACTERIZATION OF SiGe CONTACTS ON SEMICONDUCTING DIAMOND SUBSTRATES

T.P. Humphreys, P.K. Baumann, K.F. Turner and R.J. Nemanich
Department of Physics, North Carolina State University, Raleigh, North Carolina
27695-8202 USA.

R.G. Alley, D.P. Malta and J.B. Posthill
Research Triangle Institute, Research Triangle Park, North Carolina 27709-2194 USA.

Silicon-Germanium films have been grown by electron-beam deposition on
naturally occuring p-type semiconducting diamond C(001) substrates. As
evidenced by low-energy electron diffraction and scanning tunneling
microscopy the SiGe layers are polycrystalline. Corresponding current-voltage
(I-V) measurements conducted at room temperature have demonstrated the
formation of a low-barrier rectifying contact. Consistent with the observed
low-barrier height, the I-V measurements recorded at 300 °C exhibit ohmic-
behavior. In addition, subsequent post-growth annealing of the SiGe contacts
at 850 °C in ultra-high vacuum has shown an apparent degradation in the I-V
characteristics.

INTRODUCTION

At present, there is a significant scientific and technological interest in the
fabrication of stable ohmic and high-temperature rectifying contacts on diamond (1, 2).
To date, several metals (3, 4), refractory metal silicides (5) and semiconductors (6) have
been investigated as appropriate contact materials to semiconducting single crystal
diamond substrates. In particular, the authors have demonstrated that the deposition of
heteroepitaxial films of Ni on diamond exhibit excellent high-temperature rectifying
properties (4). Indeed, similar studies conducted on post-growth annealed $TiSi_2$ contacts
on diamond have also shown rectification at high-temperature (5). Moreover, it has also
been recently demonstrated by Venkatesan et al. (6) that highly doped polycrystalline Si
contacts fabricated on semiconducting diamond substrates form stable high-temperature
rectifying diodes. In particular, the Si / diamond heterostructure also affords the potential
of fabricating novel heterojunction devices which can be integrated with existing Si-
based processing technologies.

In the present study we report initial results pertaining to the growth and characterization of SiGe contacts deposited on natural p-type semiconducting diamond C(001) substrates.

EXPERIMENTAL PROCEDURE

Commercially supplied (D. Drucker & ZN.N.V) low-resitivity ($\sim 10^4 \; \Omega \cdot cm$, p-type) semiconducting natural diamond (surface orientation (001)) substrates were chemically cleaned. The cleaning procedure included boiling $CrO_3 + H_2SO_4$ (heated to 200 °C) for 10 min followed by immersion in aqua regia ($3HCl + 1HNO_3$) and standard RCA cleaning solutions. Following cleaning, the samples were mounted on a Mo sample holder and transferred into the electron-beam evaporation chamber. The base pressure in the system was typically 2×10^{-10} Torr. Prior to deposition, the substrates were heated to 550 °C for 5 minutes to thermally desorb both water vapor and possibly physi-adsorbed gas contaminants. On cooling to room temperature an unreconstructed (1x1) low-energy electron diffraction (LEED) pattern was observed from the C(001) surface. The substrate temperature was maintained at 550 °C and the SiGe films were grown by the co-deposition of Si and Ge using electron beam evaporation. The corresponding Si and Ge fluxes were calibrated to obtain SiGe layers with a 5% Ge composition. By employing a stainless steel shadow mask several SiGe dots of ~200 nm in thickness and 3×10^{-3} cm^2 in area were fabricated. Subsequent post-growth *in-situ* annealing of the samples was performed at a temperature of 850 °C at 10^{-8} Torr for 30 min.

RESULTS AND DISCUSSION

Examination of the as-grown films by LEED failed to obtain an ordered surface structure. Indeed, an inspection of the SiGe films by *ex-situ* scanning tunneling microscopy (STM) showed a highly textured surface morphology which indicated that the deposited layers were polycrystalline, as shown in Fig. 1. The STM image was obtained in the constant current mode with a tip bias of 2 V. The presence of small polycrystalline grains of ~100 nm is clearly evident. The corresponding rms surface roughness of the deposited layer has been determined to be ~ 5 nm. Also, it was apparent that the SiGe films exhibit excellent adhesion properties with the underlying diamond substrate. In contrast, STM images of the annealed films were much more difficult to obtain due to their higher resistivity. As shown in Fig. 2, the surface morphology of the annealed films was significantly smoother with a corresponding rms surface roughness of ~ 3 nm and an apparent increase in grain size.

Shown in Fig. 3 is the Raman spectrum of the SiGe films obtained at room temperature using an Ar^+ ion laser (514.5 nm) excitation source. Clearly observed are two distinct phonon peaks pertaining to Si and Ge at 518 cm^{-1} and 300 cm^{-1}, respectively. It is interesting to note that the corresponding SiGe phonon mode, indicative of alloy formation (near 400 cm^{-1}) was not observed. The absence of the SiGe phonon mode would tend to suggest an apparent segregation and clustering of Si and Ge during growth. Differences in the Si and Ge surface mobilities and/or surface energies on the chemically cleaned diamond C(001) surface during the initial stages of growth may account for this behavior (7). Further studies are currently in progress to study this growth phenomena. Following the high-temperature ultra-high vacuum annealing step only the Si phonon peak was observed in the Raman spectrum. The absence of the Ge phonon mode in the layer was attributed to the evaporation of Ge during thermal annealing.

Current-voltage (I-V) measurements were obtained by mounting the diamond substrates on a Cu plate using Ag paint to form a large area back contact and applying a bias to the SiGe contact using a W probe. The room temperature I-V characteristics obtained for the as-deposited SiGe contacts on semiconducting diamond substrates are shown in Fig. 4. The rectifying character of the SiGe contact is clearly evident. From the I-V measurements a small forward bias turn-on voltage of ~ 0.6 V was estimated. The corresponding reverse bias leakage current density was measured to be ~1.56 x 10^{-6} A / cm^2 at 20 V. Moreover, from the apparent linear region of the semilogarithmic plot of the forward characteristics an ideality factor n of 2.5 was calculated. This high n value may be an indication that the current conduction at the SiGe/diamond interface is not governed by a thermionic emission mechanism. It is interesting to note that similar observations have also been reported for Ni, $TiSi_2$ and Si contacts on semiconducting diamond C(001) substrates (4-6). In each of these studies current conduction appeared to be dominated by a space charge limited current (SCLC) mechanism. Consistent with the small turn-on voltage and the relatively high reverse leakage current, the corresponding I-V measurements recorded at 300 ^oC exhibit ohmic-like behavior.

Shown in Fig. 5 is the corresponding I-V characteristics for the high-temperature annealed SiGe contacts recorded at 25 ^oC. Clearly, in comparison with the as-deposited films, the rectifying behavior of the annealed SiGe contacts has been degraded. In particular, the forward bias turn-on voltage has been significantly reduced. From the I-V measurements a forward bias turn-on voltage of ~ 0.2 V has been estimated. Also, the reverse bias leakage current has increased to ~22 nA which corresponds to a current

density of 7.3×10^{-6} A/cm^2 at 20 V. In addition, corresponding I-V measurements conducted at 300 °C showed ohmic-like behavior.

CONCLUSIONS

In summary SiGe films have been grown by the co-deposition of Si and Ge on natural single crystal diamond C(001) substrates. As evidenced by LEED and STM analysis, the as-deposited films are polycrystalline. The I-V measurements of the SiGe contacts have demonstrated rectifying characteristics at room temperature. However, for measurements conducted at 300 °C the I-V characteristics exhibit ohmic-like behavior. Furthermore, it has also been demonstrated that subsequent post-growth annealing of the contacts has degraded the I-V characteristics.

ACKNOWLEDGMENTS

REFERENCES

1. M.W. Geis, N.N. Efremow and D.D. Rathman, J. Vac. Sci. Technolol. 6, 1953 (1988).

2. For a review see K. Das, V. Venkatesan, K. Miyata, D.L. Dreifus and J.T. Glass, Thin Solid Films. 212, 19 (1992).

3. K.L. Moazed, J.R. Zeidler and M.J. Taylor, J. Appl. Phys. 68, 2246 (1990).

4. T.P. Humphreys, J.V. LaBrasca, R.J. Nemanich, K.Das and J.B. Posthill, Jpn. J. Appl. Phys. 30, L1409 (1991).

5. T.P. Humphreys, J.V. LaBrasca, R.J. Nemanich, K.Das and J.B. Posthill, Electron. Lett. 27, 1515 (1991).

6. V. Venkatesan, D.G. Thompson and K. Das, proceedings of Symp. Mater. Res. Soc. 270, 419 (1992).

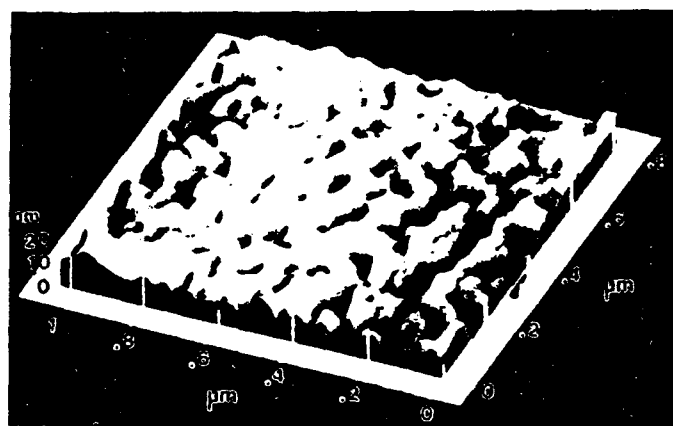7. P.C. Kelires and J. Tersoff, Phys. Rev. B 63, 1164 (1989).

Fig. 1 Topographic (constant current) STM micrograph of the surface morphology of the SiGe film deposited on natural diamond C(001) substrates.
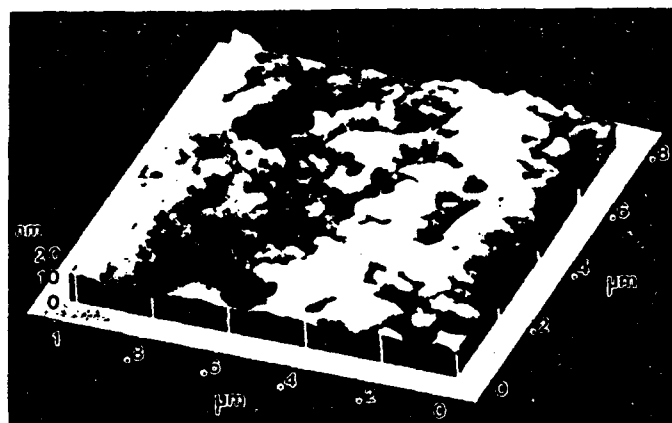

Fig. 2 Topographic (constant current) STM micrograph of the surf.ce morphology of the as-deposited SiGe film following a high-temperature anneal at 850 °C in a vacuum of 10^{-8} Torr for 30 min.
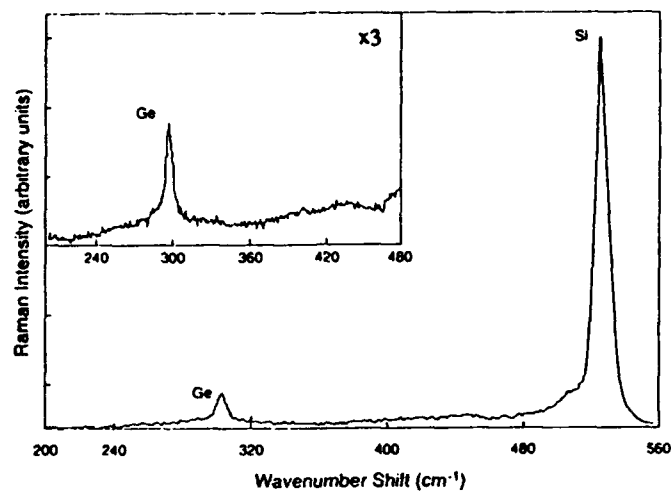
Fig. 3 Raman spectrum of the SiGe film deposited on natural C(001) diamond
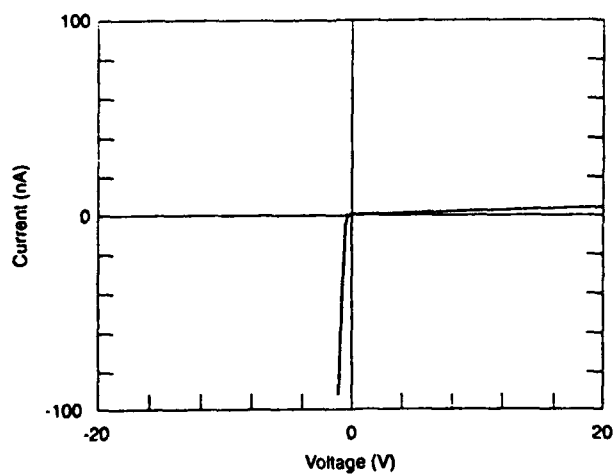substrates.

Fig. 4 Linear plot of the current-voltage (I-V) characteristics of the SiGe contacts on
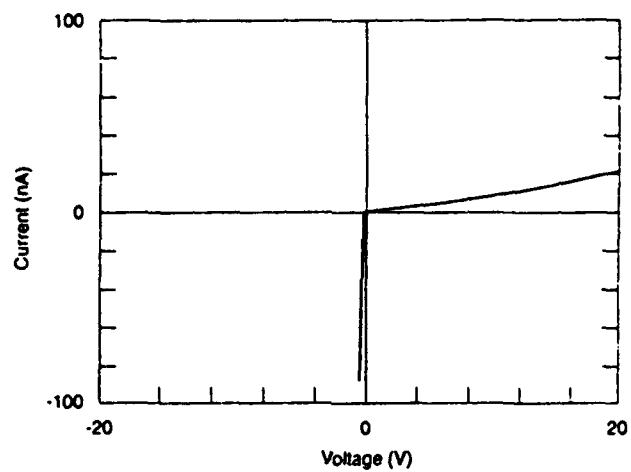semiconducting diamond C(001) substrates. Measurements were conducted at
25 °C.

Fig. 5 I-V characteristics of the post-growth high-temperature annealed SiGe contacts at
25 °C.

A SURVEY OF LOCAL CARBON SOURCES FOR ENHANCING DIAMOND NUCLEATION

R.A. Rudder, G.C. Hudson, R.E. Thomas, J.B. Posthill, and R.J. Markunas
Research Triangle Institute, P. O. Box 12194, Research Triangle Park, NC , 27709

ABSTRACT

Diamond nucleation on non-diamond substrates is an issue that has been widely studied. Many authors have correlated diamond nucleation with advantageous carbon on the wafer surface. However, the chemical constituency and the role of the carbon on the wafer surface have not been rigorously established. We have undertaken nucleation studies wherein a survey of carbon species have been applied to Si wafers without physical abrasion by diamond polish. Experiments were performed in a low pressure rf-induction plasma system using H_2-CH_4. The carbon species applied to the surface ranged from graphite powders to fluorocarbon polymers to hydrocarbon polymers to polycarbonates. These experiments show that many local carbon species promote diamond growth. We suspect that these carbon sources contribute to diamond nucleation by substantially changing the C/H/O ratios nearby the surface without distorting the balance of C/H/O in the gas phase region of the plasma. It is critical that the carbon sources upon dissolution not distort the C/H/O ratio in the plasma region, if the nucleation is to occur under conditions of high quality diamond growth (i.e., high atomic H flux).

I. INTRODUCTION

Chemical vapor deposition (CVD) of diamond films has attracted great attention in the scientific and industrial community. The extreme properties of diamond (hardness, optical transparency, thermal conductivity, etc.) offer opportunities for commercial application. Almost all of these opportunities require that diamond deposit onto a host substrate. The most traditional method for insuring diamond nucleation is to treat the host substrate with diamond powder prior to introduction into the CVD system.[1-4] These diamond treatments have involved polishing or ultrasonic techniques utilizing typically 1μm size diamond grit. Many studies have expounded the role of this diamond pretreatment. Such techniques are very successful in enhancing diamond nucleation. Diamond nucleation proceeds on residual diamond providers, at protruding surface features[5], and perhaps at unique defect sites on the Si surface. In some work, researchers have enhanced the effect of the diamond polish by performing the polish with an oil-base.[6] For many applications, this method may be totally satisfactory. However on many substrates, the damage to the substrate is intolerable. Furthermore, diamond treatments can aggravate diamond adherence problems by resulting in diamond growth on residual powders rather than diamond growth directly to the substrate material. It is, thus, highly desired to develop alternative diamond nucleation techniques wherein no diamond is applied to the substrate surface.

This paper reports on the enhancement of diamond nucleation by various "local" carbon sources which are applied to the surface prior to introduction to the CVD system. We choose to refer to these carbon sources as local to the substrate to distinguish them from gas-phase carbon as supplied by the gaseous feedstock. Previous work[7] by ourselves has shown that graphite fibers (3 - 5 μm diam.) when placed on a substrate, enhance the nucleation of diamond on the area of substrate that is directly underneath the graphite fiber. We postulate that the dissolution of the fiber changes the local gas phase carbon concentration near the substrate such that diamond nucleation is enhanced local to the dissolving fiber. It is critical not to distort the plasma gas-phase concentration. Distortion of the plasma-gas phase carbon concentration will compromise the atomic hydrogen generation.[8,9] Under these conditions, poor quality crystals would grow at the nucleation sites. The previous graphite fiber work stimulated a study to investigate the effects of various local carbon sources.

II. EXPERIMENTAL APPROACH

The system used here for the growth of diamond has been reported on previously. It is a low-pressure rf-induction plasma system operating at 13.56 MHz. This system has typically operated at pressures less than 10 Torr. The work here has been at 5 Torr. This low-pressure rf-induction system has deposited diamond from a wide variety of feedstocks including H_2/CO, H_2/CH_4, H_2/CF_4, H_2O/CH_4O, H_2O/C_2H_6O, and H_2O/C_3H_8O The work here has concentrated on nucleation enhancement using H_2/CH_4 gas. We chose to standardize the conditions at 5 Torr, 2000 W, 30 sccm of 1% CH_4 in H_2, and 800°C. The substrate temperature of 800°C is reached both through eddy-current-heating of a graphite susceptor upon which the substrate rest and through radiative heating of the susceptor by a nearby graphite resistive element. The low-pressure rf-induction plasma is observed to be confined within the 50μm dia quartz tube between the turns of the rf coil. The graphite susceptor resides 15 μm from the boundary of the intense plasma. It should be noted that the graphite susceptor supplies carbon to the gas phase through atomic-H dissolution. The area of graphite is equivalent to the area of the silicon samples which have been treated with the local carbon sources. All the effects observed here from the various local carbon sources occur under atomic H gasification of the graph susceptor. Despite the graphite susceptor dissolution in all experiments, rather dramatic differences are observed between various local carbon sources. This observation attests to the local effect of the surface carbons.

This study addressed the use of local carbon sources with varying chemical constituency, bond order, and saturation. Fluorocarbons, carbohydrates, hydrocarbons, and graphite, were applied to Si (100) surfaces. An effort was made not to abrade the surfaces during the application of these carbon sources to the surface. Teflon (without "black" pigment) was tested as a local fluorocarbon source. Sucrose was tested as a local carbohydrate source. Photoresist was tested as a local hydrocarbon source. Graphite fibers were crushed into powder and applied to a Si (100) surface as a local graphite source. No precautions were taken to control the thickness between the various pretreatments 100nm of photoresist was applied. 0.5 μm of teflon was applied. The sucrose layer thickness was not accurately known but probably was 1-5μm. The graphite powders were crushed from 3μm diam fiber stock without 100% coverage and then were dispersed on the silicon wafer.

3

III. EXPERIMENTAL RESULTS AND DISCUSSION

All carbon sources showed some nucleation enhancement as compared to an untreated Si wafer. Few of the local carbon sources showed nucleation enhancement comparable to that obtained by diamond scratching/polishing with 1 µm diamond paste. The graphite powder treatment produced a nucleation density comparable to diamond scratching. Teflon and sucrose produced substantial diamond nucleation enhancement. Photoresist showed little, if any, nucleation enhancement. All the local carbon sources, except the diamond crystal, were dissolved rapidly in the CVD growth environment.

Figures 1 and 2 shows SEM photographs of Si wafers treated with photoresist, sucrose, teflon, and graphite powders prior to introduction into the CVD chamber. In some cases, the dissolution produced observable changes in plasma emission while the carbon sources were being gassified. Saturated local carbon source such as carbohydrates and fluorocarbons are "labeled" with oxygen atoms and flourine atoms, respectively. One can observe their effect on the global gas phase concentration by a visible change in the plasma emission upon dissolution. Furthermore, their rapid dissolution does not persist long enough to greatly enhance diamond nucleation. From Figures 1d and 2d, it is apparent that the graphite powders were the most successful at diamond nucleation enhancement.

During the dissolution period, surface carbons are locally changing the gas phase concentration. Atomic hydrogen is being depleted from the gas phase as the hydrocarbon concentration is increasing. The high gas phase carbon concentration creates nucleation sites for diamond growth. Indeed other workers have used a "bilayer" processes for obtaining densely nucleated diamond films.[10] With a bilayer process, a standard diamond polished wafer showed higher diamond nucleation, if diamond was nucleated on it under microwave plasma conditions rich in carbon. This approach was also demonstrated in an oxy-acetylene diamond growth.[11] Unfortunately, nucleation conditions were conditions rich in gas-phase-carbon. This over abundance of carbon quenches the atomic H population in the gas phase. As a consequence, small grain, poor diamond is produced at the diamond/substrate interface. In this work here, the local carbon sources dissolve producing a high gas-phase carbon concentration local to the dissolution site. While the dissolution contributes hydrocarbons to the gas-phase in the plasma region, the gas-phase concentration in the plasma is much lower than at the Si surface due to volume dilution. As a consequence, the atomic hydrogen flux to the

nucleating surface is not compromised. High quality crystals are nucleated. Thus, local carbon sources create conditions of carbon supersaturation in the gas phase nearby the carbon source without compromising atomic H generation from the plasma.

Thus, local graphite sources are seen as an ideal alternative to diamond pretreatments for nucleation enhancement. The dissolution rate is high enough to enhance local nucleation without seriously degrading the global gas-phase concentration. Remember, that the samples are resting on a graphite susception which is contributing gas-phase carbon. The global-gas-phase carbon concentration is controlled by the susception dissolution and the methane to hydrogen ration in the feedstock. The local graphite carbon sources then enable a partial separation of control variables. High quality, high rate diamond deposition demands the ultimate in atomic H flux. Yet, carbon addition into the global gas phase has been reported to reduce the atomic H generation in the gas phase. By introducing local graphite carbon sources, the carbon concentration at the nucleating surface is greatly increased without compromising the atomic H flux generation from the plasma. In addition, it is hoped that the nucleation sites produced by the local change in carbon concentration under still high atomic H flux will improve the adherence and quality of the diamond nuclei. Thus, improving the performance of diamond thin film products.

IV. CONCLUSIONS

Various local carbon sources have been tested for nucleation enhancement. Of the sources tested (photoresist, sucrose, teflon, graphite powders), the graphite powders demonstrated the highest nucleation enhancement. The work here with various carbon sources shows a tendency for longer the carbon chain species to promote more nucleation. Graphite powders are then seen as an ultimate long chain carbon. Graphite dissolves at a slower rate than hydrocarbons, carbohydrates, or fluorocarbons due to its unsaturation, every carbon atom requiring at least 2 hydrogen atoms to complete gasification (i.e. acetylene) or at least 4 hydrogen atoms to complete gasification (i.e. methane) . This work demonstrates an alternative nucleation technique which avoids physical abrasion the substrate with diamond powder. It preserves the plasma gas-phase carbon concentration, thus maintaining high atomic H flux, while local to the nucleation sites providing carbon super-saturation. Diamond growth occurs on surface sites intrinsic to the substrate and not on residual diamond powder. It is thus hoped that the use of local carbon sources such as graphite will promote better adherence between the diamond film and the substrate.
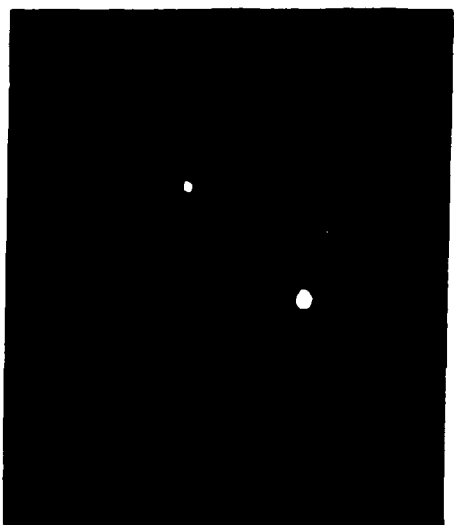
ACKNOWLEDGMENTS

REFERENCES

1.   B.V. Spitsyn, L.L. Bouilon, B.V. Deraguin, J. Cryst. Growth 52, 223 (1981).

2.   N. Setaka, Research Report No. 39, National Institute for Research in Inorganic Materials (1989).

3.   D. M. Tung, W.L. Hsu, and K.E. McCarty, Electrochem. Soc. Proc. 89-12, 500 (1989).

4.   Y. Liou, A. Inspektor, R. Weimer, D. Knight, and R. Messier, Mat. Res. Soc. Proc. 1662, 109 (1990).

5.   Paul A. Dennig and David A. Stevenson, *Applications of Diamond Films and Related Materials*, Materials Science Monographs 73, 383 (1991).

6.   Pehr. E. Pehrsson, A.A. Morrish, *New Diamond Science and Technology*, MRS Int. Conf. Proc. 397 (1991).

7.   R. A. Rudder, G. C. Hudson, R. C. Hendry, R. E. Thomas, J. B. Posthill, and R. J. Markunas, *Applications of Diamond Films and Related Materials*, Materials Science Monographs 73, 295 (1991).

8.   F. G. Celii and J. E. Butler, Applied Physics Letters 54, 1031 (1989).

9.   L. Schafer, C. P. Klages, U. Meier, and K. Kohse-H oinghaus, Applied Physics Letters 58, 571 (1991).

10.   Koji Kobashi, Kozo Nishimura, Koichi Miyata, Kazuo kumagi, and Akimitsu Nakane, J. Mater. Res. 5, 2469 (1990).

11.   K.V. Ravi and C.A. Koch, Appl. Phys. Lett 57, 348 (1990)

FIGURE CAPTIONS

Figure 1:   Low magnification SEM photographs of diamond deposition on Si(100) wafers which were treated with a) photoresist, b) teflon, c) sucrose, d) graphite powers, and e) diamond scratched.

Figure 2:   High magnification SEM photographs of diamond deposition on Si(100) wafers which were treated with a) photoresist, b) teflon, c) sucrose, d) graphite powers, and e) diamond scratched.
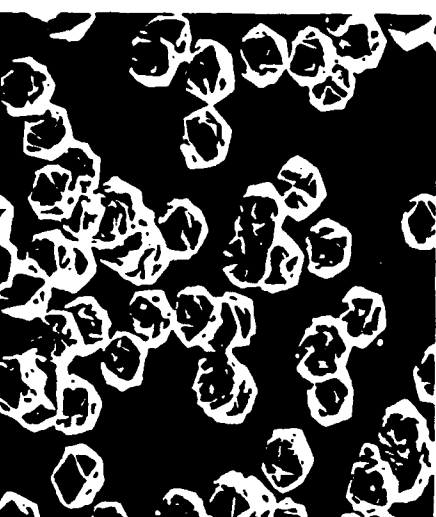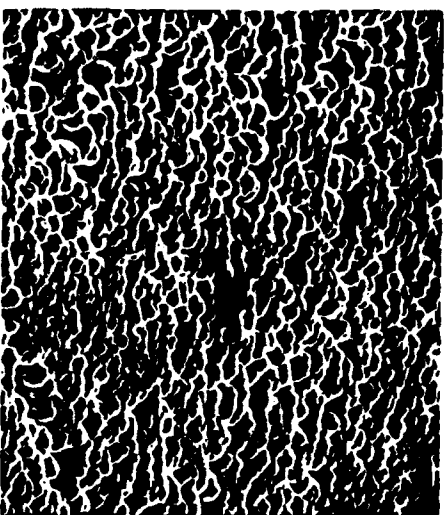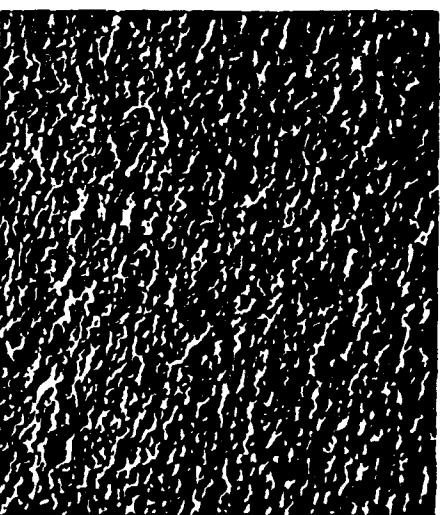
1a

1d 15 μm 15 μm
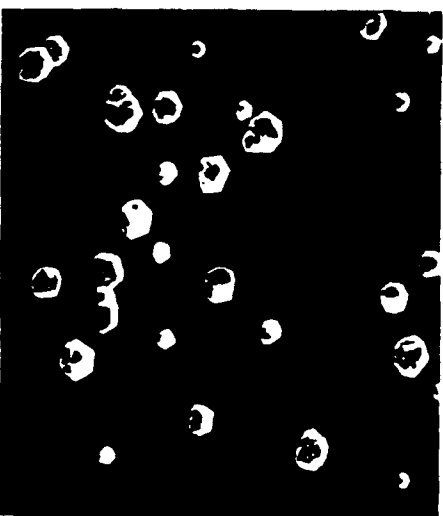
1e 15 μm 15 μm

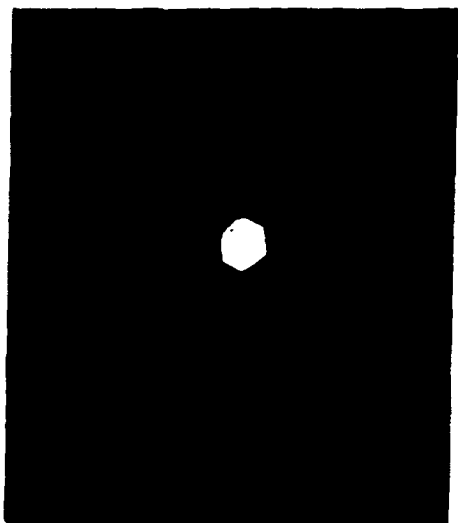1b 15 μm

1c 15 μm

2a

5 μm

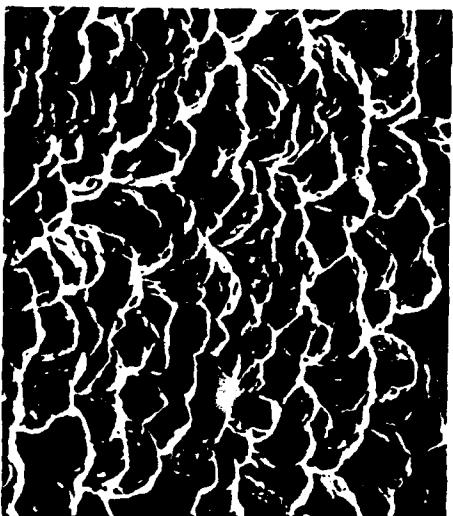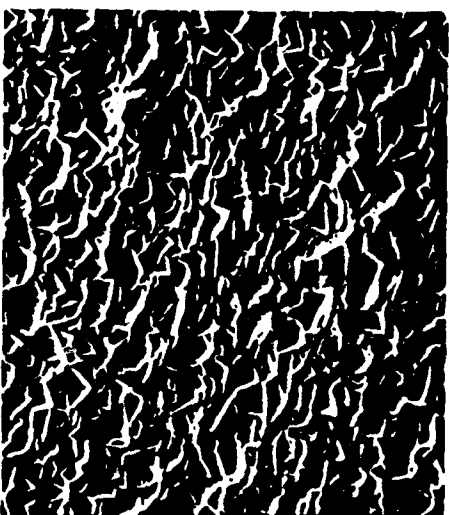2b

5 μm

2c

5 μm

2d

5 μm

2e

5 μm

DIAMOND SURFACE STUDIES OF GROWTH MECHANISMS FROM WATER- ALCOHOL DEPOSITION CHEMISTRIES

R.E. Thomas, J.B. Posthill, R.A. Rudder, and R.J. Markunas
Research Triangle Institute, Research Triangle Park, NC 27709

M. Frenklach
Department of MS&E, Pennsylvania State University,
University Park, PA 16802.

In this paper we will be presenting results from basic surface chemistry studies of interactions of atomic oxygen, atomic hydrogen and acetylene with single crystal diamond (100) surfaces. Measurements of oxygen terminated surfaces indicate an activation energy of approximately 44 kcal/mole for CO desorption and 21 kcal/mole for CO_2 desorption. Thermal desorption and LEED studies of C(100)-1×1:O surfaces indicates that the reconstruction upon CO desorption occurs in the temperature range of 450-525°C. Annealing of oxygenated surfaces in an atomic hydrogen flux does not appear to appreciably delay the onset of the reconstruction. Thermal desorption studies also indicate that CO will desorb from both saturated and partially oxygenated surfaces at temperatures in the 200-250°C range. Experiments with C^{13} homoepitaxial films indicates that C_2H_2 will preferentially adsorb at room temperature on oxygenated surfaces that have been partially desorbed. The CO desorption appears to open sites at < 300° which will easily react with acetylene.

INTRODUCTION

Hydrogen plays an integral role in many of the CVD diamond growth processes developed to date.[1] Hydrogen is thought to function in the growth process in a number of ways, including maintenance of sp^3 hybridization of carbon atoms at the growth surface Oxygen has been used in concentrations of approximately 1-2% in H_2/CH_4 plasmas to extend the diamond growth regime with respect to gas composition and substrate temperature [2,3] The role oxygen plays is perhaps more complicated. It has been suggested that oxygen increases the atomic hydrogen concentration through gas phase reactions and also etches non-diamond carbon.[2] Oxygen will also desorb from the diamond surface at temperatures much lower than hydrogen, this may allow sites to open at the surface for the addition of carbon.[4] Recently, however, oxygen has been introduced to the growth process in much larger concentrations in the form of water and alcohols.[5] In spite of numerous growth studies, the details of the roles of hydrogen and oxygen in the CVD growth environment are still unclear, as are fundamental questions concerning interactions of these two gasses with the diamond surface. Important questions remain concerning the details of the reconstruction and the effect of adsorbates on surface structure. In order to greatly simplify the systems under consideration, we have used a combination of low pressure gas dosing, temperature programmed desorption, and low energy electron diffraction (LEED) to study interactions of relatively simple gasses such as atomic hydrogen and atomic oxygen with a clean diamond surface. We have also studied the addition of carbon to the diamond surface in the form of acetylene reactions with partially deoxygenated (100) surfaces.

EXPERIMENTAL PROCEDURES

A full description of the experimental procedure is available in earlier publications and only a brief review is given here.[4] Thermal desorption spectroscopy and LEED observations were performed in a stainless steel UHV system. Sample heating was accomplished by clipping the crystals to a 0.25mm thick molybdenum resistive strip heater. The sample temperature was measured by a 0.125mm diameter chromel/alumel thermocouple threaded through a laser drilled hole in the diamond and held in tension against the crystal face. Two type IIa (100), 5×5× 0.25mm, diamond crystals were used in the course of the present study. In order to be able to more clearly differentiate CO desorbing from the sample surface, a homoepitaxial C^{13} layer was grown on the substrates. Thermal desorption from samples before and after C^{13} deposition shows no difference, aside from an increase in sensitivity, in the CO and H_2 desorption features. Approximately 2000 Å of diamond was deposited in an rf plasma reactor with a $H_2/C^{13}H_4$ discharge. To clean the surfaces, the samples are initially hand polished 5 minutes with 0.25 μm diamond grit, followed by solvent rinses. The samples are then placed in a CrO_3/H_2SO_4 (125°C) solution for 20 minutes to remove non-diamond carbon. The samples are rinsed in DI water and then boiled in a 3:1 solution of HCl/HNO_3 for 20 minutes to remove any metals contamination. Samples subjected to this cleaning process typically show a good quality 1×1 LEED pattern at beam voltages as low as 50 volts with no annealing. Auger spectroscopy of the diamond surfaces as introduced to the chamber indicates that the surface is left O-terminated following the acid cleaning. In all cases atomic hydrogen for dosing was generated via a tungsten filament operating at a temperature of approximately 1500°C. Filament temperatures were measured with a hand held optical pyrometer. Atomic oxygen was generated via an iridium filament at 1100°C. VLSI grade hydrogen and oxygen gasses were used with no further purification. No attempt was made to quantify the percentage of atomic species generated by the filaments.

RESULTS

CO and CO₂ Desorption Kinetics.

Figure 1 shows results for CO thermal desorption from oxygen covered surfaces as a function heating rate. Samples were dosed to saturation with atomic oxygen and then thermal desorption spectra were acquired at set heating rates. The activation energy is easily extracted by measuring the peak maximum and plotting $\ln(T_m^2)\beta$ vs $1/T_m$, where β refers to the heating rate and T_m refers to the temperature of the maximum desorption rate.[6] The slope of the resulting line then gives the activation energy. Since the heating rate appears in a logarithmic function, it must be varied as widely as possible. Heating rates from 2°C/s to ~ 18°C/s were used. The analysis technique also depends on several assumptions; ν (frequency factor) and E_a (activation energy) are independent of coverage and the initial surface coverage is the same for each temperature ramp. The derivation on which the activation energy extractions is based is rigorously correct only for first-order desorptions. However, simulations for second-order desorptions indicates errors of < 2% are observed when applying this analysis to second-order desorption kinetics.[6]. In the present study there is a much greater variability in the data. Using this approach, an activation energy of approximately 44 kcal/mole was obtained for CO desorption. A similar analysis for CO_2 desorption gives an activation energy of approximately 21 kcal/mole.

H/O Interactions on the C(100) Surface.

Unlike atomic hydrogen adsorption, atomic oxygen adsorption will convert the 2×1 surface to the 1×1 configuration.[4]. In the next series of experiments the effect of oxygen coverage on the conversion back to the 2×1 state was studied along with the influence of atomic hydrogen on the process. The state of the surface was determined by LEED while the oxygen coverage, relative to saturation, was determined by thermal desorption spectroscopy. Figure 2 shows a series of CO desorption curves where the surface was saturated with oxygen and then annealed at the indicated temperatures. The samples were cooled before performing LEED and thermal desorptions. LEED indicates that the surface converts to the 2×1 configuration between 450°C and 525°C for 10 minute anneals. At this point there is 35-50% coverage of oxygen, relative to the saturated surface.

The adsorbed oxygen appears to have some ability to stabilize the 1×1 configuration on the surface, but as more oxygen is lost the surface eventually converts to the 2×1 configuration. We know that exposure of the 2×1 surface to atomic hydrogen does not readily result in a 1×1 configuration but in a growth environment the surface is continually exposed to atomic hydrogen.[4]. Would atomic hydrogen stabilize the 1×1 configuration if supplied while oxygen gradually left the surface? Figure 3 shows results where oxygen saturated surfaces were annealed in an atomic hydrogen flux. The samples were then cooled to room temperature and LEED taken on the surface. Finally, thermal desorption spectra were obtained to determine the relative concentrations of H & O remaining on the surface. The curves obtained for the 500 and 625°C anneals are very similar, except that slightly less CO desorbed from the surface after annealing at 650°C. Both surfaces appeared by LEED to be left in the 2×1 configuration after annealing and hydrogen dosing. The atomic hydrogen does not appear to be able to stabilize the surface in the 1×1 configuration upon desorption of CO.

Acetylene Adsorption on CO Desorption Sites

We are clearly able to desorb CO from the surface at relatively low temperatures, and earlier work has shown that oxygen will desorb at low temperatures even for low surface coverages, < 10% [4]. If the surface does not reconstruct there will be two dangling bonds left where a carbon atom has left the surface. This should be an extremely active site and may easily accommodate a small hydrocarbon such as acetylene.[7] Figure 4 shows results of an experiment where this idea was tested. Several control experiments were performed to determine that acetylene was preferentially adsorbing on CO desorption sites. Figure 4a shows thermal desorption results from a sample where atomic oxygen was adsorbed to saturation and then the sample was exposed to acetylene. The diamond substrate consists of a C^{13} homoepitaxial layer and conventional C^{12} acetylene was used to determine if carbon addition had occurred. Masses 2, 26, 27, 28, and 29 were scanned and desorption was observed only for mass 29 or $C^{13}O$. In the second experiment, Fig. 4b, the sample was first exposed to acetylene and then atomic oxygen. Again, no evidence is seen of $C^{12}O$, to indicate acetylene adsorption. Acetone is a common contaminant of acetylene and a third control experiment was performed where the sample exposed only to acetylene. In this case neither $C^{12}O$ or $C^{13}O$ was observed. It is only for the final case, Fig 4c, that we see evidence of acetylene adsorption. In this case the oxygenated surface was partially desorbed at 350°C to approximately 85-90% oxygen coverage and then

exposed to acetylene at room temperature. Thermal desorption shows clear evidence for both $C^{12}O$ and C^{13} desorption.

DISCUSSION

Desorption Kinetics

Activation energies of 44 kcal/mole and 21 kcal/mole were measured for CO and CO_2 desorption respectively. We have not found references to earlier measurements of activation energies, but the temperatures reported here for CO desorption agree well for CO desorption from both graphite and from diamond powder [8,9,10]. For the diamond powders the desorption maximum is observed at approximately 600°C at a heating rate of .333°C/s. In contrast we observe a maximum at ~ 500°C for desorption from the C-(100) face and for a heating rate of .5° C/s. There are several experimental differences that may account for the differences observed in desorption maxima. For the powder desorptions, molecular oxygen was adsorbed at 420°C at 7.5 $\times 10^{-3}$ Torr. In the present study atomic oxygen was adsorbed, at room temperature, at an effective pressure < 1×10^{-7} Torr. In addition Fig. 3 shows the effect of annealing in shifting the desorption peak maxima to higher temperatures. However, for graphite, and certainly for diamond powders, a variety of crystallographic faces and sites are exposed. It may be that oxygen desorption from the (111), (110) faces, or sites not present in quantity on the (100) face of diamond, may show very different kinetics from those observed on the (100) face. There is some evidence of this from graphite desorptions where two distinct CO peaks are observed [9,10].

H/O Interactions

Oxygen terminated samples were annealed under an atomic hydrogen flux. We were interested in determining if hydrogen supplied during the CO evolution would be able to prevent the surface from reconstructing to the 2×1 configuration. Annealing at 550°C and 625°C converts the surface to the 2×1 configuration in spite of the hydrogen flux. At 800°C the oxygen has entirely left the surface and again the surface converts to the 2×1 configuration in spite of the atomic hydrogen flux. It does not appear that atomic hydrogen is particularly successful at maintaining the sp^3 coordination. We have observed in earlier work that hydrogen will not convert a 2×1 surface to the 1×1 configuration [4]. This of course is for the relatively low atomic hydrogen fluxes we are able to obtain in UHV with filament sources. Fluxes are obviously much greater under growth conditions which may allow the insertion reaction to proceed. Calculations on the (100) surface, however, indicate that there are steric hindrances to achieving a fully saturated dihydride phase on the (100) surface [11]. Also of interest in the growth environment is the ability of oxygen to displace hydrogen on the surface. We find that the removal of hydrogen by oxygen proceeds much faster than the reverse reaction. Depending on the relative rates of these two reactions under growth conditions this result has obvious implications for the role of oxygen in the growth environment. Based on these results it appears that oxygen will much more efficiently open sites for addition of carbon than hydrogen, both by hydrogen removal and by CO desorption.

Acetylene Adsorption

Removing a CO molecule, whether the oxygen is double bonded to the individual carbon atom or bridge bonded to two adjacent carbon atoms on the surface, requires two carbon-carbon

bonds to be broken. If all the oxygen from a saturated surface was desorbed an entire layer of carbon atoms would be removed and the surface would reconstruct to the 2×1 configuration. For a partial desorption the carbon atoms with dangling bonds are in the next plane of atoms down from the surface. The surrounding lattice can then contribute to keeping this site from reconstructing. The thermal desorption data show that at room temperature acetylene will only adsorb on surfaces that have been prepared in such a way as to leave these sites open. Methyl radicals, CO, and methane may also react at these sites. However for there to be a net addition of carbon to the surface, two carbon atoms have to be added each time a CO molecule desorbs.

SUMMARY

Atomic oxygen adsorption on the C(100)-2×1 surface will convert the surface back to the 1×1 configuration. Surfaces with full or partial oxygen coverages will lose oxygen from the surface through CO desorption at relatively low temperatures, < 300°C. The partial desorption of CO from the (100) surface presumably leaves two dangling bonds, which appear to preferentially adsorb acetylene. In addition it appears that atomic oxygen is much more efficient at removing hydrogen bonded to the diamond surface, than atomic hydrogen will remove oxygen adsorbed on the surface.

ACKNOWLEDGMENTS

REFERENCES

1.   See references in "Proceedings of the Second International Conference on New Diamond Science and Technology", edited by R. Messier, J.T. Glass, J.E. Butler, and R. Roy (Materials Research Society, Pittsburgh, PA, 1991).

2.   J.A. Mucha, D.L. Flamm, and D.E. Ibbotson, *J. Appl. Phys.* 65, pp. 3448 (1989).

3.   S.J. Harris, and A.M. Weiner, *Appl. Phys. Letts.* 55, pp. 2179 (1989)

4.   R.E. Thomas, R.A. Rudder, and R.J. Markunas, *J. Vac. Sci.* Tech. A, 10, pp. 978 (1992).

5.   R.A. Rudder, G.C. Hudson, J.B. Posthill, R.E. Thomas, R.C. Hendry, D.P. Malta, R.J. Markunas, T.P. Humphreys, and R.J. Nemanich, *Appl. Phys. Lett.*, 60, pp. 329 (1992).

6.   F.M. Lord, and J.S. Kittleberger, *Surf. Sci.*, 43, pp. 173 (1974).

7.   D. Huang, and M. Frenklach, *J. Phys. Chem.*, 96, pp. 1868 (1992).

8.   S. Matsumoto, Y. Sato, and N. Setaka, Carbon 19, pp. 232 (1981)

9.   B. Marchon, J. Carrazza, H. Heinemann, and G.A. Somorjai, Carbon, 26, pp. 507 (1988).

10.   M.J. Nowakowski, J.M. Vohs, and D.A. Bonnell, *Surf. Sci. Letts.*, 271, L351 (1992).

11.   Y.L. Yang, and M.P. D'Evelyn, *J. Am. Chem. Soc.*, 114, pp. 2796 (1992)
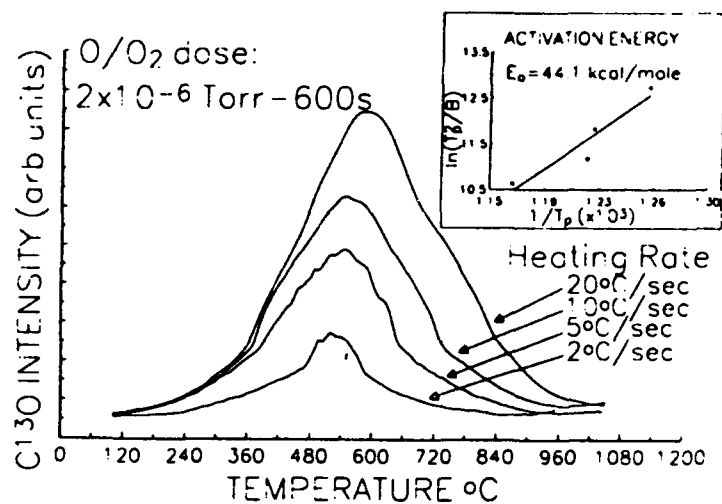
Figure 1 Plot of $C^{13}O$ desorption as a function of heating rate to extract the activation energy for desorption.
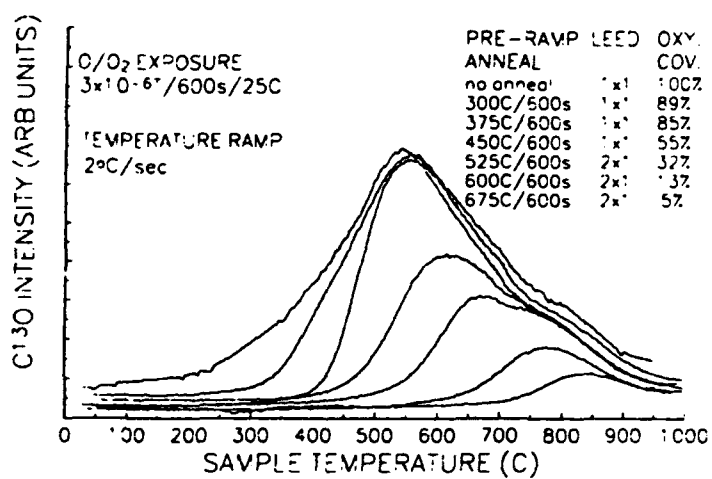

Figure 2. Plot of $C^{13}O$ desorption spectra from oxygen saturated surfaces as a function of annealing.
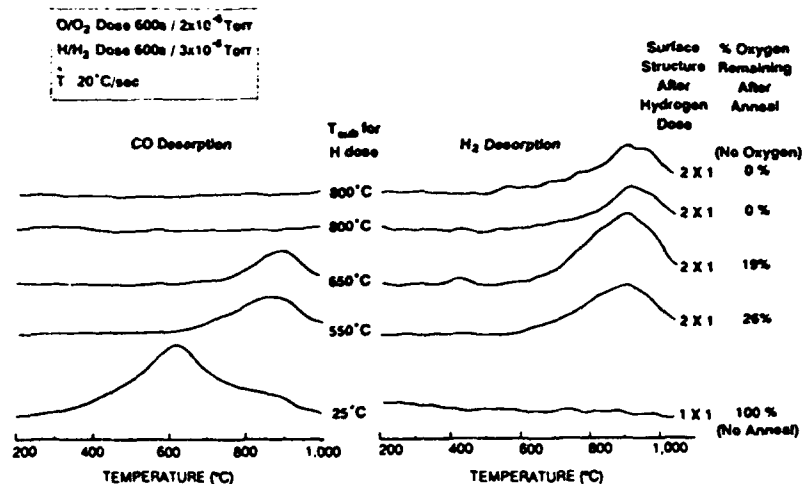
Figure 3.   Effect of atomic hydrogen on C(100) surface structure at elevated temperatures
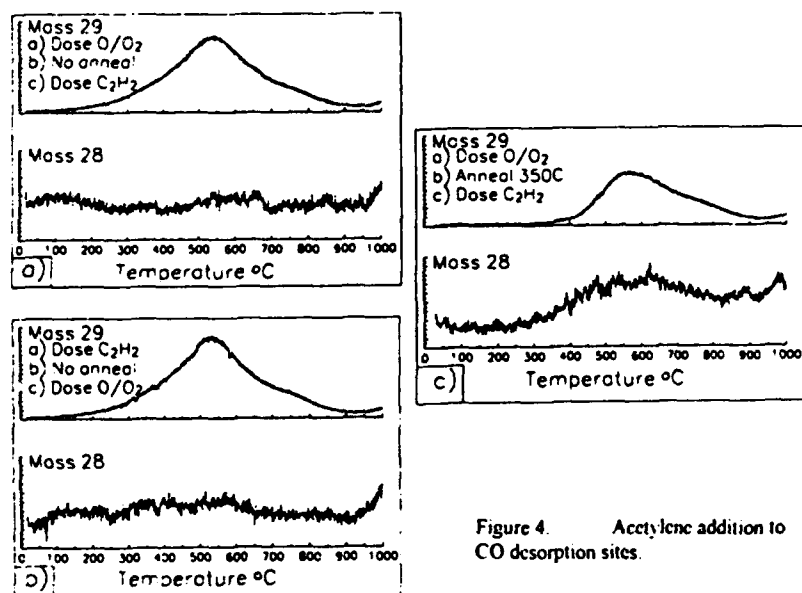

Figure 4.   Acetylene addition to CO desorption sites.

Surface Processes Associated with Diamond Growth From Water Alcohol Deposition Chemistries

R. E. Thomas, R. A. Rudder, and R. J. Markunas

Center for Semiconductor Research, Research Triangle Institute, Research Triangle Park, NC 27709, U.S.A.

Electron energy loss spectroscopy (EELS) and low energy electron diffraction (LEED) have been used to study the effects of atomic oxygen dosing and atomic hydrogen dosing on the diamond (100) surface. Terminated surfaces appear very similar with EELS although the oxygenated surface gives a 1x1 LEED pattern and the hydrogenated surface gives a 2x1 LEED pattern. Annealing of both surfaces gives rise to a new loss peak at approximately 5 eV from the elastic peak. This peak is thought to arise from dangling bonds on the surface

1. INTRODUCTION

Although a wide variety of growth chemistries and techniques have been developed for the chemical vapor deposition of diamond, fundamental questions remain unresolved concerning surface processes during diamond growth. A number of diamond growth mechanisms have been proposed which involve atomic hydrogen and hydrocarbon species.[1] In addition, numerous growth studies have shown that oxygen, in the form of CO, H_2O, or alcohols, can contribute to diamond formation.[1] Previous surface studies have shown that atomic oxygen will convert a C:(100)-2x1: surface to 1x1 configuration.[2] Upon heating the oxygen leaves the surface predominantly in the form of CO with some CO_2 also desorbed. The maximum desorption rate for CO occurs at approximately 600°C for a heating rate of 5C/s, and significant desorption occurs at temperatures less than 400°C, well below the peak maximum. As CO desorbs from the surface the surface reverts to the 2x1 configuration. The desorption of CO from the surface at relatively low temperatures has the potential for opening sites for the addition of carbon to the diamond lattice. However, the nature of these sites is unclear. In the present study we have used electron energy loss spectroscopy (EELS) and low energy electron diffraction (LEED) to study the transition from the 1x1 to the 2x1 structure upon CO evolution and to probe the surface sites resulting from CO desorption. Comparisons are made of both hydrogen and oxygen terminated surfaces and graphite surfaces.

2. EXPERIMENTAL PROCEDURES

A full description of the experimental procedure is available in earlier publications and only a brief review is given here.[2] EELS and LEED observations were performed in a stainless steel UHV system. Sample heating was accomplished by clipping the crystals to a 0.25 mm thick molybdenum resistive strip heater. The sample temperature was measured by a 0.125 mm diameter chromel/alumel thermocouple threaded through a laser drilled hole in the diamond and held in tension against the crystal face. Two type IIa (100), 5x5x0.25 mm, diamond crystals were used in the course of the present study. To clean the surfaces, the samples are initially hand polished 5 minutes with 0.25 μm diamond grit, followed by solvent rinses. The samples are then placed in a CrO_3/H_2SO_4 (125°C) solution for 20

minutes to remove non-diamond carbon. The samples are rinsed in DI water and then boiled in a 3:1 solution of HCl/HNO$_3$ for 20 minutes to remove any metals contamination. Samples subjected to this cleaning process typically show a good quality 1x1 LEED pattern at beam voltages as low as 50 volts with no annealing. Auger spectroscopy of the diamond surfaces as introduced to the chamber indicates that the surface is left O-terminated following the acid cleaning. In all cases atomic hydrogen for dosing was generated via a tungsten filament operating at a temperature of approximately 1500°C. Filament temperatures were measured with a hand held optical pyrometer. Atomic oxygen was generated via an iridium filament at 1100°C. VLSI grade hydrogen and oxygen gasses were used with no further purification. No attempt was made to quantify the percentage of atomic species generated by the filaments. EELS data were collected with a Perkin-Elmer single pass cylindrical mirror analyzer. The elastic peak was set at approximately 150 eV for all spectra to maximize surface sensitivity. Differentiation of the spectra was performed digitally using a Savitsky-Golay differentiation and smoothing routine.

3. RESULTS AND DISCUSSION

Figure 1 shows derivative EELS spectra obtained from annealing of a hydrogen terminated sample. The hydrogen dosed samples remained in a 2x1 configuration after exposure to the atomic hydrogen, with each dangling bond now terminated by a hydrogen. The unannealed sample shows large peaks at approximately 8 eV, 23 eV, and 33 eV away from the elastic peak. Upon annealing of the hydrogen terminated surface the 23 eV peak gradually diminishes in intensity relative to the 33 eV peak. The 8 eV peak grows in intensity relative to the other peaks and we observe the appearance of a new peak approximately 5 eV from the elastic peak
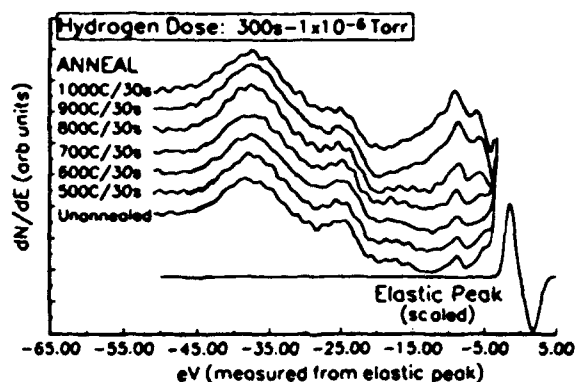
Figure 1. Electron energy loss spectra from diamond (2x1):H surface.

following the anneal at 700°C. Fig 1. The 5 eV peak grows in magnitude with subsequent anneals at 800°C and 900°C. The temperature at which the 5 eV feature first appears corresponds very well with the onset of hydrogen desorption from the surface measured in earlier thermal desorption experiments.[2] The differentiation process emphasizes changes in the peak structure, however peak positions quoted in the text refer to the undifferentiated spectra for consistency with previous literature. Figure 2 shows a comparison of differentiated and undifferentiated spectra. The evolution of EELS structure for oxygen

Figure 2. Comparison of differentiated and undifferentiated spectra from hydrogen-dosed sample.

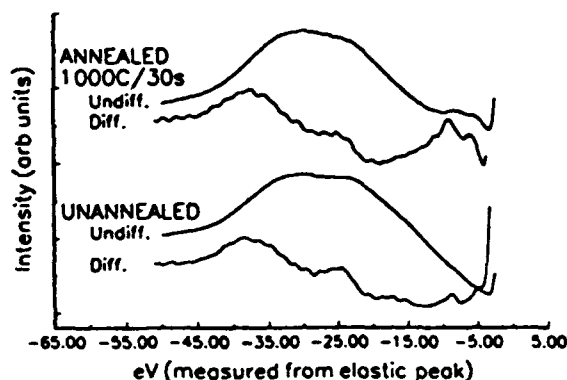terminated surfaces is more complex as can be seen in Figure 3. The oxygen dosed samples also exhibited a peak at 5 eV away from the elastic peak after annealing. The peak appeared at approximately 600°C, which again corresponds quite well with thermal desorption data.[2] However from Figure 3 one can see that the peak at approximately 8 eV undergoes more complex transformations. Following the anneal at 1000°C all of the oxygen has desorbed from the surface and the surface is left in a 2x1 configuration with 1 dangling bond per carbon atom. If the surface is then exposed to atomic hydrogen Figure 3 shows that the peaks at both 5 eV and 8 eV are suppressed.
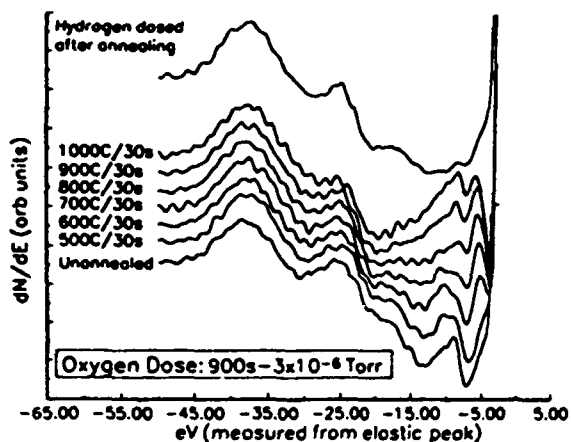

Figure 3.   Electron energy loss spectra from diamond (1x1):0 surface.

For comparison purposes EELS spectra were obtained from pyrolytic graphite samples using the same apparatus and geometry. Results from graphite surfaces are shown in Figure 4 along with spectra from hydrogen dosed samples. In the case of graphite the most prominent feature is a loss peak at approximately 6 eV. From the plot one can see that this feature is clearly at a different energy than the 5 eV loss feature seen on diamond surfaces.

The peak at 33 eV is associated with a bulk plasmon in diamond [3], and we do not see much
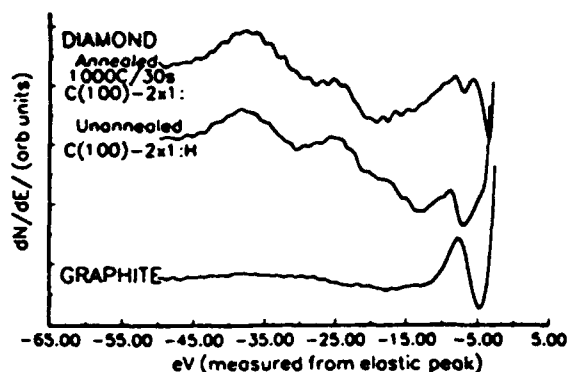

Figure 4   Comparison of EELS spectra from clean graphite and hydrogen-dosed diamond samples.

change in this feature as a function of surface structure or termination. The peak at 23 eV has been correlated with plasmon and/or interband excitations and the peak at 8-10 eV with interband transitions.[3]   The peak at 23 eV diminishes upon annealing for both H-termination and O-termination even though the surface structure remains in a 2x1 configuration throughout the process for hydrogenated surfaces and reconstructs from a 1x1 to a 2x1 structure in the case of oxygenated surfaces. It is not surprising that both desorption series converge to the same EELS spectra since equivalent 2x1 reconstructed surfaces are obtained via each path. Apparently the presence of dangling bonds serves to suppress or shift the frequency of the surface plasmon mode. Zangwill has pointed out that the zero point energy of the plasmon oscillator system increases as the electron density increases.[4] With dangling bonds on the surface we have effectively increased the electron density and we expect the plasmon frequency to shift to higher energies. With the resolution available in the present arrangement it is difficult to observe this shift but what may be happening is that the surface plasmon energy shifts towards the bulk plasmon and cannot be resolved. The behavior of the peak at 8-10 eV is more difficult to explain. This peak has been associated with a transition

from the valence band to the conduction band.[3] The behavior of the peak is also more complicated and distinct differences are observed between samples with oxygen termination and hydrogen termination. The evolution of surface structure accompanying oxygen desorption is more involved than the case for hydrogen. CO desorbs from oxygenated surfaces causing a loss of carbon and then the surface reconstructs.

We also observe the appearance of a peak at approximately 5 eV from the elastic peak after annealing both oxygen and hydrogen terminated surfaces. A similar feature has been observed following annealing of as deposited and oxygenated polycrystalline diamond.[5] The as deposited material was presumed to be hydrogen terminated. The 5 eV feature has been associated with band gap excitation.[3] Alternative explanations include surface states induced by dangling bonds or plasmon losses from π bonding as the surface reconstructs. The 5 eV loss feature disappears after the surface is dosed with atomic hydrogen. We do not expect band-gap excitation to disappear with hydrogen dosing. However the dangling bonds would be filled and/or π bonds lifted from the surface dimers. Several facts point to dangling bonds as the source of the loss peak at 5 eV. High resolution electron energy loss spectroscopy of (111) and (100) surfaces shows the presence of a C=C double bond on the (111) surface but not on the (100) surface.[6] The C=C double bond is seen on the (111) surface after hydrogenation, so the addition of atomic hydrogen does not necessarily break all of the double bonds on the surface. Double bonds may also exist on the (100) surface but cannot be resolved by the HREELS measurement. Recent quantum chemical calculations show the dimer bond on the (100) surface does not contain a significant π component.[7] Finally, EELS spectra from graphite surfaces taken under the same conditions show the π plasmon on graphite shifted by approximately 1 eV from the 5 eV loss feature observed on diamond.

4.0 SUMMARY

Electron energy loss spectroscopy has been used to study hydrogen and oxygen terminated diamond surfaces and graphite. Both terminated diamond surfaces exhibit similar loss spectra with major peaks at 33, 23, and 8 eV. Annealing of the samples gave rise to a new loss feature at 5 eV thought to be a result of the appearance of dangling bonds on the surface.

ACKNOWLEDGMENTS

REFERENCES

1. See references in Proceedings of the Third International Conference on the New Diamond Science and Technology, edited by D. K. Bachmann, A. T. Collins, and M. Seal (Elsevier Sequoia, Lausanne Switzerland, 1993).
2. R. E. Thomas, R. A. Rudder, and R. J. Markunas, J. Vac. Sci. Technol. A10 (1992) 2451.
3. P. G. Lurie and J. M. Wilson, Surf. Sci. 65 (1977) 453.
4. A. Zangwill, Physics at Surfaces (Cambridge University, Cambridge, England, 1988) 144.
5. Y. Mori, N. Eimori, J. S. Ma, T. Ito, and A. Hiraki, Appl. Surf. Sci., 56-58 (1992) 89.
6. S.-T. Lee. and G. Apai., Phys. Rev. B 48 (1993) 2684.
7. M. Frenklach, private communication.

Effects of oxygen on surface reconstruction of carbon

Jerry L. Whitten, Pietro Cremaschi [1,*]

Department of Chemistry, North Carolina State University, Raleigh, NC 27695-8204, USA

Raymond E. Thomas, Ronald A. Rudder, Robert J. Markunas

Research Triangle Institute, Research Triangle Park, NC 27709-2194, USA

Abstract

Recent experiments on diamond growth by chemical vapor deposition indicate that atomic oxygen converts the diamond (100)-(2 × 1) surface to the (1 × 1) structure. Ab initio total energy calculations are performed on a cluster of carbon atoms simulating the (100) surface in order to investigate the effect of oxygen on surface reconstruction. Calculations are reported for the clean surface and for O atoms adsorbed atop carbon and at a C-C bridge site. Bridge and atop carbon sites for oxygen have nearly identical adsorption energies and adsorption of O at either site prevents the C(100)-1 × 1 to 2 × 1 dimerization reconstruction. Adsorption of oxygen at one bridge site affects, but does not prevent, the dimerization of an adjacent pair of surface carbon atoms.

1. Introduction

The application of chemical vapor deposition techniques to grow diamond is under intense investigation in many laboratories [1-10]. In plasma or hot filament techniques, high concentrations of hydrogen in source gases are generally employed in order to maintain tetrahedral, sp^3, bonding of the surface carbon; H atoms subsequently abstract surface hydrogen to form H$_2$

and growth continues at unsaturated carbon sites by the addition of hydrocarbon fragments [1,10-13]. The openness of the ideal C(100) surface and the nature of its surface sites would make this a preferred surface for film growth. However, the ideal surface, C(100)-1 × 1, readily undergoes reconstruction to form a dimerized C(100)-2 × 1 structure [15-18]. This dimerized surface, depicted in Fig. 1, can easily add one hydrogen per carbon, but unlike Si(100), the distance between adjacent carbon atoms on C(100) is too short to accommodate two additional hydrogens [19]. Consequently, the dimerized surface less readily adds additional carbon. Incompletely hydrogenated surfaces, e.g., the addition of three H atoms to a pair of carbon atoms, convert to the

---

* Corresponding author.

[1] Permanent address: Centro CNR, Dipartimento di Chimica Fisica ed Elettrochimica, Universita di Milano, Milano, I-20133 Italy.
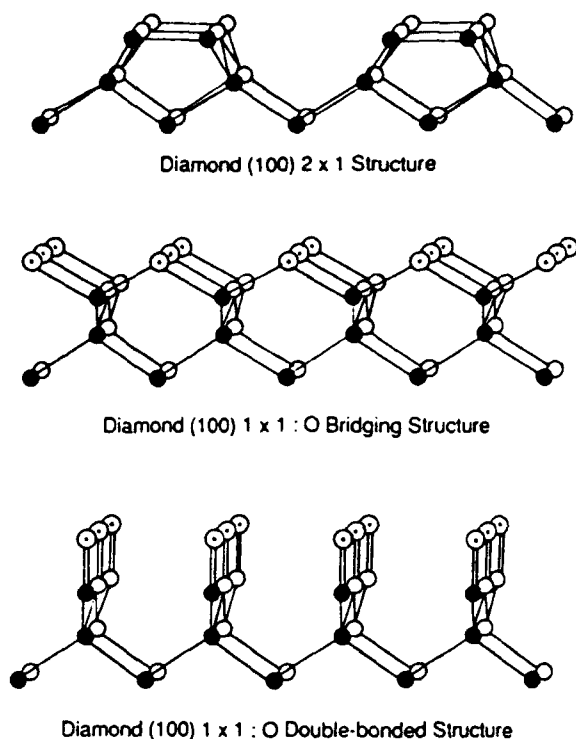
Diamond (100) 2 x 1 Structure

Diamond (100) 1 x 1 : O Bridging Structure

Diamond (100) 1 x 1 : O Double-bonded Structure

Fig. 1. Diamond (100) surface showing the 2×1 dimer reconstruction and possible adsorption sites for oxygen.

2×1 configuration when hydrogen is removed [18].

LEED studies have shown that adsorption of atomic oxygen is able to convert the 2×1 surface to 1×1 [14,15]. Large amounts of oxygen will saturate the surface sites, but less than one-half a monolayer of oxygen would leave carbon sites available for reaction with carbon containing CVD species [14,18,20]. Annealing studies of oxygen-terminated (100) surfaces show that surfaces that are only partially covered with oxygen are able to maintain the 1×1 configuration [14]. In addition, thermal desorption studies have shown that desorption of CO from the (100) surface can occur as low as 200°C [14]. Thus, dosing C(100) surfaces with oxygen shows promising in enabling low temperature epitaxial growth of diamond [14,18,20–24].

The nature of the C(100)-1×1 surface, its distances and tetrahedral structure of C-C bonds to the lattice, suggest that oxygen could add to

the surface to form C–O–C (ether) or C=O (ketone) linkages commonly found in organic compounds. Thus, full monolayer coverages involving one O per surface carbon as well as half monolayer coverages of one O per two surface carbons are likely, see Fig 1. It is unclear from either experimental or theoretical studies exactly how much oxygen on the surface is required to produce a C(100)-1×1 structure [13,25,26].

The purpose of this study is to investigate, using first-principles theory, the adsorption of oxygen atoms on C(100). Adsorption energetics and the energetics of different surface reconstructions are calculated. Since we are primarily interested in a detailed account of the structure and energetics of the region around the adsorbate, a cluster model of the surface is used. This approach allows the application of ab initio configuration interaction theory to produce an accurate description of various stages of the dimerization reconstruction and a determination of oxygen–carbon and carbon–carbon distances and angles in the vicinity of the adsorption site.

2. Theory

In this work, calculations are carried out for the full electrostatic Hamiltonian of the system, with wavefunctions constructed by self-consistent field (SCF) and configuration interaction (CI) expansions. There are no empirical parameters and distances and angles in the vicinity of the oxygen adsorbate are optimized in all calculations. For N electrons, Q nuclei

$$H = \sum_i^N -1/2\nabla_i^2 + \sum_i^N \sum_k^Q -Z_k/r_{ki} + \sum_{ij}^N 1/r_{ij}$$

CI wavefunctions are generated from an initial SCF configuration, or from multiple parent configurations in the case of stretched or broken bonds, by one- and two-particle excitations from the main components of the wavefunction to give expansions of the form

$$\psi = \sum_k \lambda_k A\left(\chi_1^k \chi_2^k \cdots \chi_n^k\right).$$

In the CI calculations, the occupied and virtual orbitals of the SCF solution are transformed separately to obtain orbitals with varying degrees of localization about the oxygen adsorbate and surface carbon atoms undergoing dimerization. This unitary transformation of orbitals which is based upon exchange maximization with the valence orbitals of atoms in the dimer region of the cluster enhances convergence of the configuration interaction (CI) expansion. Perturbation theory is used to incorporate numerous small contributions not explicitly included in the CI expansion. Details of the theory have been reported elsewhere [27–30].

3. Clean surface studies

In this section, we consider the dimerization of C(100) using the cluster of carbon atoms depicted in Fig. 2 to describe the surface. This particular cluster has all of the nearest neighbor and bulk next nearest neighbor atoms of the C_1–C_2 pair of atoms undergoing dimerization. Carbon atoms on the boundary of the cluster, except C_1 and C_2, are saturated by hydrogen atoms to simulate continuation of the lattice. The energy change on reconstruction, as a function of the angle of rotation about the second layer atoms, α, is reported in Table 1 for three spin states, $S = 2$, $S = 1$ and $S = 0$, of the pair of carbon atoms C_1–C_2. The lowest state is for $S = 0$, corresponding to a strong interaction between the interior dangling bonds and a weak coupling of the dangling orbitals depicted as arrows extending outward as depicted in Fig. 2. If the latter two orbitals are triplet coupled, the energy increases by 0.33 eV for the ideal surface ($\alpha = 0$). As shown in Table 1, as α

Fig. 2. C(100) clean surface reconstruction. The dimerization of surface atoms C_1–C_2 as a function of angle α is treated by configuration interaction theory for three different spin states of the system.

Table 1
C(100) clean surface reconstruction

Angle α	R_{CC} (Å)	Spin state (eV)		
		$S = 2$	$S = 1$	$S = 0$
0°	2.52	0.63	0.33	0.0 [a]
25°	1.76	8.16	−2.49	−2.58
30°	1.63	9.61	−2.51	−2.84
35°	1.50	10.8	−2.06	−3.01
40°	1.38		−0.91	−2.78
45°	1.26			−2.06

The dimerization of surface atoms C_1–C_2 as a function of α, depicted in Fig. 2, is treated by configuration interaction theory for three different spin states of the system. The most stable structure is a singlet, 3.01 eV exothermic compared to the ideal surface, with $\alpha = 35°$ corresponding to a C–C distance of 1.50 Å. Energies, in eV, are relative to the ideal surface $S = 0$ state.
[a] Total energy: −463.5980 a.u.

increases, the energy of the high spin state increases sharply due to the Pauli repulsion of electrons in the inward directed hybrid orbitals, whereas the energies of the $S = 1$ and $S = 0$ spin states decrease. The lowest energy state, $S = 0$, shows an energy minimum at $\alpha = 35°$ which corresponds to a C_1–C_2 distance of 1.50 Å and a large energy lowering on dimerization of 3.0 eV. From the shape of the ground state potential curve, the uncertainty in the equilibrium distance is ~ 0.05 Å. Subsequent studies show that α is the appropriate variable to describe the dimerization since this rotation preserves bond lengths between atoms C_1 and C_2 and the remainder of the lattice. This is consistent with data for many organic compounds in which one finds fairly constant C–C bond lengths within the respective classes of single, double and triple bonds. Note that the C–C bond length in diamond is 1.544 Å which is similar to the C–C single bond in organic compounds. Thus, the calculated reconstruction of the C(100) surface results in a distance for the dimerizing carbon atoms slightly shorter than a typical C–C single bond.

4. O adsorption on C(100)

Adsorption of atomic oxygen is first considered at atop C and C–C bridge sites on the

unreconstructed C(100)-1 × 1 surface. The distance of oxygen from the surface is varied and calculated energies are reported in Table 2. The total energies for the atop and bridge sites are found to be nearly identical, differing by less than 0.2 eV. For the atop atom site, the CO distance is 1.23 Å, a value similar to that for a typical ketone double bond. The CO distance for the bridge site is 1.48 Å, slightly longer than the CO distance in dimethyl ether.

In the next series of calculations, the C_1-C_2 dimer length is optimized for the two cases: O adsorbed at the bridge site and O at an atop C site. Total energy calculations as a function of the angle of rotation, α, and vertical O distance variations are reported in Table 3 for the bridge O site. These data show that the minimum in energy will be around $\alpha = 7°$ which would correspond to a decrease of only 0.22 Å from the ideal surface C_1-C_2 distance of 2.52 Å. By comparison, the dimerization reconstruction for the clean surface corresponds to a decrease in C_1-C_2 distance of 1.02 Å. Calculations were also performed to determine whether oxygen at the bridge site would weaken the bonds between the C_1-C_2 atoms and the remainder of the lattice. Changing the vertical distance of the C_1-O-C_2 unit by 0.05 Å caused a 0.18 eV increase in energy, thus implying that bond length changes due to oxygen adsorption will be quite small. After the small dimerization reconstruction of the C-C bridge, this site becomes slightly lower in energy than for atop carbon adsorption. Similar studies were carried out for oxygen adsorbed atop one of the

Table 3
Effect of O adsorption on C(100)-2 × 1 surface reconstruction

Angle α	R_{CO} (Å)	ΔE (eV)
0°	1.43	0.07
	1.48	0.0 [a]
	1.54	0.17
7°	1.32	0.10
	1.37	−0.45
	1.43	−0.43
10°	1.31	−0.11
	1.36	−0.35
	1.43	−0.21
15°	1.26	0.73
	1.36	0.31
	1.43	0.60

O is adsorbed at a C-C bridge site. The dimerization of the C-C bridge atoms is investigated by varying the angle, α, defined in Fig. 2. For each angle, the vertical distance of oxygen from the surface is varied and results are reported in terms of the corresponding CO distance.
[a] Total energy: −538.66715 a.u.

carbon atoms of the C_1-C_2 pair. On rotating these carbons by $\alpha = 10°$, the energy increased by 0.2 eV. This means that oxygen adsorption atop alternate C atoms, at a half monolayer coverage, would prevent the dimerization reconstruction, a result that is not surprising since formation of one C=O double bond removes the driving force for pairing dangling bond orbitals.

In the final series of calculations, an O atom was adsorbed at one bridge site, and the dimerization of the adjacent C_1-C_2 pair of atoms was investigated using the cluster depicted in Fig. 3. This system is found to behave somewhat like the clean surface except that the energy of dimeriza-
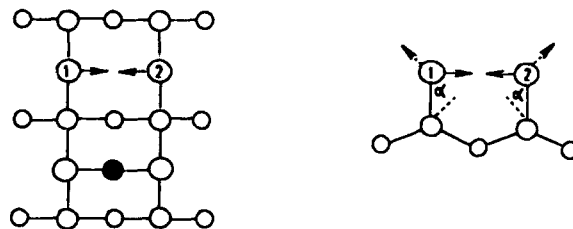
Table 2
Adsorption of O atop C and at the C_1-C_2 bridge site in Fig. 2 for the unreconstructed C(100) surface geometry; the vertical distance of O from the surface, z_0, is varied

Atop site		Bridge site	
z_0 (Å)	ΔE (eV)	z_0 (Å)	ΔE (eV)
1.33	+0.47	0.88	+0.17
1.23	0.0 [a]	0.78	0.0 [b]
1.12	+0.43	0.67	+0.07

[a] Total energy: −538.6737 a.u.
[b] Total energy: −538.6672 a.u. The distance $z_0 = 0.78$ Å corresponds to a CO distance of 1.48 Å.

Fig. 3. C(100) surface with O adsorbed at a bridge site. The dimerization of surface atoms C_1-C_2 as a function of angle α is treated by configuration interaction theory for three different spin states of the system. The solid circle denotes the oxygen adsorption site.

Table 4
Effect of bridge O adsorption on adjacent C–C dimerization

Angle α	R_{CC} (Å)	Spin state (eV)		
		$S = 3$	$S = 2$	$S = 1$ [a]
$0°$	2.52	0.60	0.30	0.0 [b]
$25°$	1.76	7.49	−2.42	−2.46
$30°$	1.63	8.86	−2.46	−2.78
$35°$	1.50	10.3	−1.98	−2.50
$40°$	1.38		−0.78	−2.63
$45°$	1.26		1.70	−1.84

The dimerization of surface atoms C_1-C_2, depicted in Fig. 3, as a function of α is treated by configuration interaction theory for three different spin states of the system.
[a] The carbon atoms bonded to oxygen are triplet spin coupled in all cases; thus, $S = 1$ for the present case corresponds to the singlet coupling of the dimerizing carbon atoms.
[b] Total energy: −806.5908 a.u.

tion is less, 2.8 eV compared to 3.0 eV, and the equilibrium distance between the dimerized C atoms is longer, 1.63 Å (uncertainty of ~0.05 Å) compared to 1.50 Å for the clean surface. Table 4 gives the relative energies of the three relevant spin states as a function of the dimerization reconstruction. The trends for each spin state are the same as shown in Table 1 for the clean surface dimerization. The ground state shows a double minimum at 30° and 40°, separated by a small barrier. Although the double minimum persists for multiple parent CI treatments, a more thorough investigation of the surface is needed before concluding that the effect is real. On the principal point, the results of the calculations are conclusive: the presence of O adsorbed at a bridge site affects, but does not prevent, the dimerization of the adjacent pair of surface carbon atoms.

5. Conclusions

The results of the present theoretical investigation lead to the following conclusions:

(1) The dimerization reconstruction of the C(100) surface occurs by a rotation of surface carbon atoms about atoms in the second layer, preserving the bond lengths between the pair of carbon atoms undergoing dimerization and the remainder of the lattice. The dimerization is 3.0

eV exothermic and produces surface dimers with a C–C distance of ~1.50 Å, a value slightly shorter than for a typical C–C single bond in organic compounds.

(2) Adsorption of O atoms can occur at atop carbon and C–C bridge sites; adsorption energies at these two sites are nearly identical for the unreconstructed surface. After the accompanying very small reconstruction, the bridge site is lower in energy, but adsorption of O at either the atop site or bridge site prevents significant dimerization of surface carbon atoms.

(3) Optimized C–O distances are similar to those found for C=O double bonds in ketones (for atop C adsorption) and similar to typical values in ether compounds (for C–C bridge adsorption).

(4) Adsorption of oxygen at one bridge site on the surface is found to affect, but does not prevent, the dimerization reconstruction of an adjacent pair of surface carbon atoms.

Acknowledgements

References

[1] R. Messier, J.T. Glass, J.E. Butler and R. Roy, Eds., New Diamond Science and Technology (Mater. Res. Soc., Pittsburgh, PA, 1991).
[2] R.A. Rudder, G.C. Hudson, J.B. Posthill, R.E. Thomas, R.J. Markunas, T.P. Humphreys and R.J. Nemanich, Appl. Phys. Lett. 60 (1992) 329.
[3] R.F. Davis, Z. Sitar, B.E. Williams, H.S. Kong, H.J. Kim, J.W. Palmour, J.A. Edmond, J. Ryu, J.T. Glass and C.H. Carter, Jr., Mater. Sci. Eng. B 1 (1988) 77.
[4] R.A. Rudder, J.B. Posthill and R.J. Markunas, Electron. Lett. 25 (1989) 1220.
[5] K.E. Spear, J. Am. Ceram. Soc. 72 (1989) 171.
[6] H. Kawarada, J.S. Ma, T. Yonehara and A. Hiraki, Mater. Res. Soc. Symp. Proc. 162 (1990) 195.

[7] H. Itoh, T. Nakamura, H. Iwahara and H. Sakamoto, in: New Diamond Science and Technology, Eds. R. Messier, J.T. Glass, J.E. Butler and R. Roy (Mater. Res. Soc., Pittsburgh, PA, 1991) p. 929.

[8] W.A. Yarbrough, J. Vac. Sci. Technol. A 9 (1991) 1145.

[9] J.F. Prins and H.L. Gaigher, in: New Diamond Science and Technology, Eds. R. Messier, J.T. Glass, J.E. Butler and R. Roy (Mater. Res. Soc., Pittsburgh, PA, 1991) p. 561.

[10] R.A. Rudder, G.C. Hudson, Y.M. LeGrice, M.J. Mantini, J.B. Posthill, R.J. Nemanich and R.J. Markunas, 1989 MRS Meeting, San Diego, CA, EA-19 (1989) 89.

[11] W.S. Verwoerd, Surf. Sci. 108 (1981) 153.

[12] X.M. Zheng and P.V. Smith, Surf. Sci. 256 (1991) 1.

[13] R.E. Thomas, R.A. Rudder, R.J. Markunas, O. Huang and M. Frenklach, J. Chem. Vapor Dep. 1 (1992) 6.

[14] R.E. Thomas, R.A. Rudder, R.J. Markunas, J. Vac. Sci. Technol. A 10 (1992) 2451.

[15] A.V. Hamza, G.D. Kubiak and R.H. Stulen, Surf. Sci. 237 (1990) 35.

[16] P.G. Lurie and J.M. Wilson, Surf. Sci. 65 (1977) 453.

[17] B.B. Pate, Surf. Sci. 165 (1986) 83.

[18] R.E. Thomas, R.A. Rudder, R.J. Markunas, Proc. 2nd Int. Symp. on Diamond Materials, Eds. A.J. Purdes, J.C. Angus, B.M. Meyerson, K.E. Spear, R.F. Davis and M. Yoder, 1991, p. 186.

[19] Y.L. Yang and M.P. D'Evelyn, J. Am. Chem. Soc. (1992).

[20] S. Matsumoto and N. Setaka, Carbon 17 (1979) 485.

[21] J.A. Mucha, D.L. Flamm and D.E. Ibbotson, J. Appl. Phys. 65 (1989) 3448.

[22] S.J. Harris and A.M. Weiner, Appl. Phys. Lett. 55 (1989) 2179.

[23] W. Shu, X. Hong Wang, A. Badzian and R. Messier, New Diamond Science and Technology, Washington, DC, MRS Conf. Proc. 812 (1990).

[24] R.A. Rudder, G.C. Hudson, J.B. Posthill, R.E. Thomas, R.C. Hendry, D.P. Malta and R.J. Markunas, Appl. Phys. Lett. 60 (1992) 329.

[25] S.P. Mehandru and A.B. Anderson, Surf. Sci. 248 (1991) 369.

[26] J.J. Boland, Surf. Sci. 261 (1992) 17.

[27] J.L. Whitten, Theoretical Studies of Surface Reactions on Metals: Cluster and Embedding Theory, in: Cluster Models for Surface and Bulk Phenomena, Eds. G. Pacchioni and P.S. Bagus (Plenum, New York, 1992) p. 375.

[28] H. Yang, J.L. Whitten, J. Chem. Phys. 96 (1992) 5529; Surf Sci. 255 (1991) 193, and references therein.

[29] J.C. Malvido and J.L. Whitten, Phys. Rev. B 26 (1982) 4458.

[30] A. Chattopadhyay, P. Madhavan, R. Fischer, I.P. Batra and J.L. Whitten, J. Mol. Struct. (Theochem) 163 (1988) 63.

Activation energy and mechanism of CO desorption from (100) diamond surface

M. Frenklach and D. Huang
Department of Materials Science and Engineering, The Pennsylvania State University, University Park, Pennsylvania 16802

R. E. Thomas, R. A. Rudder, and R. J. Markunas
Research Triangle Institute, Research Triangle Park, North Carolina 27709

An apparent activation energy for CO desorption from (100) diamond surfaces exposed to atomic oxygen was determined by thermal desorption spectroscopy performed in ultrahigh vacuum and found to be equal to 45.0 kcal/mol. A minimum potential-energy reaction path was identified by semiempirical quantum chemical calculations. Starting with an O-on-top radical site, the reaction proceeds through a β-scission of the C—CO bond, formation of a dimer C—C bond, and finally cleavage of the second C—CO bond. The largest barrier along this pathway is that of the final desorption step; it is equal to 38.4 kcal/mol, in reasonable agreement with the experimental activation energy. Taken together, the broad experimental desorption-peak feature and the multitude of possible desorption sites with differing potential-energy barriers, suggests the existence of a distribution of CO sites on diamond surfaces.

Deposition of diamond in oxygen-containing environments has received widespread attention and the beneficial effects of oxygen on the growth of diamond films have been reported.[1] Little, however, is known on the fundamental aspects of the interaction between oxygen and diamond surfaces. Recently, Thomas et al.[2] carried out an experimental study on desorption of CO from diamond surfaces. In their experiments, atomic oxygen was adsorbed on a (100) diamond face at room temperature, and then the species desorbing upon heating were monitored by mass spectrometry. In this letter, we report on determination of an apparent activation energy for desorption of CO in these experiments, present results of semiempirical quantum chemical calculations, and suggest a plausible reaction mechanism that is consistent with the experimental observations.

Details of the experimental procedure are available in earlier publications[2] and only a brief summary is given here. In order to more clearly distinguish CO desorption from the sample surface, a 2000 Å homoepitaxial ^{13}C layer was deposited on a natural diamond substrate in a rf plasma reactor with a $H_2/^{13}CH_4$ discharge. Thermal desorption from samples before and after ^{13}C deposition shows no difference, aside from an increase in sensitivity, in the CO desorption features. Atomic oxygen for dosing was generated via an iridium filament at 1100 °C.

There are several methods for extracting activation energies for desorption processes.[3] In the present study, we have chosen the method of varying the heating rate and measuring the desorption peak temperature.[4] For a first order process, the peak T_m is related to the heating rate β in the following manner:

$$\ln \frac{T_m^2}{\beta} = \frac{E_a}{RT_m} + \ln \frac{E_a}{vR},$$

where R is the universal gas constant and v the pre-exponential factor. The apparent activation energy of CO

desorption E_a was extracted by measuring the peak T_m for various heating rates and plotting $\ln(T_m^2/\beta)$ vs $1/T_m$.[4] Figure 1 shows such a plot for samples which have been saturated with oxygen and for which heating rates from 0.5 to ~14 °C/s were used. A line fit to the data yields a slope of 2.27×10^4 or $E_a = 45.0$ kcal/mol and an intercept of -16.34 or $v = 2.8 \times 10^{11}$ s^{-1}.

The analysis technique depends on several assumptions: the initial surface coverage is the same for each temperature ramp, and v and E_a are independent of coverage. The dosing process is designed to ensure that samples receive an equivalent exposure to atomic oxygen prior to each thermal desorption. Samples are annealed to remove any adsorbates and exposed to oxygen for the same time and at the same pressure for each temperature ramp. Given the extremely wide desorption peaks observed for CO desorption, FWHM ≈ 260 °C, it is not clear that a single ac-
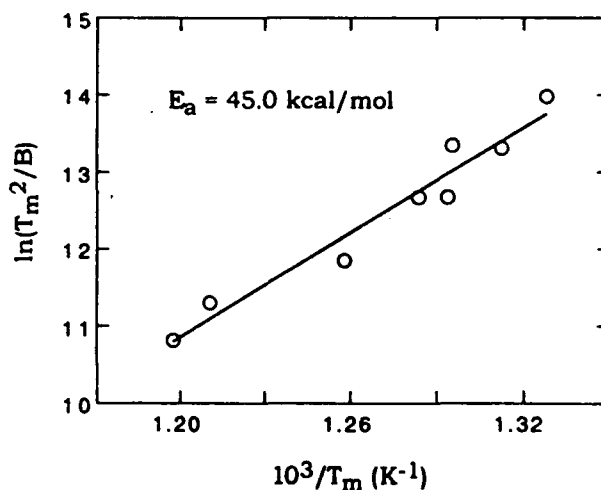

FIG. 1. Arrhenius plot for thermal desorption of CO. The circles are experimental data and the line is the least-squares fit.
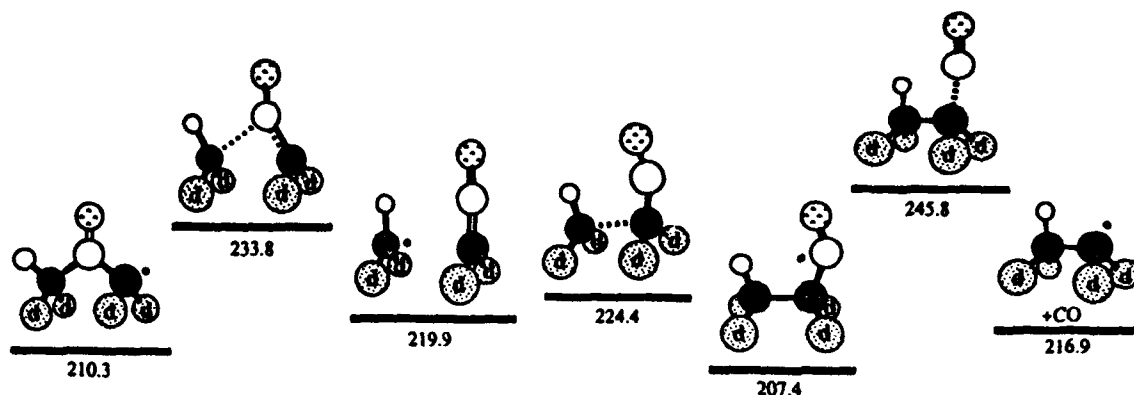
FIG. 2. Potential energy diagram for CO desorption from an O-on-top (100) diamond radical site. The designation of atoms follows Ref. 6: The filled circles designate carbon atoms, except for the uppermost one which represents an oxygen atom. The open circles are hydrogen atoms. Carbon atoms of different layers are shaded with different patterns and labeled in accordance with Ref. 6. The numbers are the enthalpies of formation in kcal/mol.

tivation energy can be used to characterize the desorption. There may exist a range of activation energies associated with sites on the surface which sum to produce a very broad desorption curve. We see no clear evidence for multiple peaks in the desorption curves which implies closely spaced activation energies if this explanation obtains. Although the surface is likely roughened by the desorption of CO, it does not appear that this alone can account for the broad desorption features seen. Identical desorption spectra are obtained directly after homoepitaxial growth of the ^{13}C layer. No differences in the width or shape of the desorption curves were noted after multiple desorptions. If a range of energies exists, the present analysis will simply give the activation energy for the dominant process. Desorption processes with larger and smaller activation energies may also be occurring. In addition, the analysis is rigorously correct only for first order desorption processes. Previous thermal desorption studies have shown that the peak tends to decrease in temperature as the coverage increases.[2] After Redhead,[5] a plot was made of $\ln(\sigma_0 T_m^2)$ vs $1/T_m$, where σ_0 is the initial surface coverage, to determine if the activation energy was coverage dependent. The plot gave a straight line indicating second-order kinetics with a constant activation energy. The derivation on which the activation energy extractions is based is rigorously correct only for first-order desorptions. However, when the above analysis was applied to data simulating second-order thermal desorption,[4] errors of less than 2% were obtained.

To investigate for a possible reaction mechanism of CO desorption, semiempirical quantum chemical potential-energy calculations were carried out. These calculations were performed, as in the previous studies[6] and to be consistent with them, using the modified neglect of diatomic overlap (MNDO) all-valence electron parameterization of the neglect of diatomic differential overlap self-consistent field (NDDO-SCF) approximation.[7] Calculations were of restricted Hartree–Fock type with the half-electron method being used for radical species.[8] The computations were performed with the AMPAC computer program developed by Dewar and co-workers.[9] The background (100) surface element was represented, as in the previous study,[6]

by a $C_{28}H_{48}$ cluster—a model compound comprised of three layers of carbon atoms whose dangling bonds are saturated with hydrogen atoms.

First, we calculated the two geometries identified to be the most stable for oxygen adsorption on (100) diamond surface,[10] bridge and on-top configurations. For the bridge configuration, the C—O bond length was computed to be 1.48 Å, the same as reported by Badziag and Verwoerd[11] and in good agreement with the result of Zheng and Smith,[10] 1.49 Å, but somewhat apart from the result of Russo,[12] 1.40 Å. For the on-top configuration, the C—O bond length was computed to be 1.22 Å, the same as reported by Russo[12] and in good agreement with the result of Zheng and Smith,[10] 1.25 Å. Referenced to the ideal undistorted clean surface, the chemisorption energies obtained in the present study were 172 and 162 kcal/mol per oxygen for the bridge and on-top configurations, respectively. These can be compared to the values reported by Zheng and Smith,[10] 194 and 198 kcal/mol, Russo,[12] 133 and 185 kcal/mol, and Badziag and Verwoerd,[11] 143 kcal/mol for the bridge site configuration. High resolution electron energy loss spectroscopy confirms the presence of carbonyl bonding on the (100) diamond surface after exposure to atomic oxygen.[13]

The minimum-energy reaction path identified in our calculations is shown in Fig. 2. The starting configuration is an O-on-top radical site shown as the left most configuration in Fig. 2. The minimum-energy reaction path then proceeds through a β-scission of the C—CO bond, formation of a dimer C—C bond, and finally cleavage of the second C—CO bond, as shown in Fig. 2. The largest potential-energy barrier encountered during this reaction sequence is that of the final desorption step; it is equal to 38.4 kcal/mol, relatively close to (within the accuracy of the MNDO potential) but slightly lower than the experimental activation energy for CO desorption of 45.0 kcal/mol described earlier in this letter.

The H atom connected to one of the C atoms in Fig. 2 is used, as described above, to aid the calculations by saturating a dangling bond. In reality, this C-atom valence is not necessarily capped by a H atom, but may be vacant or

connected to another C atom. In such cases, the energetics of CO desorption becomes less favorable; for example, the barrier for the first step is increased to 45.2 and 35.8 kcal/mol, respectively, from 23.5 kcal/mol shown in Fig. 2. On the other hand, the assumption of at least one radical site in the initial structure, as shown in Fig. 2, seems to be critical for obtaining a low activation energy, because then the cleavage of the C—C bond is accompanied by the formation of a π bond (i.e., a β-scission reaction). For example, at the same level of theory, the expulsion of CO from a fully hydrogenated site encounters a barrier[6] of 67.6 kcal/mol (for further comparison, a similar expulsion of CO with the two H atoms removed results in a 116 kcal/mol barrier). These considerations point out an array of possible CO desorption sites, some with close and some with vastly different potential energy barriers. Additional variation in the desorption energies may result from the multitude of ways in which the radical sites can be created. The existence of a distribution in activation energies is in general agreement with the interpretation given to the broad desorption peak observed in the experiment.

We also note that the reverse of the reaction pathway depicted in Fig. 2 is the insertion of CO into a (100)-(2×1) dimer, similar to the insertion of methyl.[6,14] The initial step of this insertion is the addition of CO to a dimer radical, with the computed barrier of 28.9 kcal/mol, close to 32.6 kcal/mol obtained for a similar addition of methyl.[6] The subsequent steps follow a two-step mechanism similar to one identified in molecular dynamics studies of Garrison et al.[14] for methyl. The potential energy barriers computed here are 17.0 kcal/mol for the cleavage of the dimer C—C bond and 13.9 kcal/mol for the formation of the O-on-top configuration (see Fig. 2). By comparison, for the methyl insertion, the MNDO calculations resulted in 14.2 and 18.3 kcal/mol, respectively. Thus, the energetics of the two-step CO dimer insertion are close to a similar insertion of methyl and are more favorable than the addition of CO to a triplet diradical, which has a prohibitively large (51 kcal/mol) potential energy barrier.[6] The present results make it feasible for CO to contribute to the growth of diamond, via the two-step insertion mechanism. Indeed, carbon monoxide, either formed in large quantities in oxygen-containing environments or used as the initial reactant,[1,15] has been implicated as a diamond growth species.[16]

In summary, an apparent activation energy of CO desorption from the (100) diamond surface was determined by thermal desorption spectroscopy and found to be equal 45.0 kcal/mol. A minimum potential-energy reaction path was identified by quantum chemical calculations with the semiempirical MNDO Hamiltonian. The largest barrier along this pathway is 38.4 kcal/mol, in reasonable agreement with the experimental activation energy. Taken together, the broad experimental desorption-peak feature and the multitude of possible desorption sites with differing potential-energy barriers, suggests the existence of a distribution of CO sites on diamond surfaces.

[1] See, e.g., recent reviews: P. K. Bachmann, D. Leers, and H. Lydtin, Diamond Relat. Mater. 1, 1 (1992); F. G. Celii and J. E. Butler, Ann. Rev. Phys. Chem. 42, 643 (1991).
[2] R. E. Thomas, R. A. Rudder, and R. J. Markunas, J. Vac. Sci. Technol. A 10, 2451 (1992).
[3] A. M. de Jong and J. W. Niemantsverdriet, Surf. Sci. 233, 355 (1990).
[4] F. M. Lord and J. S. Kittleberger, Surf. Sci. 43, 173 (1974).
[5] P. A. Redhead, Vacuum 12, 203 (1962).
[6] D. Huang and M. Frenklach, J. Phys. Chem. 96, 1868 (1992).
[7] M. J. S. Dewar and W. Theil, J. Am. Chem. Soc. 99, 4899 (1977).
[8] For example, J. Sadlej, Semi-Empirical Methods of Quantum Chemistry, translated by I. L. Cooper (Ellis Horwood, Chichester, 1985).
[9] Available from the Quantum Chemistry Program Exchange (Chemistry Department, Indiana University) as QCPE Program No. 506 (1985).
[10] X. M. Zheng and P. V. Smith, Surf. Sci. 262, 219 (1992).
[11] P. Badziag and W. S. Verwoerd, Surf. Sci. 183, 469 (1987).
[12] N. Russo, in Structure and Reactivity of Surfaces, edited by C. Morterra, A. Zecchina, and G. Costa (Elsevier, Amsterdam, 1989), p. 809.
[13] P. Pehrsson (personal communication).
[14] B. J. Garrison, E. J. Dawnkaski, D. Srivastava, and D. W. Brenner, Science 255, 835 (1992).
[15] F. M. Cerio, W. A. Weimer, and C. E. Johnson, J. Mater. Res. 7, 1195 (1992).
[16] K. M. McNamara and K. K. Gleason, J. Appl. Phys. 71, 2884 (1992); J. Electrochem. Soc. 140, L22 1993).

ELECTRON MICROSCOPY OF NATURAL AND EPITAXIAL DIAMOND

J.B. Posthill*, T. George**, D.P. Malta*, T.P. Humphreys***, R.A. Rudder*, G.C. Hudson*,
R.E. Thomas*, and R.J. Markunas*

*   Research Triangle Institute, Research Triangle Park, NC 27709-2194
** Center for Space Microelectronics Tech., JPL, Calif. Inst. of Tech., Pasadena, CA 91109
*** Department of Physics, North Carolina State University, Raleigh, NC 27695-8202

Semiconducting diamond films have the potential for use as a material in which to build active electronic devices capable of operating at high temperatures or in high radiation environments. Ultimately, it is preferable to use low-defect-density single crystal diamond for device fabrication. We have previously investigated polycrystalline diamond films with transmission electron microscopy (TEM) and scanning electron microscopy (SEM)[ref 1], and homoepitaxial films with SEM-based techniques[ref 2]. This contribution describes some of our most recent observations of the microstructure of natural diamond single crystals and homoepitaxial diamond thin films using TEM.

We are developing techniques to thin diamonds to electron transparency in the region of interest; particularly as diamond is difficult to mechanically thin. One simple (but time consuming) approach for the fabrication of plan-view diamond TEM samples is to thin only by ion milling. Figs. 1 and 2 show TEM micrographs taken from a (100) natural type IIb (semiconducting) diamond crystal and a (100) natural type Ia diamond that have been ion milled to electron transparency. The mottled background contrast observed in both images is believed to be an artifact due to ion milling. An average dislocation density of $\sim 5 \times 10^7$ cm^{-2} was observed in the type IIb material, and the dislocation distribution was found to be nonuniform. Dislocations were not observed via TEM in the type Ia diamond (dislocation density $< 10^5$ cm^{-2}), but nitrogen-containing platelets that lie on $\{100\}$ planes, characteristic of type Ia diamond, were observed. A technique for more rapid thinning for plan-view TEM sample preparation was achieved by laser ablation (Fig. 3), which is described in more detail elsewhere[3]. Although it is recognized that defect densities will vary from stone to stone for natural diamond, type Ia has consistently been found to show lower dislocation densities.

Homoepitaxial diamond films were grown on (100) type Ia diamond substrates using water/methanol mixtures in an rf-driven plasma-enhanced chemical vapor deposition (PECVD) reactor. The growth conditions were comparable to that described elsewhere[4]. They were then ion milled from the back-side for plan-view TEM examination. Figs. 4 and 5 respectively show the featureless topography recorded by a field emission gun SEM and dislocations observed by TEM in a film grown for 50 minutes. The average dislocation density was found to be $\sim 5 \times 10^6$ cm^{-2}, and no other types of defects were observed. This dislocation density would be considered high by single crystal Si standards, but it does represent the current benchmark for diamond epitaxy. We are certain we are observing the epilayer because of the absence of nitrogen-containing platelets. Note also that the micro-Raman spectrum of the diamond epitaxial layer showed the characteristic LO phonon peak with a FWHM of 2.4 cm^{-1}, comparable to that of the substrate. These results show that growth of homoepitaxial diamond can be achieved on natural type Ia diamond to a reasonable standard. In other words, the presence of the nitrogen-containing platelets in the substrate does not result in catastrophic dislocation densities in the diamond epilayer.[5]

References

1. J.B. Posthill, et al., Proc. 47th Ann. Meet. Electron Microsc. Soc. of America. 592 (1989).

2. D.P. Malta, et al., Proc. 49th Ann. Meet. Electron Microsc. Soc. of America, 880 (1991).

3. T. George, et al., Appl. Phys. Lett., in press.

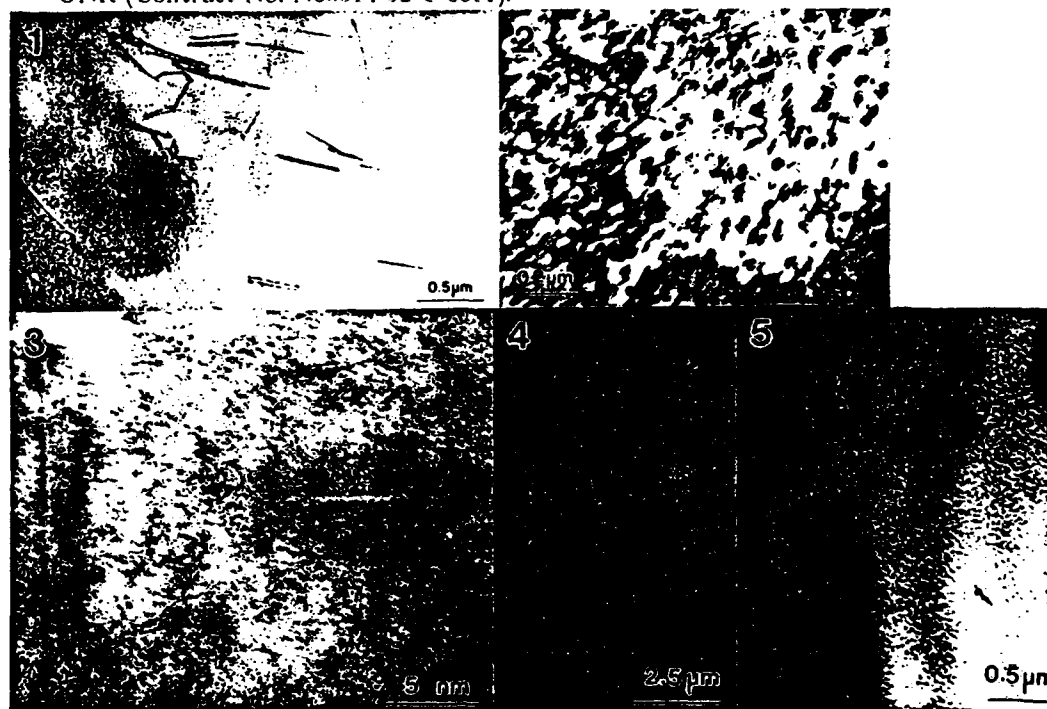4. R.A. Rudder, et al., Appl. Phys. Lett., 60 329 (1992).

FIG. 1.--TEM of single crystal C(100) [type IIb]. Note high dislocation density. Sample prepared by ion milling.

FIG. 2.--TEM of single crystal C(100) [type Ia]. Note the presence of {100} nitrogen platelets (shown inclined in this [110] orientation) characteristic of natural type Ia diamond. Sample prepared by ion milling.

FIG. 3.--Higher magnification TEM of single crystal C(100) [type Ia] in [100] orientation. Sample prepared by laser ablation.

FIG. 4.--SEM topographical image of diamond homoepitaxial film grown using water/methanol mixture. The surface is featureless.

FIG. 5.--TEM plan-view of diamond homoepitaxial film grown using water/methanol mixture. Sample prepared by ion milling.